QUANTIFICATION OF PRESTRESSED CONCRETE RAILWAY CROSSTIE FLEXURAL RESPONSE: IMPLICATIONS FOR MECHANISTIC DESIGN

BY

JOHN RILEY EDWARDS

DISSERTATION

Submitted in partial fulfillment of the requirements
for the degree of Doctor of Philosophy in Civil Engineering
in the Graduate College of the
University of Illinois at Urbana-Champaign, 2019

Urbana, Illinois

Doctoral Committee:

Professor Christopher P.L. Barkan, Chair
Professor David A. Lange, Co-Chair
Professor Erol Tutumluer
Professor David Clarke, University of Tennessee – Knoxville

ABSTRACT

Concrete is the dominant crosstie material choice for demanding locations on heavy axle load (HAL) freight railroads with steep grades, sharp curves, and high annual gross tonnage. Concrete crossties are also used in rail transit applications where safety and reliability of infrastructure is at a premium and maintenance time is often limited. As such, development and implementation of a structural design method that enables optimization of crosstie design for varied applications and loading environments will reduce initial capital cost and recurring maintenance expense.

Center flexural cracking is one of the most common factors limiting the service life of concrete crossties in North America, and rail seat cracking has been documented as a performance concern. Improving the understanding of crosstie flexure can help reduce the occurrences of cracked crossties by ensuring that designs conform to the field conditions in which they are used. To date, few methods have been proposed to accurately quantify the revenue service field bending moments of concrete crossties and their variability due to support conditions and other factors. This dissertation describes the development, deployment, and validation of a method to quantify crosstie bending moments using concrete surface strain gauges.

Data collected using this method at field installations throughout the United States were used to investigate the effects of thermal gradient, axle load, axle location, support condition, and rail mode on crosstie bending moments. Results indicated that thermal gradient is significant and should be considered in crosstie flexural design, especially at the crosstie center. Additionally, crosstie support condition is the largest source of variability in crosstie bending moments and its effect is most pronounced on HAL freight railroads. The field results indicated

the need for development and application of a probabilistic design method for the flexural capacity of concrete crossties. I developed a design process based on structural reliability analysis concepts whereby target values for reliability indices (β) for new designs are obtained and compared with existing designs for further design optimization. New (proposed) designs are more economical, having a center negative moment capacity reduction of 50% for heavy rail transit. For HAL freight, a reduction in rail seat bending capacity of approximately 40% is justified, reducing the size of the rail seat cross section by approximately the same magnitude. In most cases the proposed designs for both rail modes have fewer prestressing wires and a higher centroid of prestressing steel. In all cases the flexural capacities at the crosstie center and rail seat are better balanced from a structural reliability standpoint.

The probabilistic method using structural reliability analysis fundamentals that is proposed and demonstrated in this dissertation constitutes a critical step in the development of mechanistic-empirical practices for the design of concrete crossties. Additionally, this framework for probabilistic design provides a foundation for the future application of mechanistic-empirical design practices to other railway track components.

ACKNOWLEDGMENTS

Research is a team sport, and I am convinced that great research is unlikely to emerge from a researcher operating in isolation. I have learned this firsthand over the past 13 years, and most importantly, I have seen this demonstrated by my supervisor and advisor, Christopher P.L. Barkan who has encouraged me to take an inter-disciplinary, team approach to addressing challenging research questions.

First and foremost, it is my desire that the glory associated with this dissertation go to Jesus Christ, my Lord and chief exemplar. I also desire that this recognition of Jesus not be in a manner that is religious and distant, but rather one that demonstrates my personal connection and reliance on Him. Secondly, I am greatly indebted to my wife Kristin and my children for allowing me to undertake this academic endeavor at a challenging life stage. They have been patient and encouraging, and I am fortunate that this process was largely completed before the arrival of my third child. I am prayerfully hopeful that this dissertation and degree can be used to serve them, and will allow me to impact the world.

I am very respectful and deeply appreciative of my advisers for this dissertation, and their personal time commitment and intentional encouragement they have provided to me as a non-traditional PhD student. I have been fortunate to work with Chris Barkan since 2004 in a variety of roles, and respect his keen intellect and passion for rail engineering that is unmatched the world over (I have amassed a significant volume of empirical data to support this claim). His relational attitude toward his employees and students is contagious, and is his attribute that I am most hopeful of replicating in my own career. I have also been fortunate to work with David Lange in a variety of capacities, both in and out of the University, and I appreciate his intellect

and well-rounded manner by which he pursues life and work and has engaged me in engineering conversations. A special thanks to Erol Tutumluer is also due. Erol is a gifted academic with a keen intellect. He is a tremendously kind and welcoming individual that stands out in field that tends to promote self-centeredness. Finally, but by no means least, is David Clarke. Having Prof. Clarke as a member of this committee has been a tremendous gift to me, as I have long respected his intellect and knowledge of rail engineering, along with his choice of state to reside in (Tennessee, my home state). Other RailTEC and CEE faculty, past and present, including Don Uzarski, Ernie Barenberg, and Marshall Thompson, have provided focused and timely encouragement that I greatly appreciate.

The core technical team that I have been fortunate to be a part of for the past decade played a major role in developing a collective momentum that has allowed me to pursue much of the research that is included in this dissertation. I am indebted to all of my co-workers, graduate research assistants, and undergraduate students. A specific thanks to Marcus Dersch for his continued growth in the workplace, which has played a role in allowing me to focus more time on writing this dissertation. I am also very thankful for his friendship in and out of the workplace. In addition to Marcus, I am very grateful for the full time technical staff I have collaborated with over the past eight years including Ryan Kernes, Yu Qian, Matthew Csenge, and most recently, Arthur de Oliveira Lima.

Specific personal acknowledgement of both Yubing Liang and Alvaro Canga Ruiz is warranted, as they collaborated with me over the past several years, and are both gifted researchers. I have been encouraged by them along the way, and was frequently impressed with their intellect as we advanced our understanding of the design and performance of track components.

Strong industry support in the form of research funding was provided by the Federal Railroad Administration (FRA) and the Federal Transit Administration (FTA), two modal administrations of the United States Department of Transportation (US DOT). I am specifically grateful to Cam Stuart and Gary Carr of FRA and Terrell Williams of FTA for their confidence in funding the research program that I have been fortunate to manage at UIUC. The material in this dissertation represents the position of the author and not necessarily that of FRA or FTA. I am also grateful to the sponsors that have supported my research program over the past decade, starting with the Association of American Railroads (AAR) Technology Scanning Program.

I would like to acknowledge the following industry partners that have provided either research funding or emotional support related to this dissertation, at the risk of leaving out some organizations that have provided valuable contributions: Union Pacific Railroad; BNSF Railway; National Railway Passenger Corporation (Amtrak); Progress Rail Services, a Caterpillar Company; Gutanna Technologies; Hanson Professional Services, Inc.; Rocla/Vossloh Concrete Ties and Fastening Systems, voestalpine Nortrak, Pandrol, and CXT Concrete Ties, Inc., an LB Foster Company.

Finally, a portion of my funding has been provided through grants to UIUC's RailTEC from CN and Hanson Professional Services, Inc. I am grateful to the generosity of these organizations and the opportunity I have had to build relationships with individuals at both CN and Hanson. I would like to personally acknowledge Kevin Day and Dave Ferryman at CN and Sergio (Satch) Pecori, Gary Potts, and Mat Fletcher at Hanson for their support and friendship over the past 15 years.

To all of the people that I have left out, you have been no less impactful in my life and the development of this research program and dissertation.

To my family,

Kristin, Elijah, Oliver, and Caroline Edwards

And our Leader,

He is before all things, and in Him all things hold together.

(Colossians 1:17)

TABLE OF CONTENTS

CHAPTER 1: INTRODUCTION

1.1 Purpose

The purpose of my dissertation research is to quantify the magnitude and variability of concrete crosstie (referred to internationally as a "sleeper") field bending moments under revenue service train operations. Additionally, I develop a method of predicting crosstie flexural demand given knowledge of a rail line's operational characteristics. Finally, these data and methods are used to develop and demonstrate a framework for probabilistic design of future concrete crossties, and provide a means of quantifying the reserve capacity of existing designs.

1.2 Background

The majority of railroad track worldwide is supported by stone ballast. A ballasted track system consists of the rail, fastening systems, crossties, ballast, sub-ballast, and subgrade (Hay, 1982; Kerr, 2003). In North America, concrete is the second most common material used to manufacture crossties, but it is the dominant material used for crossties elsewhere in the world (Zeman, 2010; Senese, 2016). Combining Class I heavy axle load (HAL) freight railroads, Amtrak, and rail transit properties, there are approximately 35 million concrete crossties installed in track in North America, with approximately 750,000 to 1,500,000 additional new crossties manufactured and installed each year.

Pre-tensioning is the most common practice used to manufacture concrete crossties in North America (Van Dyk, 2014), with some post-tensioning or hybrid (e.g. pre-tensioned with end plates) operations beginning to emerge. Due to the increased flexural strength, ductility, and

resistance to cracking produced by the "pre-tensioned" steel wires (Naaman, 2004), prestressed concrete crossties can withstand the high dynamic loading environment imparted by passing trains. Prestressed concrete crossties are commonly used in the most demanding service conditions in the United States such as freight railroad trackage with extensive curvature, steep grades, and heavy freight tonnage (in terms of both axle load and total gross tonnage); very high and higher-speed passenger train traffic; and rail transit applications where reliability of infrastructure is at a premium (Jimenez and LoPresti, 2004; Zeman, 2010; Van Dyk, 2014).

Railroads, concrete crosstie manufacturers, and researchers have ranked cracking from center binding (support under the center of member and not the ends) among the most critical problems limiting the service life of concrete crossties (Van Dyk, 2014). Additionally, rail seat cracks have also been cited as a performance problem for concrete crossties and have been the subject of considerable research (Zakeri and Rezvani, 2012; Domingo et al., 2014). Both of these failures relate to the structural integrity and flexural resistance of the crosstie. The relative ranking of crosstie failure mechanisms and areas of concern vary considerably between North America and elsewhere in the world (for more discussion of these differences see Van Dyk et al (2014) (Table 1.1). My dissertation addresses cracking from dynamic loads and center binding.

Table 1.1: Rank of problems in concrete crosstie track on a scale of 1-8, with 8 being the most critical (modified from Van Dyk 2014).

Most Critical Concrete Crosstie Problems	Average Rank	
	North America	Elsewhere
Rail seat deterioration (RSD)	6.4	3.2
Shoulder/fastening system wear or fatigue	6.4	5.5
Cracking from dynamic loads	4.8	5.2
Derailment damage	4.6	4.6
Cracking from center binding	4.5	5.4
Tamping damage	4.1	6.1
Other (ex. manufacture defect)	3.6	4.1
Cracking due to environmental/chemical degradation	3.5	4.7

Because of the increasing use of prestressed concrete crossties in demanding operating environments, it is important to understand the factors that cause crossties to crack at the rail seat and center. The input loading, support configurations, and resulting bending experienced by the crosstie can be investigated through data collection, experimentation, and finite element (FE) modeling. In 2011, an extensive concrete crosstie research effort was begun by the Rail Transportation and Engineering Center (RailTEC) at the University of Illinois at Urbana-Champaign (UIUC) to quantify these factors (Grassé, 2013; Grassé et al., 2014; Edwards et al., 2017a, 2017b). This research program was funded by the US DOT Federal Railroad Administration (FRA) under the 2010 Broad Agency Announcement (BAA) program. It was the first large-scale concrete crosstie research effort commissioned in the U.S. since the 1970's, when research was conducted on Amtrak's Northeast Corridor (NEC) and at the Transportation Test Center (TTC) (Harrison et al., 1984) during the early years of concrete crosstie adoption in North America.

Despite these research efforts, and recent development of a preliminary framework for mechanistic design of crossties (Van Dyk et al., 2013; Edwards et al., 2017a, 2017b), further research is required to generate a robust and repeatable method for collecting field bending strains that can be used to address critical questions related to mechanistic crosstie design. Collecting and interpreting accurate and reliable field data on concrete crosstie flexural performance provides information needed to properly design laboratory experiments, calibrate FE models, and ultimately is essential to develop optimized designs for concrete crossties.

This line of research provides a means of accurately analyzing the demand on current concrete crossties, which when compared to their capacity, allows us to quantify residual (excess) capacity to either first crack or ultimate failure. This can be done both deterministically

and probabilistically, as will be discussed in subsequent chapters. To achieve accurate measurements and quantify the bending behavior of concrete crossties under revenue service train traffic, an instrumentation methodology was designed, developed, and deployed. In this dissertation, I will demonstrate its application for addressing a number of critical track superstructure research questions related to the design and performance of concrete crossties.

1.3 Recent Crosstie Research

Over the past decade, substantial research has been conducted on the structural performance of concrete crossties via laboratory experimentation (Taherinezhad et al., 2013; César Bastos, 2016; César Bastos et al., 2016) and analytical evaluation using FE modeling (Chen et al., 2013; Chen et al., 2014a; Chen et al., 2014b; Yu and Jeong, 2014; Chen et al., 2016). There has been comparatively little research aimed at quantifying and understanding the magnitude of, and variation in, flexural demands placed on concrete crossties in the field. Additionally, there is no documented method for accurately collecting these bending moment data in the field or laboratory, especially over long time periods.

Although not exhaustive, Table 1.2 provides an overview of the subjects of concrete crosstie research over the past decade. While the crosstie and fastening system are closely linked and should be considered as a system, this list excludes research focused only on fastening systems. The dominant research evident from the literature relates to the crosstie's response to dynamic and impact loading, or its ultimate capacity. There has also been research focusing on concrete materials, largely driven by field failures such as rail seat deterioration (RSD) and questions related to freeze thaw durability and the adequacy of existing standardized testing procedures.

Table 1.2: Crosstie research topic areas and select references

Crosstie Research Area	Sub-area	Select references
Rail seat deterioration (RSD)	Mechanisms	(Choros et al., 2007; Zeman, 2010; Kernes, 2014)
	Materials	(Van Dam, 2014; Shurpali et al., 2014; Shurpali et al., 2017)
Concrete materials	Air voids and freeze thaw	(Albahttiti et al., 2015; Song et al., 2017b)
Cracking	Loading, Impact loads	(Kaewunruen and Remennikov, 2009a; Kaewunruen and Remennikov, 2009b; Jokūbaitis et al., 2016; Ngamkhanong et al., 2017)
Center flexure	Bending capacity	(Wolf, 2015a; César Bastos, 2016)
	Cracking	(César Bastos et al., 2016)
	Thermal effects	(Wolf et al., 2016b)
Prestressing	Transfer length	(Zhao et al., 2012; Zhao et al., 2013a)
Field response	Bending moments	(RSMA 1970; Wolf, 2015a; Wolf et al., 2016a; Wolf et al. 2016b; Mayville et al., 2014)

1.4 Crosstie Design Considerations

Preliminary research at UIUC showed significant variability in the flexural demands on concrete crossties in the field (Gao et al., 2016), largely due to support conditions. This variation has a major influence on crosstie design and represents a disparity between field response and demand prediction methods within current design procedures. Crosstie flexural demand variability can occur due to a number of factors including: loading magnitude, support conditions, properties of the crosstie itself, duration of load application, temperature gradient, and climate. Each of these factors needs to be further studied in order to develop optimized, mechanistically-designed concrete crossties.

1.4.1 Considerations for Concrete Monoblock Crosstie Design

There are multiple design elements to be considered when assessing the performance of, or generating a design for, prestressed monoblock railway crossties (Figure 1.1). In addition to its flexural strength (resistance to bending under load), which is widely considered to be the most critical element of crosstie design, the allowable ballast pressure must not be exceeded (AREMA, 2016) and the rail seat area should be robust to a variety of proposed failure mechanisms (Choros et al., 2007; Zeman, 2010). The latter is primarily driven by the reduction in pressure at the rail seat through geometry changes, premium materials, improved rail pads, and other fastening system components.

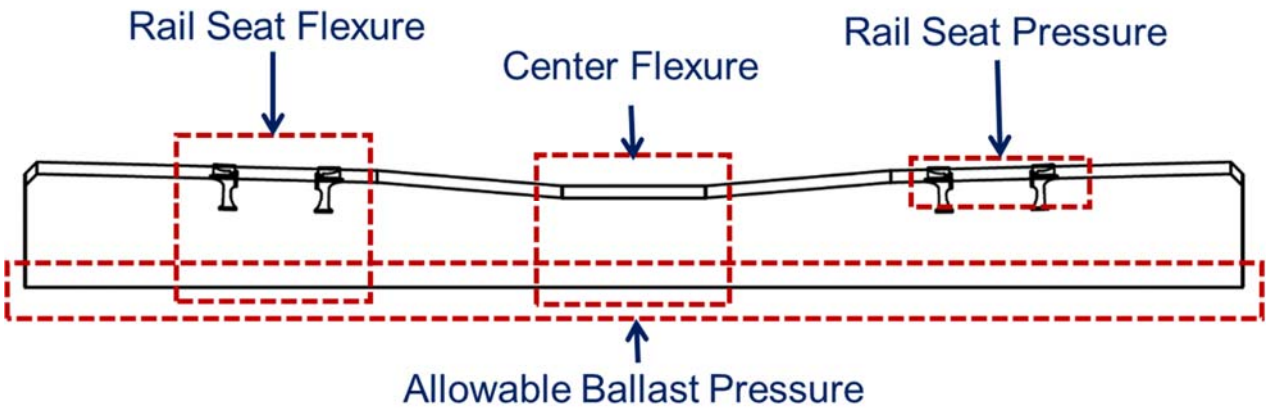

Figure 1.1: Critical considerations for concrete crosstie design.

1.4.2 Crosstie Materials and Structural Design Consideration

In addition to structural design, which is largely associated with the location, magnitude, and eccentricity of the centroid of prestressing wires or strands, the materials selection and mixture design of the crosstie must be considered. Concrete material choices also have an effect on the flexural performance, rail seat integrity, and ballast pressure (as it relates to possible abrasion on the bottom of the crosstie). Table 1.3 identifies which design element must be

considered for each crosstie design characteristic. For example, crosstie geometry, materials / mixture design, and prestress design all must be considered when designing the flexural characteristics of the rail seat and crosstie center. Designing a rail seat that is robust to the magnitude and duration of expected loads, and is resistant to abrasion that may be caused by displacements, should consider both crosstie geometry (i.e. rail seat dimensions and area) and the abrasion resistance of the concrete mixture design and its constituent materials.

Table 1.3: Integration of concrete crosstie design elements

Crosstie Design Characteristic	Crosstie Design Elements		
	Geometry	Materials	Prestress
Rail Seat Flexure	●	●	●
Center Flexure	●	●	●
Rail Seat Pressure	●	●	
Allowable Ballast Pressure	●	●	

Changes to one design characteristic will likely necessitate a change in the parameters of other's, and optimizing these areas in isolation is unlikely to generate a globally optimal design solution. Previous concrete crosstie design and performance research conducted at UIUC has been undertaken from a multi-disciplinary standpoint, drawing upon knowledge in each of the aforementioned focus areas (Edwards et al., 2017a, 2017b). The research I describe in this dissertation will be a continuation of this holistic, multi-disciplinary approach to improving concrete crosstie design and performance.

1.4.3 Crosstie Center and Rail Seat Bending Moments

The two locations on the crosstie that are most critical to flexural design are the rail seat and center. Specifically, concrete crosstie design is typically governed by center negative and rail seat positive bending moments (Figure 1.2). The other, "minor" bending moments of center positive and rail seat negative would rarely, if ever, generate moments that govern the overall flexural design of the crosstie, but they will nevertheless be considered in this research and documented in this dissertation.

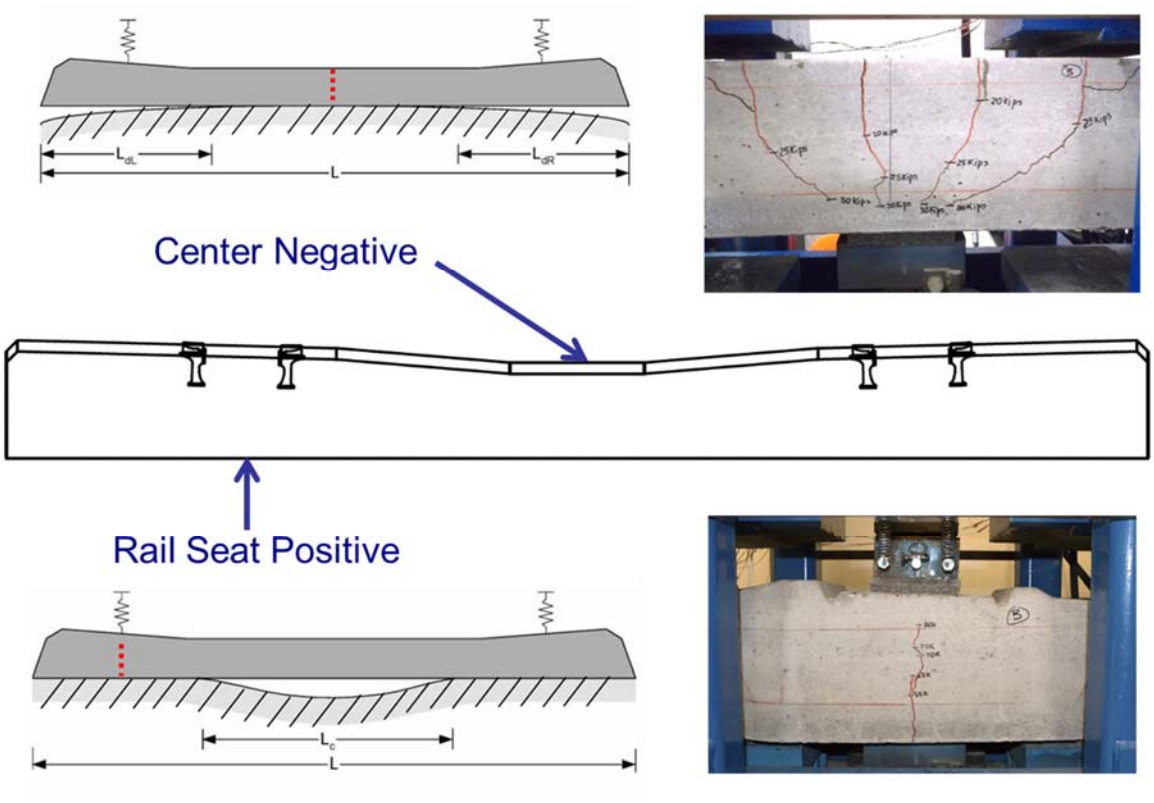

Figure 1.2: Two critical regions for flexural design consideration and images of typical flexural cracking patterns.

The flexural design of crossties in North America is based on Chapter 30 (Ties) of the American Railway Engineering and Maintenance-of-Way Association (AREMA) Manual for Railway Engineering (hereafter referred to as the "AREMA Manual") (2016) that references use

of American Concrete Institute (ACI) 318-14 (2014) design criteria, which are largely based on allowable stress design principles. The contents of the AREMA Manual are updated on an annual basis and references in this dissertation to specific release dates of the AREMA Manual are intentional.

1.4.4 Prestress Concrete Design Fundamentals

Prestressing of concrete provides a variety of benefits over reinforced concrete, including greater moment capacity at first crack, and improved moment-curvature characteristics between first crack and ultimate failure (Lin and Burns, 1981; Naaman, 2004). ACI 318-14 (2014) design recommendations provide guidance on quantifying stresses and ensure that under expected service loads members do not fail in either compression or tension. Typically, prestressed concrete crossties are designed as Class U (uncracked) members per ACI 318-14 (2014), thus their flexural capacity is defined based on first crack at the extreme tensile fiber. This generally conforms to what AREMA (2016) states, although the AREMA definition requires a crack to penetrate to the first level of prestressing from the tensile surface of the crosstie. The evaluation of stresses and strains described below is based on the Euler-Bernoulli beam theory for small deformations (Timoshenko, 1953).

The total stresses at the extreme tensile (i.e. top of crosstie) fiber cannot exceed the modulus of rupture (f_r) of the concrete (Equation 1.1). The three terms demonstrate precompression, the internal moment caused by the eccentric of the prestressing, and the external moment due to axle loads. For concrete with a compressive strength (f'_c) of 7 ksi (typical for concrete used to manufacture concrete crossties) the value for f_r is 0.627 ksi according to ACI 318-14, Table 24.5.4.1 (2014).

$$-\frac{F_{se}}{A_c}-\frac{F_{se}(e)c}{I_c}+\frac{M_c c}{I_c}\leq f_r \quad (1.1)$$

Where:
f_r = modulus of rupture of concrete (ksi) [0.627 ksi for f'_c of 7 ksi]
M_c = center negative bending moment (kip-in)
F_{se} = effective prestressing force (after losses) (kips)
A_c = cross-sectional area (in^2)
I_c = section moment of inertia (in^4)
e = eccentricity of prestress centroid (in)
c = distance from neutral axis to extreme fiber (in)

In conventional solid mechanics terminology, compressive stresses are characterized as positive, and tensile stresses negative. Additionally, the negative second term in Equation 1.1 ($\frac{F_{se}(e)c}{I_c}$) indicates that the eccentricity induced by the prestress produces compression in the top of the crosstie that is used to counteract a positive bending moment. The stresses listed in Equation 1.1 can also be represented graphically (Figure 1.3).

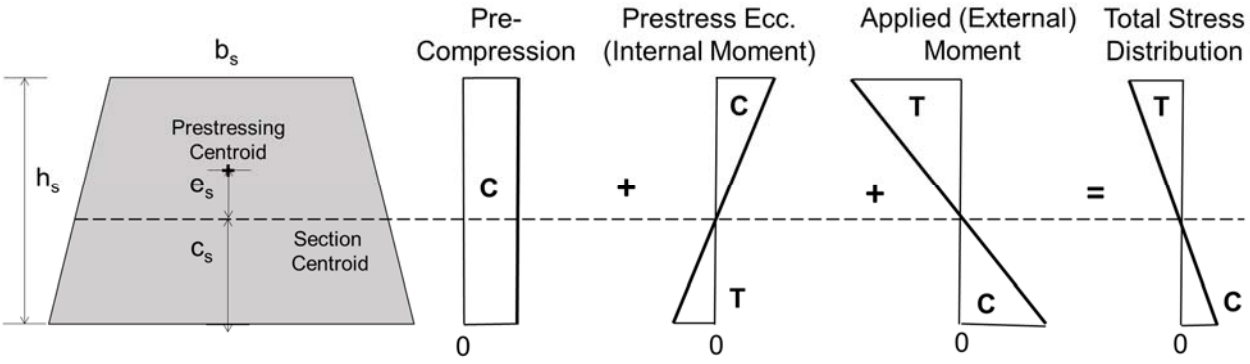

Figure 1.3: Graphical representation of stresses within concrete crosstie center cross section assuming an external moment is applied causing tensile forces in the top surface.

The critical value to quantify in relation to induced stresses, and identification of when the structural member will crack (or fail), is the bending moment. One can solve Equation 1.1

for the cracking moment that would indicate that the total stresses in the tensile surface equal f_r (Equation 1.2), which defines the maximum moment capacity prior to cracking of the member.

$$M_{cr} = \frac{I_c}{c_{tens}}\left(f_r + \frac{F_{se}}{A_c} - \frac{F_{se}(e)c_{tens}}{I_c}\right) \quad (1.2)$$

Where:
f_r = modulus of rupture (ksi)
M_{cr} = cracking moment (kip-in)
c_{tens} = distance from neutral axis to extreme tensile fiber (in)

The strength of a prestressed concrete member is typically governed by cracking at the tensile surface, as opposed to crushing in the compression region. This is primarily due to the manner in which it is loaded (e.g. uniform load or two distributed rail seat loads). Additionally, the crushing limit for concrete is much higher than the tensile limit, on the order of 4.2 ksi for concrete with a compressive strength (f_c') of 7 ksi according to ACI 318-14 (2014).

For the sake of brevity, only the crosstie center region will be considered, and the tensile (top) surface will be the location of greatest attention assuming that the crosstie is experiencing negative bending. The rail seat flexural considerations are similar, albeit limited by tension on the bottom surface of the crosstie as a result of positive bending moments.

The aforementioned discussion related to the calculation of first crack, and was in the linear elastic range of expected behavior of prestressed concrete components, but the ultimate strength and curvature is also of specific interest in prestress design. This process is undertaken either by use of an approximate formula such as can be found in ACI 318-14 (2014), or through a procedure referred to as strain compatibility that provides a more exact estimate of the flexural capacity of the member, which is also referenced in ACI 318-14 (2014).

There are a number of other considerations with respect to prestressed concrete design, including stresses at the end section at transfer or prestress, development length, and long-term effects of creep and shrinkage. Development length, i.e. the length over which the prestress is transferred from the steel prestressing strands to the concrete, is less critical at the center of a crosstie, but can affect the flexural performance of the rail seat given its proximity to the end of the crosstie. As such, a number of studies have been conducted to understand bond requirements in prestressed concrete (Zhao et al., 2012; Bodapati et al., 2013; Zhao et al., 2013a; Zhao et al., 2013b; Bodapati et al., 2014; Zhao et al., 2014). Stresses at the ends of crossties are typically controlled by ensuring that the concrete reaches a specified "transfer" strength prior to transfer of prestress forces to the concrete (typically with f'_c of 4.5 to 5.0 ksi), which increases the threshold for stresses (and strains) that would result in cracking.

1.4.5 General Comments on Crosstie Support Conditions

There has been considerable research on the global load-deflection characteristics of the track structure as measured through the composite metric of "track modulus" (Talbot, 1919; Kerr, 2000; Kerr, 2003). Much less attention has been given to understanding individual crosstie-to-crosstie variability. Research has also been conducted in the laboratory and using analytical modeling to provide insight into settlement characteristics of crossties and the variability associated with different support conditions (Hou et al., 2018). This body of research has largely focused on the behavior of the track substructure (i.e. beneath the crosstie). Support conditions also play a major role in the response of the track superstructure (i.e. crosstie, fastening system, and rail); consequently, it is important to be able to quantify them. Gao et al. (2016) addressed this by developing a support condition back-calculator and several pilot studies attempted to quantify the effect of varied support conditions (Edwards et al., 2017b).

An example of recent field research aimed at quantifying variability of support conditions conducted by the Association of American Railroads (AAR) found a wide range of pressures beneath adjacent crossties (McHenry, 2013). Laboratory experimentation on other crosstie materials found similar variability (Song et al., 2017a).

1.4.6 AREMA Method for Representing Support Conditions

Support conditions play an important role in the magnitude of the bending moment induced, and small changes in support beneath the crosstie can have disproportionate effects on the bending moments, especially at the crosstie center. To calculate maximum bending moments, Equations 1.3 and 1.4 were developed by Wolf (2015a) and recently adopted by AREMA (2017) to better align with international design standards for concrete crossties. Equation 1.3 is used to calculate maximum rail seat positive bending moments and Equation 1.4 is used for center negative bending moment calculation.

$$M_{RS+} = \frac{1}{8}\left[\left(\frac{2R}{2(L-g)+\alpha(c)}\right)(L-g)^2 - Rs\right] \quad (1.3)$$

Where:
M_{RS+} = rail seat positive bending moment (kip-in)
R = design rail seat load (kip)
L = crosstie length (in)
g = rail center-to-center spacing (in)
α = center support factor (-)
c = 2g-L = center support section (in)
s = rail seat width (in)

$$M_{C-} = \frac{1}{2}R\left[\frac{L^2-(1-\alpha)c^2}{2(L-(1-\alpha)c)} - g\right] \quad (1.4)$$

Where:
M_{C-} = center negative bending moment (kip-in)

These equations are calculated with a variable center reaction reduction coefficient (α) that ranges from 0.66 to 0.86. This coefficient varies depending on the length of the crosstie and assumes a uniformly distributed rail seat load. It provides a means of calculating the moments defined in the preceding section. The variables related to loading and support conditions can be depicted graphically (Figure 1.4).

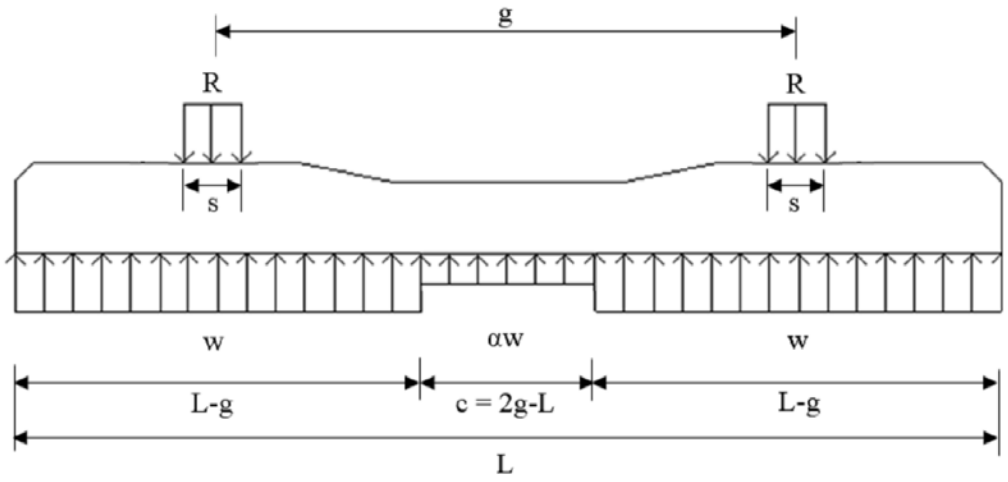

Figure 1.4: Variables for estimation of design bending moment and support conditions (Wolf, 2015a; AREMA, 2017).

While the equations above facilitate calculation of expected bending moments for concrete crossties, the majority of this dissertation focuses on field quantification of these moments, as opposed to further study of the validity of these bending moment estimation methods.

1.5 Iterative Design

Iterative design processes have generally been used for the design of railway track components such as crossties. These processes rely heavily on practical experience, and field performance, rather than being derived from a clear understanding of the load environment in

which they will be installed and failure mechanisms and causes that can be expected. At a minimum, this approach has led to inefficient designs and may be responsible for a subset of the documented performance problems and service failures. This process has also led to the multitude of designs present in current railway infrastructure. This has created confusion, reduced compatibility and potential economies of scale due to the trial-and-error process, and lack of a standard design optimization method.

1.6 Introduction to Concept of Mechanistic-Empirical Design

Over the past few decades, the concept of mechanistic-empirical design has been developed and applied to highway pavements (Thompson, 1996; ARA, 2004; Von Quintus and Moulthrop, 2007; AASHTO, 2008; Pavement Interactive, 2012). In the context of highway pavements, the mechanistic-empirical pavement design guide (MEPDG) (AASHTO, 2008) was developed to identify the causes of stress in pavement structures and to map these to observed performance (Pavement Interactive, 2012; Al-Qadi, 2018) (Figure 1.5). As is the case in traditional design, an iterative element remains in the mechanistic-empirical design process, but the mechanistic-empirical process is rooted in the mechanics of the behavior of the pavement system and iterations are only necessary due to most design problems not having a closed form solution.

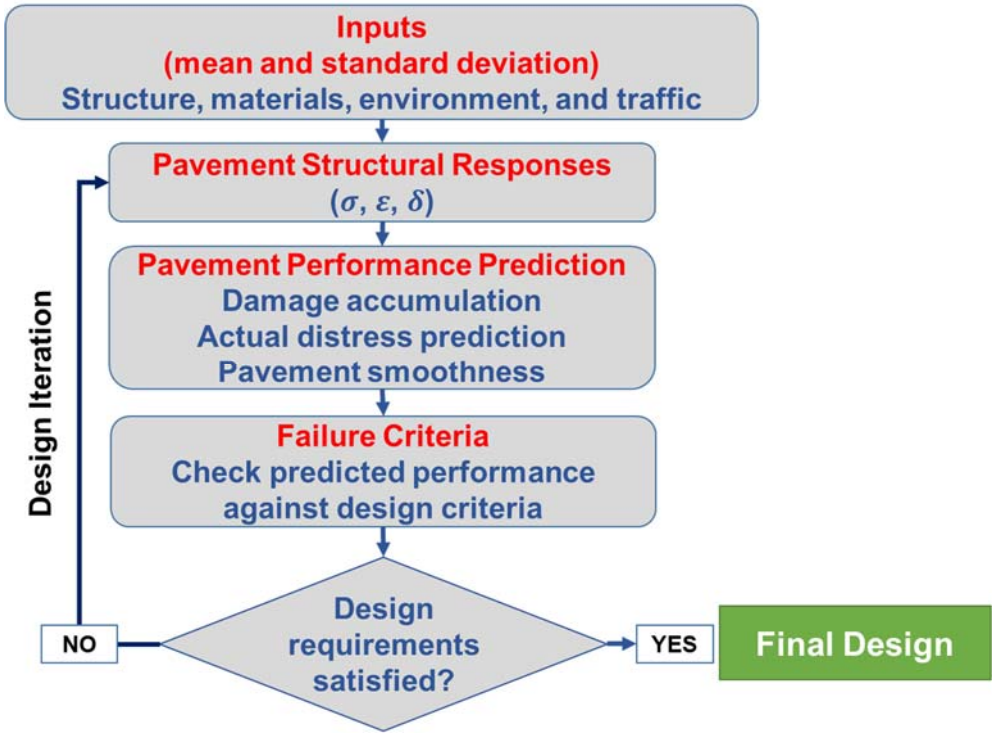

Figure 1.5: Flow chart representation of the Mechanistic-Empirical Pavement Design Guide (MEPDG) method for highway pavement design (modified from Al-Qadi, 2018).

According to Pavement Interactive (2012) the mechanistic-empirical approach to pavement design is defined by the focus on physical causes (the "mechanistic" part) and using observed performance to determine relationships (the "empirical" part). It is not possible to have a purely mechanistic deterioration (performance) model prior to the proper design and execution of experiments to understand physical deterioration rates as a function of climate, time, traffic, and other factors.

1.7 Mechanistic-Empirical Deign of Railway Track and its Components

While traditional design takes advantage of empirical relationships, these mostly relate to secondary responses of components. Thus, it is rare that these relationships were generated based on a thorough investigation of the mechanistic response of a component to load. There are

exceptions, however, and examples include attempts to consider probabilistic approaches to the design and performance of the track substructure. Analogous to the highway pavement example, collecting loads, stresses, strains, and/or bending moments within the track structure is the "mechanistic" component, and equating these values to the expected field performance currently requires an "empirical" element to the design process.

Initial suggestions for the application of a mechanistic-empirical design approach in the rail domain were documented by Csenge et al (2015) and Van Dyk et al (2013) and further developed by Quirós-Orozco (2018). More research is needed to fully implement this methodology in the field of rail engineering in general, and track components in particular. Several aspects of this approach are undertaken in this dissertation. Specifically, the mechanistic portion of response quantification based on allowable stress thresholds is advanced in my dissertation in the context of concrete crossties. These can be further developed using finite element modeling to study scenarios that would be too costly to investigate in the field.

The empirical portion of mechanistic-empirical design for railway infrastructure is more challenging to address, and requires further research. To date, most track design processes do not consider the effects of repeated load application and life cycle estimation (Hay 1982; Kerr 2003). There are, however, interim steps to implementing time and tonnage into a mechanistic-empirical design process. One such step is to use the literature that quantifies long-term performance and deterioration curves. Track geometry deterioration rates and other indicators could be used as a proxy for component deterioration rates. Examples include research by Zarembski (2010) related to timber crosstie track and research by Lovett (2017) related to the life cycle of track and maintenance prioritization.

A proposed framework for mechanistic-empirical design of railway track and its components is shown in Figure 1.6.

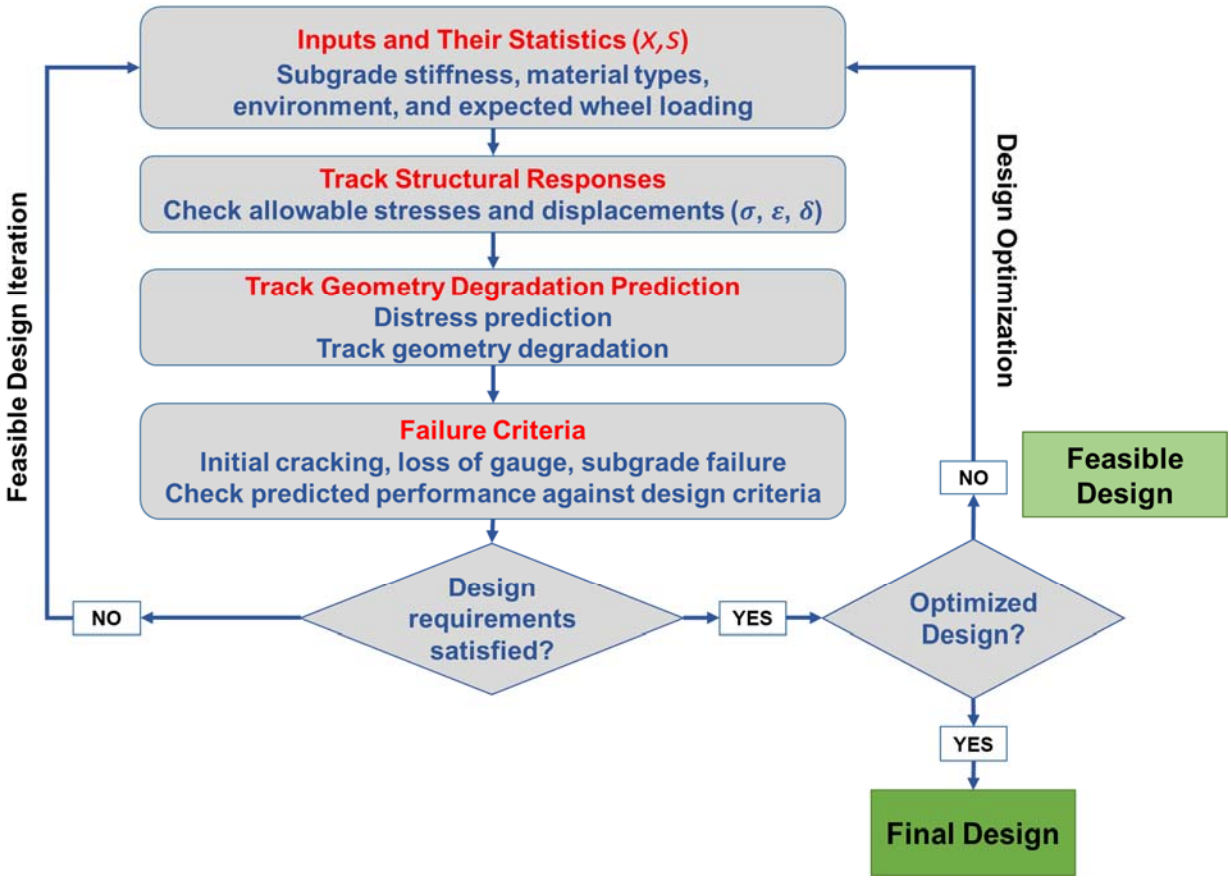

Figure 1.6: Proposed framework for application of mechanistic-empirical design to railroad track infrastructure.

If the sole criteria for the success of a given design is whether or not it will function over its intended life cycle, it is simple to generate a feasible design solution. However, the inclusion of methods for optimization such as structural reliability analysis or other probabilistic procedures is critical to obtaining economic design solutions. Such a procedure can incorporate prior allowable stress procedures for designing track components such as those proposed by Kerr (2003) to evaluate design alternatives. Finally, the method should consider the design of the

track substructure beneath the crosstie, and the interaction of the track substructure and superstructure. When fully implemented, this design procedure will facilitate the life cycle estimation of track and its individual components.

1.8 Mechanistic Response Quantification and Design of Concrete Crossties

My dissertation will focus on the process of collecting loads and bending moments (the mechanistic component), because this is of greater importance in establishing a mechanistic design process. It is also the most feasible element of a proposed mechanistic-empirical process to integrate with current static design procedures. Given that what is actually being studied are concrete crosstie flexural "responses" and the factors that influence them, I will adopt the term *Mechanistic Response* for the work described in my dissertation. This research is important because the response of components must be well understood before inferences can be made as to how they should be designed. A discussion of design based on the quantified mechanistic responses quantified is included in Chapter 6; however, the empirical portion of mechanistic design relating to degradation mechanisms or rates is outside the scope of this discussion.

The application of mechanistic response quantification for a component within the track structure should be done with care, given that track is a system of interconnected, interacting parts that must function together (Hay, 1982; Kerr, 2003). Nevertheless, it is important to consider the application of a mechanistic design approach by starting at a component level, to avoid system-level complexities that are of secondary concern at this stage.

If we envision a continuum between traditional iterative (empirical) design and purely mechanistic design, Figure 1.7 shows the relative position of current concrete crosstie design standards and an ideal solution that should be the objective of future research.

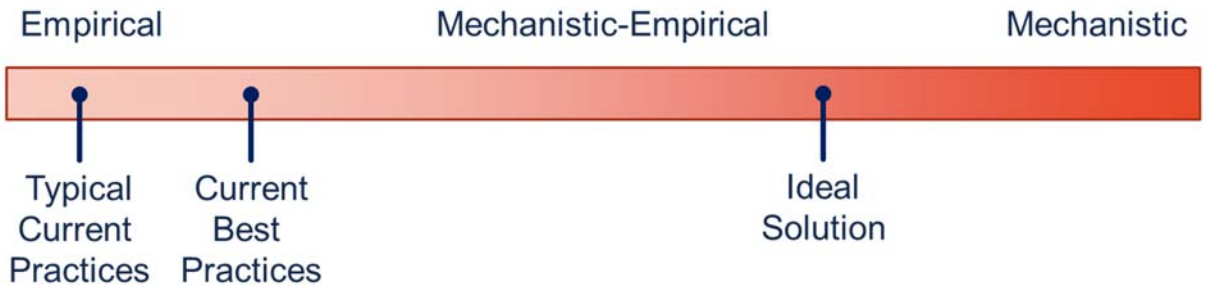

Figure 1.7: Flow chart representation of the application of mechanistic response and design to rail engineering in the context of concrete crossties.

1.9 Research Scope

My research addresses the above questions in the context of both United States rail transit and HAL freight railroad applications. Rail transit applications were given priority in this research because of the relative paucity of rail transit infrastructure research compared to HAL freight infrastructure. Furthermore, the use of different modes including light, heavy, and commuter rail transit and HAL freight provides a much broader range of loads thereby facilitating more robust statistical approaches. Light, heavy, and commuter rail are categorized below using definitions from the American Public Transportation Association (APTA) (2019). Their typical static wheel loads are discussed in Chapter 3.

- **Commuter Rail** is a mode of transit service characterized by an electric or diesel propelled railway for urban passenger train service consisting of local short distance travel operating between a central city and adjacent suburbs.
- **Heavy Rail** is a mode of transit service (also called metro, subway, rapid transit, or rapid rail) operating on an electric railway with the capacity for a heavy volume of traffic. It is characterized by high speed and rapid acceleration passenger rail cars operating singly or in multi-car trains on fixed rails; separate rights-of-way from which all other vehicular and foot traffic are excluded; sophisticated signaling, and high platform loading.

- **Light Rail** is a mode of transit service operating passenger rail cars singly (or in short, usually two-car or three-car, trains) on fixed rails in right-of-way that is often separated from other traffic for part or much of the way. Light rail vehicles are typically driven electrically with power being drawn from an overhead electric line.

HAL freight refers to typical North American freight railroad rolling stock in unrestricted interchange. A commonly referenced freight car used for track component design has a gross rail load of 286,000 lbs., corresponding to a wheel load of 35,750 lbs.

The varying operational environments within rail transit, and between rail transit and HAL freight (Table 1.4), illustrate non-linear elements of crosstie flexural behavior and the varying levels of reserve flexural capacity. These in turn suggest the need for design optimization. Additional differences in HAL freight and rail transit also include typical maintenance practices, the number of unique track component designs, and existing instrumentation installed in track that may be of use to researchers (Table 1.4).

Table 1.4: Comparison of HAL freight and rail transit attributes

HAL Freight	Rail Transit
Established research and findings	Limited infrastructure research
Very heterogeneous fleet in unrestricted interchange throughout network	Homogeneous fleet in closed systems
Performance-based wheel maintenance	Mileage-based wheel maintenance
Extensive field instrumentation (WILDs)	Relatively little field instrumentation
Few crosstie designs	Many crosstie designs
Crossties designed by manufacturers, based on guidance from railroads	Limited transit agency involvement in design process, largely engineering firms
Tamping cycle is tonnage-based or driven by geometry deviations	Maintenance due to poor support or geometry deviations is rarely required

1.10 Objective

The objective of my research is development of a general approach to mechanistic response (demand) quantification for railway track infrastructure components with a particular focus on its application to prestressed, precast concrete crossties. This research advances our fundamental understanding of the mechanistic performance of concrete railway crossties by quantifying their response to load. Specifically, I quantify the relationships between revenue service flexural performance (i.e. demand) and flexural rigidity of crossties (i.e. capacity). Achieving these objectives provides a framework and case study of design to be undertaken using mechanistic response values based on structural reliability analysis (SRA) methods rooted in probabilistic design.

1.11 Scope and Research Questions

Within this dissertation I answer the following questions:

- Can a surface-mounted, non-destructive instrumentation technique be developed and implemented to reliably capture concrete crosstie field bending moments over long durations in a variety of different rail transport modes?
- Given that input loads are critical to the estimation of flexural demands, what loads are induced by rail transit vehicles, and can these loads be represented using standard distributions? How do these impact factors differ from HAL freight, and how will they influence the design of concrete crossties for rail transit applications?
- How do rail transit concrete crosstie bending moments compare to current crosstie flexural capacities? How do these values vary from crosstie-to-crosstie, and between rail transit modes?

- Which factors influence the bending moment demand for concrete crossties (e.g. temperature gradient, axle location, train speed, vertical axle load, etc.)? Are these factors similar in terms of their relative effect among a variety of rail modes? Can a model be generated to accurately predict crosstie center bending moments?
- Using mechanistic response data, what is the optimal design for a crosstie considering a probabilistic design method based on SRA principals that consider moment demand, variability in materials, etc.?

1.12 Dissertation Structure

The structure of this dissertation (Figure 1.8) generally follows the mechanistic response and design process as applied to concrete crossties (introduced in Sections 1.6 through 1.8). It consists of the development of a method to quantify crosstie bending moments, quantification of input loads at the wheel-rail interface, application of the methods, and proposes a design optimization method that considers the field data and probabilistic distributions for crosstie capacity.

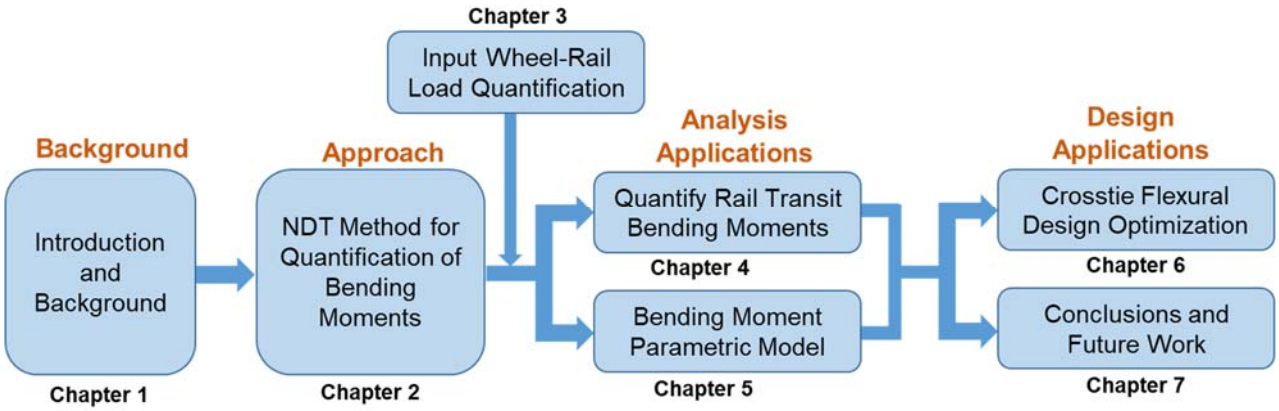

Figure 1.8: Structure of dissertation chapters.

Additionally, I organized my dissertation chapters to achieve the initial steps toward quantification of concrete crosstie inputs needed for a mechanistic-empirical design process as proposed in Section 1.7. The manner in which they map to the steps in the mechanistic-empirical design process is shown in Figure 1.9. The only step of the proposed mechanistic-empirical design process that is not addressed in my dissertation is the prediction of distress predication and track geometry degradation. I discuss next steps and research needs related to track distress prediction in Section 7.1.6.

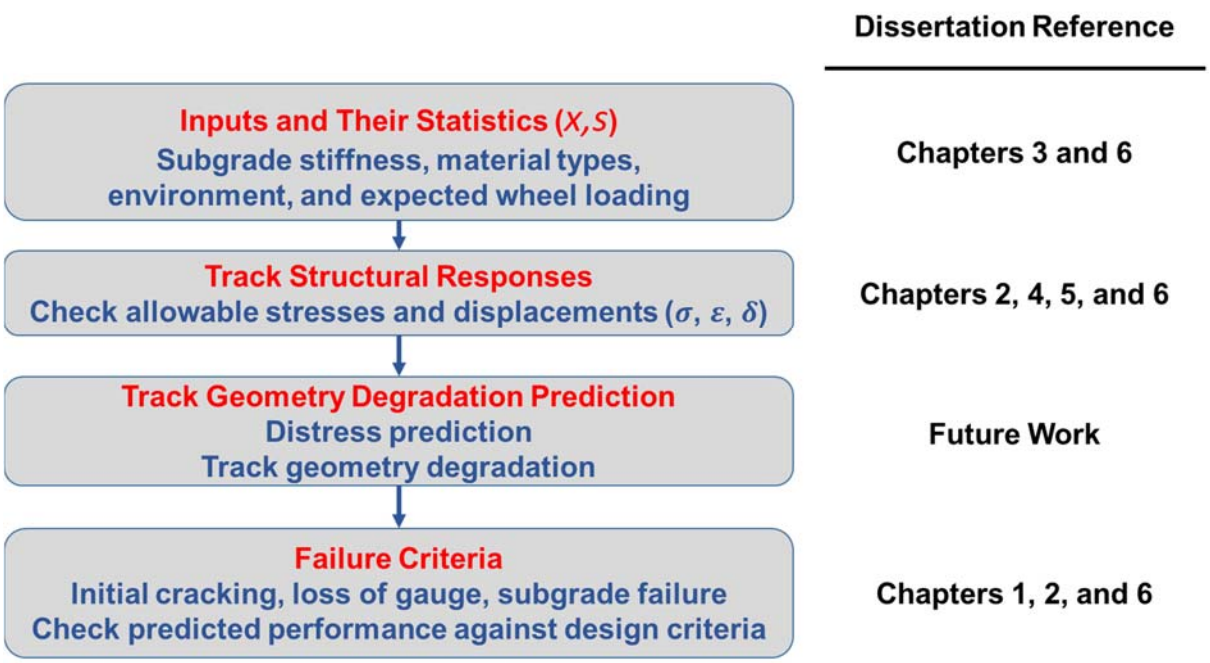

Figure 1.9: Connection between dissertation chapters and elements of proposed framework for mechanistic-empirical design of railroad track infrastructure components.

Chapter 2 begins with additional background on previous concrete crosstie flexural performance research and provides a detailed explanation of the proposed methodology. The chapter also includes examples of crosstie flexural performance data to illustrate the validity of the methodology and a range of questions that can be addressed.

Chapter 3 provides quantification of input loads for rail transit, as measured at the wheel-rail interface, over a one-year period. Methods of modeling the distribution of loads at field sites on light and heavy rail transit infrastructure are developed as they relate to the input loads required to interpret or obtain crosstie bending moments.

Chapter 4 includes a case study of light and heavy rail transit crosstie bending moments, to understand the variability for each mode, and how they relate to existing crosstie design capacities for the two modes. The chapter then expands upon the methodology described in Chapter 2, and provides a means of applying the method to different rail transit modes to incorporate factors related to seasonal effects, crosstie support condition variation, and axle location (leading vs. trailing).

Chapter 5 describes development of a multivariate regression model for center bending moments (i.e. response variable) for concrete crossties, taking into consideration a variety of predictor variables. Regression models are developed for both rail transit and HAL freight applications, and predictor variables and their significance evaluated to determine how much error they explain for each mode.

Chapter 6 presents a method for optimization of concrete crosstie design by taking into consideration the field bending moment data and a probabilistic approach to design that considers a level of assumed risk. SRA concepts are also employed to improve the robustness of the process and map to conventional structural design processes.

Chapter 7 summarizes the principal findings of this dissertation, its contributions to the research and practitioner communities, advancements to the development of a mechanistic design process for track components, and suggests topics warranting future research.

CHAPTER 2: QUANTIFICATION OF CONCRETE RAILWAY CROSSTIE BENDING MOMENTS USING SURFACE STRAIN GAUGES

2.1 Background and Methodology

In this chapter I introduce a novel methodology for the quantification of concrete crosstie flexural demand using a non-destructive and non-intrusive approach. The method consists of mapping surface strains collected under revenue service operations to bending moments generated through analytical calculations or laboratory calibration.

2.1.1 Prior Approaches to Flexural Demand Quantification

An international review of prior instrumentation and experimental efforts aimed at quantifying in-field revenue service concrete crosstie bending moments revealed a limited number of deployments. The projects identified used either embedded or surface strain gauges (Venuti, 1970; Prause et al., 1977; Venuti, 1990; Mayville et al., 2014; Kerokoski et al., 2016; Edwards et al., 2017a), or fiber optic sensors (Consolis, 2017). Most of the instrumentation was deployed at either the proof-of-concept level or in a temporary manner. A drawback to embedded strain gauge methods is the need to cast gauges into the crosstie during the manufacturing process. This limits the breadth of use, and eliminates the option of conducting experimentation on existing crossties installed in track.

Protecting gauges is important using either embedded or surface methods given the demanding loading and environmental conditions encountered in revenue service railroad track (Edwards et al., 2017a, 2017b). While using surface-deployed instrumentation, Venuti (1990) documented interference related to signal noise and post processing of the data that were not

easily overcome. These problems must be overcome to ensure that reliable information is obtained from the data collected.

2.1.2 Proposed Instrumentation Technology

Given manufacturing and breadth-of-use limitations to embedded strain gauging, and that concrete surface strain gauging has proven reliable in other applications (Yu et al., 1998; Roesler and Barenberg, 1999; Chen et al., 2013; Cheng et al., 2014), this method was chosen to instrument several large-scale, field research projects at the University of Illinois at Urbana-Champaign (UIUC) (Wolf et al., 2014; Wolf et al., 2015; Wolf, 2015; Gao et al., 2016; Wolf et al., 2016a). Strain gauges are versatile instrumentation hardware that were used as early as the 1940s (Hannah and Reed, 1992; Window, 1992) and have long been used to monitor the performance of transportation facilities (Khan and Wang, 2001). They have also been used for numerous railway engineering applications (Venuti, 1970; Venuti, 1990; Stratman et al., 2007; Yang et al., 2008; Mayville et al., 2014; Cortis et al., 2017).

Building on the aforementioned experience, I selected 120-ohm strain gauges of type PFL-30-11-3LT from Texas Measurements (Vishay Micro-Measurements, 2015b). This type of strain gauge (Figure 2.1) is specifically designed for use with concrete materials, based on information obtained from the manufacturer (TML, 2017).

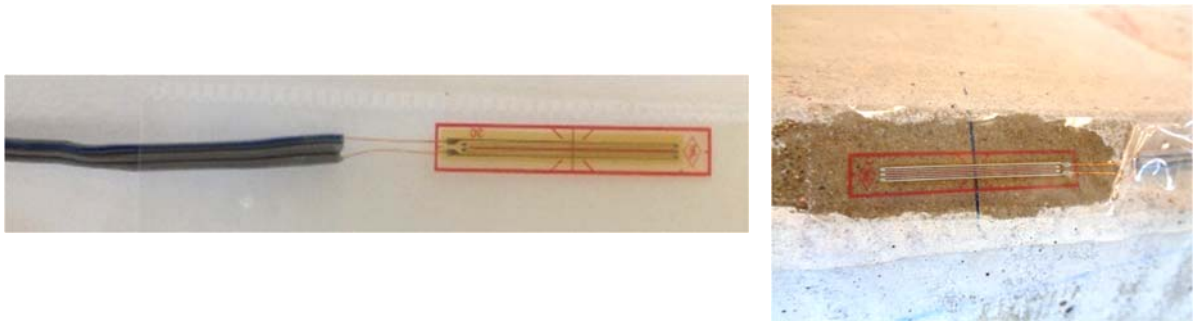

Figure 2.1: Standard 120-Ohm concrete strain gauge before (left) and after (right) installation on concrete crosstie (Wolf, 2015b).

Longer gauges are recommended for heterogeneous specimens such as concrete, because the gauge will span the disparate elements of the specimen under investigation (HBM, 2017). In this particular case, the length of the gauge (1.2 in [30 mm]) allows it to span multiple pieces of aggregate and sections of mortar paste within the concrete element, thus the strain being reported is an average strain, rather than a localized strain in a piece of aggregate or section of mortar paste (Vishay Micro-Measurements, 2015b). For reference, the typical maximum size for concrete crosstie coarse aggregate is around 0.4 in (10 mm), which is approximately 1/3rd of the strain gauge length.

There are, however, limitations to using surface strain gauges on concrete materials. One is the ability to accurately measure strain across cracks that open after the surface strain gauge is installed (Roesler and Barenberg, 1999). If the first-crack capacity of the object in question is likely to be exceeded during testing, another instrumentation type (e.g. crack opening gauges, digital image correlation [DIC], etc.) should be considered. For the range of strains expected in concrete crossties for this research, which was in the linear-elastic range, cracking of specimens was not expected.

Data from strain gauges were collected using the National Instruments (NI) compact data acquisition system (cDAQ), which provided compact and reliable hardware that would perform in a robust manner in the demanding field environment (Figure 2.2) (Wolf, 2015a; National Instruments, 2017).

Figure 2.2: Compact Data Acquisition (cDAQ) chassis with interchangeable modules (National Instruments, 2017).

The instrumentation setup was designed to be temperature compensating to minimize error due to temperature fluctuations from direct sunlight, shading from passing trains, and seasonal climate conditions. Pilot projects conducted in both laboratory and field settings used this instrumentation technology, and it was both cost effective and reliable (Wolf, 2015a; Edwards et al., 2017a). cDAQ output signals from instrumentation were recorded through a NI LabVIEW virtual instrument (VI) developed for the site-specific instrumentation associated with this experimental program (e.g. varied number of channels, data acquisition rate, number of modules, etc.).

Shielded wiring was used to minimize electrical interference and "cross talk" between the various channels of data being collected. Expert opinion and findings from prior research (Venuti, 1990) has also indicated that this is especially critical in an environment that involves use of electrified propulsion systems to avoid the effect of stray currents that are present in most light and heavy rail transit systems.

A minimum sampling rate was determined based on the maximum authorized train speed at each field experimentation location and the desired data sampling resolution, where the

resolution is the distance the train travels between consecutive samples. The desired sampling resolution for the example heavy axle load (HAL) freight railroad application discussed in this chapter was 12.7 mm (0.5 inches). Based on these requirements, prior experience, and expert recommendation, the sampling rate was set at 2,000 Hertz.

Prior experience and documentation from manufacturers (Vishay Micro-Measurements, 2015a) has also shown the importance of providing adequate protection for the strain gauges. This is especially important given the demanding field environment in which they are expected to perform reliably over long periods of time and accumulated gross tonnage of rail traffic. As such, a protection plan was implemented for each strain gauge placed on the concrete crossties (Figure 2.3, Table 2.1).

Of particular importance is the type of epoxy used to ensure that its expansion and contraction characteristics did not interfere with the data collection process. Devcon 2-Ton® clear epoxy was found to be the best option given that it had thermal expansion properties similar to the concrete substrate.

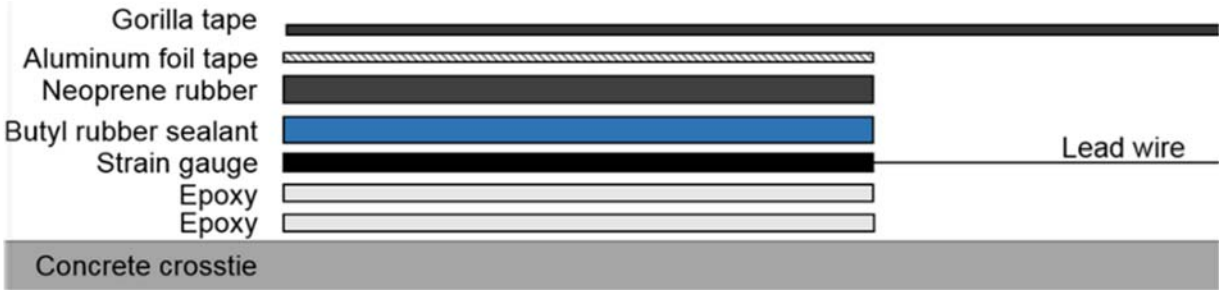

Figure 2.3: Concrete surface strain gauge protection plan (Wolf, 2015a).

Table 2.1: Explanation of strain gauge protection plan layers (Wolf, 2015a)

Layer	Description	Purpose
Epoxy (Bottom)	Two-part epoxy, applied in two coats: primer and secondary	Primer coat bonds with concrete surface and provides smooth surface to mount gauge, secondary coat bonds strain gauge to primer
Strain gauge	Sensor that measures change in resistance caused by induced strains	Measures the change in strain experienced by the concrete under an applied load
Butyl rubber sealant	Sticky rubber layer	Provides moisture and mechanical protection for gauge
Neoprene rubber	Harder, stiffer rubber layer	Provides mechanical protection for gauge
Aluminum foil tape	Reflective tape layer	Provides moisture protection to gauge and holds all lower protection layers in place
Lead wire	Three-wire insulated bundled wire	Transmits strain signal recorded by gauge to data acquisition
Gorilla Tape® (Top)	Resilient tape layer	Holds all lower protection layers in place

2.1.3 Instrumentation Deployment on Crosstie

In order to quantify the flexural behavior of the crosstie under load, bending strains were measured at critical locations along the length of the crosstie. Concrete surface strain gauges were applied oriented longitudinally along the chamfer near the top surface of the crosstie. For some of the crossties at each field-testing location, five strain gauges (labeled A – E) were applied, with one at each of the two rail seats, one at the center, and another located approximately halfway between each rail seat and the crosstie center (Figure 2.4). The initial locations for the gauges were developed and documented by Wolf (2015).

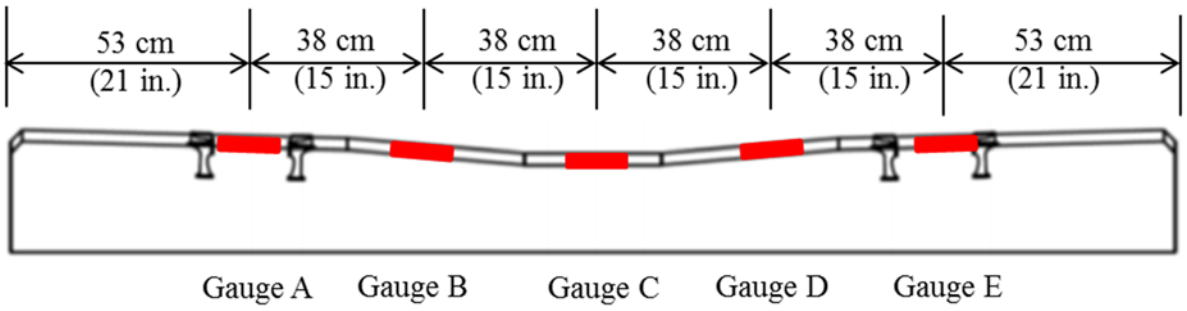

Figure 2.4: Profile view of crosstie showing locations of strain gauges (Wolf, 2015a).

Given the comparatively greater importance of capturing the center and rail seat bending moments, additional crossties at each site were instrumented with strain gauges only at locations A, C, and E. The dimensions shown in Figure 2.4 account for a specific instrumented crosstie with a total length of 102 in. (258 cm), a common crosstie type used in the United States on HAL freight railroads. Images of instrumented crossties in the field with fully protected gages can be seen in Figure 2.5.

The most critical locations in terms of analyzing the flexural service demands on the crosstie are the crosstie center (Gauge C) and rail seat (Gauges A and E). To relate the measured strains to bending moments, calibration factors were determined using two methods that are discussed in the next section.

Figure 2.5: Images of crossties instrumented with concrete surface strain gauges at a heavy-haul freight railroad field experimentation location.

2.1.4 Interpretation of Data and Generation of Results

Measured crosstie strains from field sites and revenue service loading conditions must be correlated to bending moments using factors that are generated by one of three methods:

1) use of a calibration constant from calculations based on known crosstie sectional geometries and concrete properties, 2) generating laboratory calibration curves by applying known moments under controlled experiments (i.e. loading conditions and support configurations), or

3) calibrating each crosstie while they are installed in track. The latter method, while documented in the literature (Mayville et al., 2014), was deemed impractical for my purposes given the number of required field sites and individual crossties that would be instrumented, and

the safety and operational constraints of working in an active railway environment. The former two methods are discussed in greater detail in the following sub-sections.

2.1.4.1 Laboratory Calibration

Laboratory calibration was conducted using the Static Tie Tester (STT) (Figure 2.6) at UIUC's Research and Innovation Laboratory (RAIL) in the Harry Schnabel Jr. Building in Champaign, IL. The STT can apply known loads to test the flexural and/or compressive behavior of concrete crossties. The STT uses a hydraulic cylinder to apply loads to the rail seat or center of a crosstie up to approximately 100,000 lbf (4,450 kN). A calibrated load cell is used to monitor the applied loads to relate strain and bending moments.

Figure 2.6: Static Tie Tester (STT) at UIUC used for laboratory calibration of concrete crossties.

Calibration of surface strain gauges requires a crosstie of the same design, strength, and approximate age (to represent overall manufacturing processes at the time) to be instrumented with surface strain gauges using the procedure described above, and then subjected to a known

applied bending moment. Laboratory calibration included rail seat positive and negative bending tests and crosstie center positive and negative bending tests. Moments were applied by loading the crosstie using pre-established procedures outlined in Sections 4.9.1.4 and 4.9.1.6 of the AREMA Manual (2016). These procedures specify placement of supports and equations for determining the moment induced in the crosstie from the load applied. Load and strain data were collected throughout the test so that I could determine the relationship between strain and moment for each crosstie. Tests were performed on the rail seat and center sections of each crosstie (Figures 2.7 and 2.8).

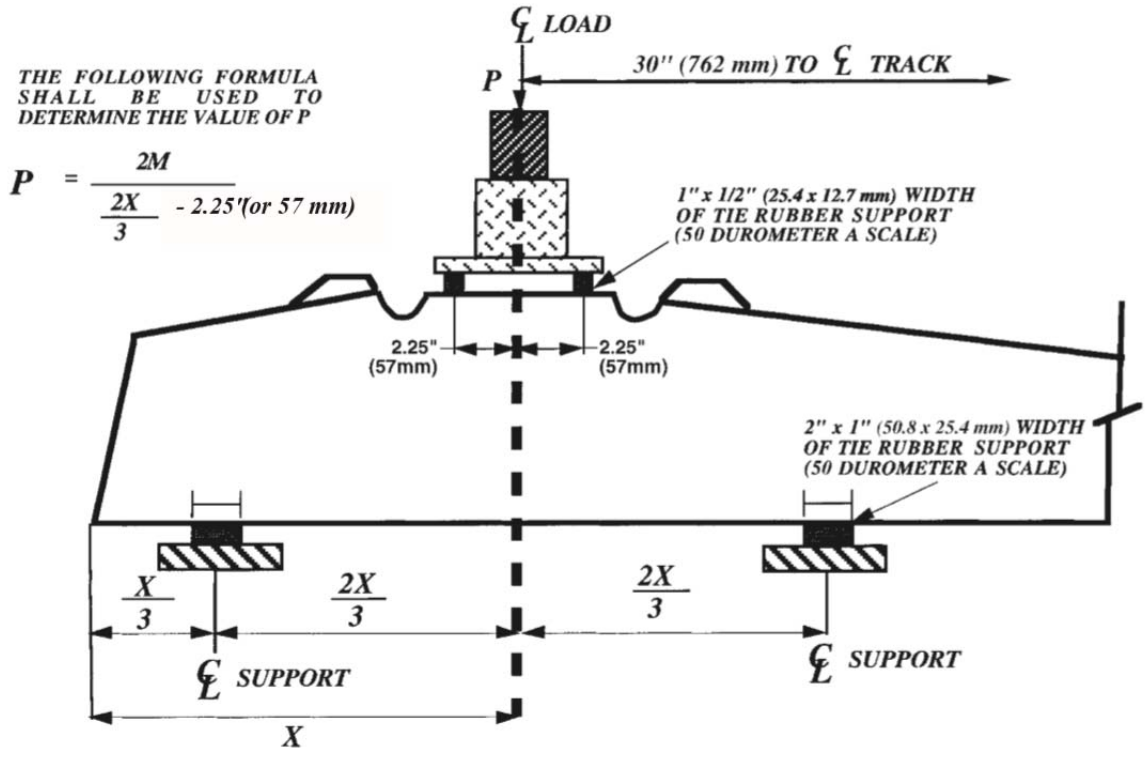

Figure 2.7: Rail seat positive bending moment test protocol used for laboratory calibration of concrete crossties (AREMA, 2016).

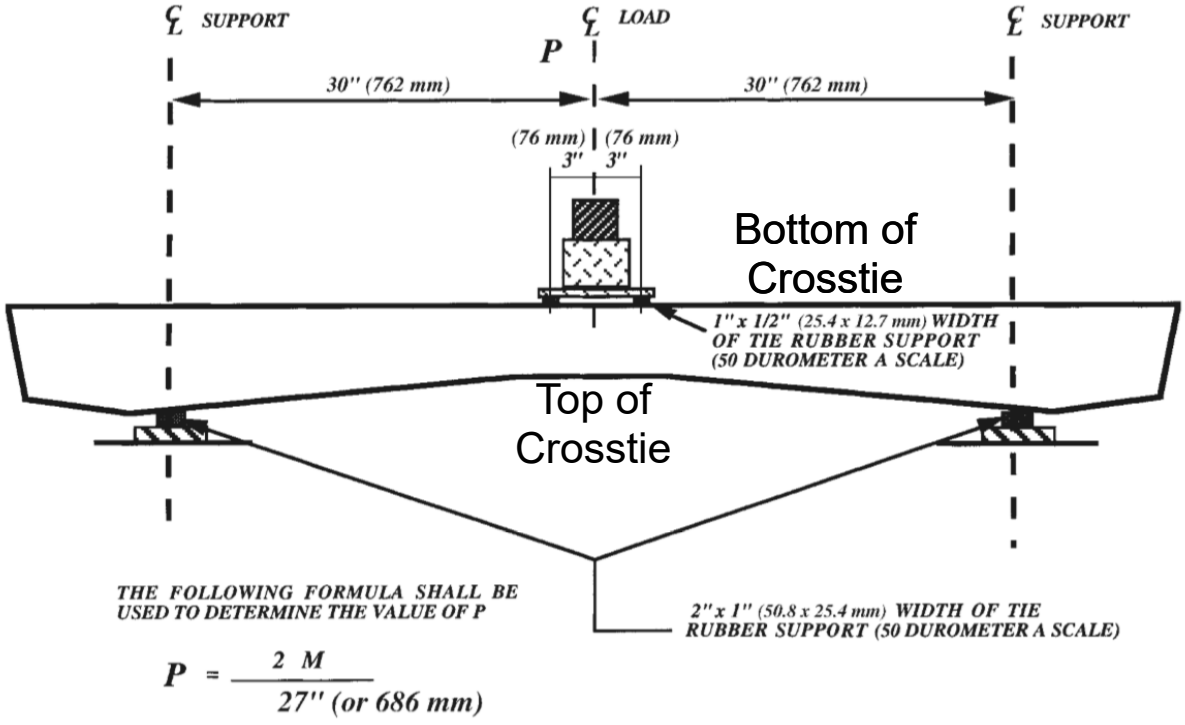

Figure 2.8: Center negative bending moment test protocol used for laboratory calibration of concrete crossties (AREMA, 2016).

These procedures specify placement of supports and equations to be used to determine the moment induced in the crosstie from the load applied. As was the case with the rail seat, load and strain data were collected throughout the test to determine the relationship between strain and moment for each crosstie.

The calibration process uses the relationship described in Equation 2.1 to relate a known bending moment to the concrete crosstie's sectional properties and response to load:

$$M_s = \frac{\varepsilon_s E_c I_s}{d_s} \tag{2.1}$$

Where:
M_s is the crosstie bending moment at section "s", kip-in (kNm)
ε_s is the strain measurement from the surface strain gauge at section "s", in/in (mm/mm)

E_c is the elastic modulus of the concrete, psi (kPa)
I_s is the moment of inertia at section "s", in^4 (mm^4)
d_s is the distance from the surface strain gauge to the neutral axis of bending of the crosstie at section "s", in. (mm)

Section "s" refers to the cross-section of the crosstie where the strain gauge is located, which must be consistent between the calibration crosstie and the test crosstie in the field. The terms E_c, I_s, and d_s are unique to the crosstie and are determined in an aggregate fashion through laboratory calibration. For the experimentation that will be described in this chapter to illustrate the measurement technique, the laboratory calibration factors were found to be 790,928 kip-in/ε (89,363 kNm/ε), 684,533 kip-in/ε (77,342 kNm/ε), and 591,921 kip-in/ε (66,878 kNm/ε) for Gauges A and E, Gauges B and D, and Gauge C, respectively.

Rail seat gauges were calibrated during the rail seat positive bending moment test (Figure 2.7) and center and intermediate gauges were calibrated during the center negative bending moment test (Figure 2.8). In order to minimize error and reduce variability, it was determined that three replicates of each calibration test should be conducted on each crosstie, and three crossties of each design and age were tested, for a total of 9 tests. Calibration loads were calculated such that the first crack design capacity of the crosstie as described by AREMA (2016) would not be exceeded. Specifications used for calibration of both types of concrete crossties discussed in this chapter can be found in Table 2.2.

Table 2.2: Geometric and prestress orientation properties required for calibration of concrete crossties used in example rail transit and HAL freight railroad applications

Location	Property	Rail Transit		Class I Freight	
Overall	Length	8.5 ft	2.6 m	8.5 ft	2.6 m
	x-Value	21.0 in	53.3 cm	21.0 in	53.3 cm
Center	Depth	6.8 in	17.1 cm	6.8 in	17.1 cm
	Top Width	8.4 in	21.4 cm	9.0 in	22.9 cm
	Bottom Width	10.5 in	26.7 cm	11.0 in	27.9 cm
	Eccentricity	-0.4 in	-1.0 cm	0.3 in	0.8 cm
Rail Seat	Depth	8.56 in	21.8 cm	8.8 in	22.2 cm
	Top Width	8.44 in	21.4 cm	9.0 in	22.9 cm
	Bottom Width	10.5 in	26.7 cm	11.0 in	27.9 cm
	Eccentricity	0.459 in	1.2 cm	0.6 in	1.5 cm

An example of the laboratory calibration curves can be found in Figure 2.9. The points represent the laboratory data recorded during a crosstie center gauge calibration, and the blue dashed line corresponds to the linear best fit of the laboratory data. The slope of the dashed line is the laboratory calibration factor for the concrete crosstie center gauge and was calculated to be 492,620.3 kip-in/ε (55,658.6 kNm/ε).

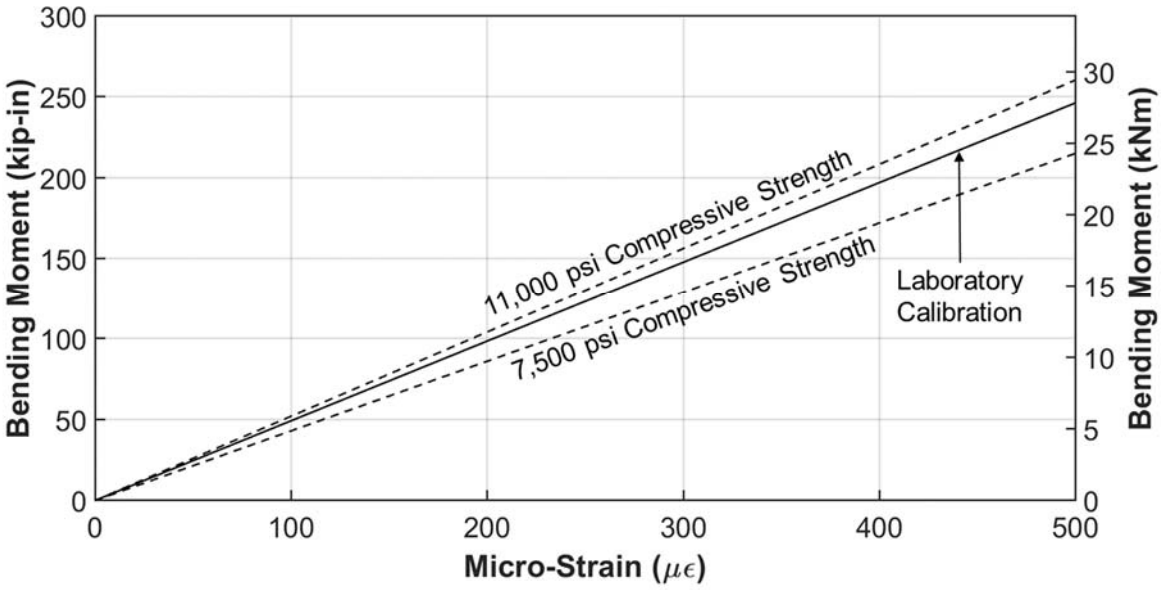

Figure 2.9: Comparison of data from concrete crosstie center calibration in the laboratory (red scattered points) and analytical calculations (black lines) for a HAL freight crosstie.

The laboratory experimentation enabled me to determine the adequacy and accuracy of strain gauge placement, thereby addressing the question of whether a strain gauge located on the chamfer of the rail seat (compression side) of the crosstie could reliably capture rail seat positive bending. Results demonstrated that gauges could accurately be placed at either top or bottom to capture bending strain, with clear advantages of placement on the top surface in the field due to accessibility. This is also consistent with fundamental mechanics given the linear nature of the strain profile discussed in Chapter 1.

2.1.4.2 Analytical Calculations Using Fundamental Equations

As shown in Equation 2.1, the calibration factor is defined as $\frac{E_c I_s}{d_s}$, in which all of the terms can be calculated taking into account the geometric properties of the crosstie, the effect of prestressing the concrete, and the concrete material properties. Given that the crosstie's cross-section was simplified as an isosceles trapezoid (Figure 2.10), I_s was computed using Equation 2.2. The effects of prestress, including the prestress force magnitude and the location and layout of the prestressing strands, were taken into consideration by eccentricity, which was defined as the distance between the center of gravity of the prestress wires and the neutral axis of the section. The neutral axis is higher than the center of gravity (Figure 2.10), indicating a negative eccentricity, which is typical of rail seat geometry and prestress configuration. However, the neutral axis can be lower than the center of gravity, creating a positive eccentricity, which is often the case at the crosstie center.

$$I_s = \frac{{h_s}^3({a_s}^2 + 4a_s b_s + {b_s}^2)}{36(a_s + b_s)} + {e_s}^2\left[\frac{h_s(a_s + b_s)}{2} + \left(\frac{E_{ps}}{E_c} - 1\right)A_{ps}\right] \qquad (2.2)$$

Where,
a_s is the top width at section "s", in. (mm)

b_s is the bottom width at section "s", in. (mm)
h_s is the total depth at section "s", in. (mm)
e_s is the eccentricity at section "s", in. (mm)
E_{ps} is the elastic modulus of the prestressing strands, psi (kPa)
E_c is the elastic modulus of the concrete, psi (kPa)
A_{ps} is the area of prestressing strands at section "s", in^2 (mm^2)

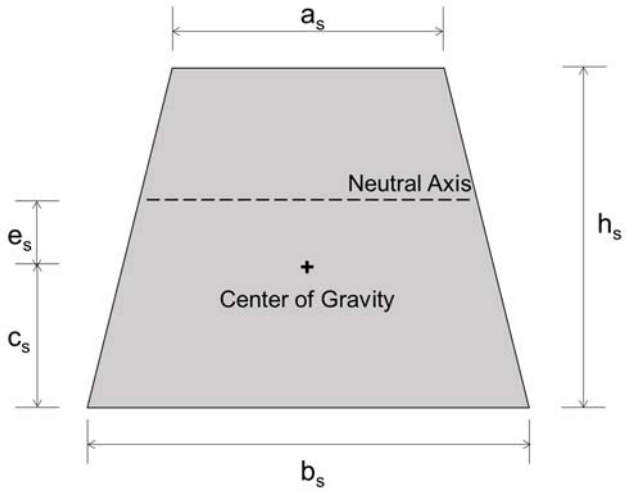

Figure 2.10: Schematic showing example concrete crosstie cross-sectional view and location of critical sectional elements.

In order to calculate d_s, the location of the center of gravity was first determined based on the geometric properties of the crossties (Equation 2.3). Next, d_s was determined using Equation 2.4 in which the eccentricity was included in the computation.

$$c_s = \frac{h_s}{3}\left(\frac{2a_s + b_s}{a_s + b_s}\right) \tag{2.3}$$

Where c_s is the height of the center of gravity at section "s", in. (m).

$$d_s = h_s + e_s - c_s - g_s \tag{2.4}$$

g_s is the vertical distance between the horizontal centerline of the surface strain gauge and the top of the crosstie at section "s", in. (m).

Concrete compressive strength and concrete unit weight were both considered in the calculation of E_c (Equation 2.5). Conversations with United States crosstie suppliers led us to bound the expected range of concrete compressive strengths to a minimum of 7,500 psi (51,711 kPa) and a maximum of 11,000 psi (75,842 kPa).

$$E_c = 0.043 w_c^{1.5} \sqrt{f'_c} \qquad (2.5)$$

Where,
w_c is the unit weight of the concrete (kg/m^3) and
f'_c is the concrete compressive strength (MPa).

After obtaining the sectional properties, the eccentricity, and the concrete weight, the calibration factor for the crosstie center was calculated to be 430,232 kip-in/ε (48,610 kNm/ε) at the minimum concrete compressive strength, and 520,840 kip-in/ε (58,847 kNm/ε) at the maximum compressive strength. The range of the calibration factors was depicted as the area between the two solid black lines in Figure 2.9. The calibration factor obtained in the laboratory was located at the upper portion of the range, indicating that the concrete compressive strengths of the instrumented crossties were closer to the maximum expected value.

Given that the instrumented crossties had previously been in service for several years before they were taken out of the track for this project (Figure 2.4), and concrete compressive strength increases over time (Mindess et al., 2003), it was reasonable that the results obtained from laboratory and hand calculation methods would be consistent. The interpretation of field bending moment results introduced in subsequent sections in this chapter use laboratory calibrations generated using the procedure referenced in this section.

2.2 Field Deployment

2.2.1 Example Field Instrumentation Deployment

Between 2015 and 2017, seven field deployments using this technology were installed throughout the United States to answer a variety of questions requiring quantification of field concrete crosstie bending moments. To demonstrate the instrumentation methodology and repeatability of results, this chapter includes example data related to the quantification of bending moments for assessing crosstie-to-crosstie variability. Quantifying bending moment variability is a critical step in the development of future mechanistic recommendations (Van Dyk et al., 2013) for concrete crosstie flexural design.

The specific field instrumentation discussed in this dissertation was conducted on a ballasted HAL freight railroad line in the western United States. Because of the high variability of support conditions observed in past field tests (Edwards et al., 2017a), instrumentation was placed in two locations, or "zones," of tangent (i.e. straight) track, spaced approximately 60 ft. (18.3 m) apart on center (Figure 2.11). Each zone consisted of five concrete crossties, based on the well documented distribution of vertical load to five consecutive crossties (Hay, 1982; Van Dyk, 2014) (Figure 2.11). A complete site of ten crossties was used to address the need for replicate data and provide insight into the variability of support conditions in this specific section of track.

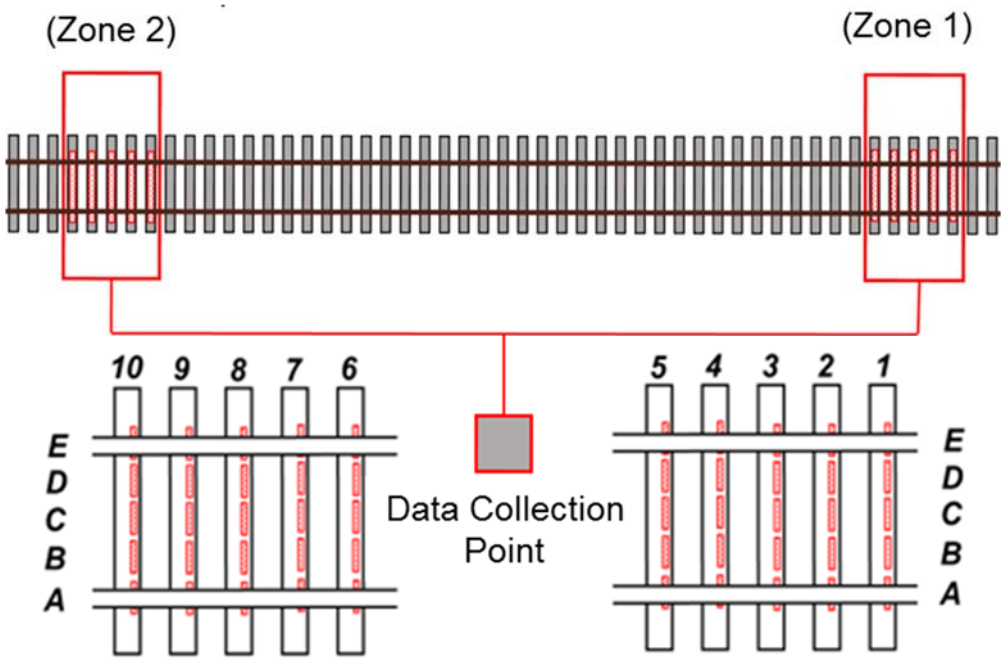

Figure 2.11: Field site layout with ten crossties in two test zones (Wolf, 2015a).

2.3 Data Analysis

To quantify the bending moments concrete crossties experience in revenue service, peaks in the strain gauge signal caused by crosstie bending due to a wheel or axle load were extracted from the data stream collected at 2,000 Hertz. This was accomplished using the "findpeaks" function in MATLAB (2012). To improve the performance of this function for this application, several of the built-in options were used, and additional modifications were made to the code that was originally developed by Wolf (2015a). To ensure that the program was recording the true peaks, as opposed to false peaks that did not represent the extreme strain reading for a given axle pass, a minimum spacing (MinPeakDistance) between the peaks was specified and a minimum value (MinPeakHeight) for all peaks was set. Before peaks were obtained, the strain signal was zeroed using data captured before the arrival of the lead axle on the first locomotive, smoothed using a moving average filter of five data points, and a linear baseline correction was applied to

adjust for any signal drift over the course of a single train pass. Data collection was initiated several seconds prior to the arrival of the lead axle of the first locomotive. This provided a stable zero point for the crosstie under no applied load. Additionally, the data collection was ended several seconds after the final train axle passed to serve as an end point for the baseline correction.

For instrumentation sites with a single train traffic type, the number of axles was a fixed value determined by the car configuration; for other sites, the number of axles was computed using a manually-adjusted "findpeaks" function. When the instrumentation sites were located close to wheel impact load detectors (WILDs) (a separate wayside inspection system used to measure vertical input loads at the wheel rail interface) the total number of axles could be obtained from the WILD data.

The value of "MinPeakDistance" was based on the axle spacing and train speed, whereas the value of "MinPeakHeight" was based on the axle load. Once the number of axles was determined, peaks could be pulled from all the strain gauge signals. The bisection method was implemented to shorten the processing time. For each strain gauge signal, the global maximum value was first obtained. This value was then halved and used as the "MinPeakHeight" in the "findpeaks" function. If the number of axles generated from the function was lower than the actual number, meaning that the "MinPeakHeight" was higher than some peaks, the "MinPeakHeight" would be further halved and used as the new input in the "findpeaks" function. If the number of axles generated from the function was greater than the actual number, indicating that the "MinPeakHeight" was lower than all peaks, the "MinPeakHeight" would be increased by half of its value and executed in the new "findpeaks" function. The iterations would stop once

the output number of axles matched the actual axle count and all peaks were confirmed to have been extracted from the signal.

Figure 2.12 (left vertical axis) shows an example of a typical strain gauge signal for a center gauge. The signal was zeroed and the peaks were numbered in sequence, which were eventually converted into bending moments using the laboratory moment calibration factors mentioned above (Figure 2.12, right vertical axis).

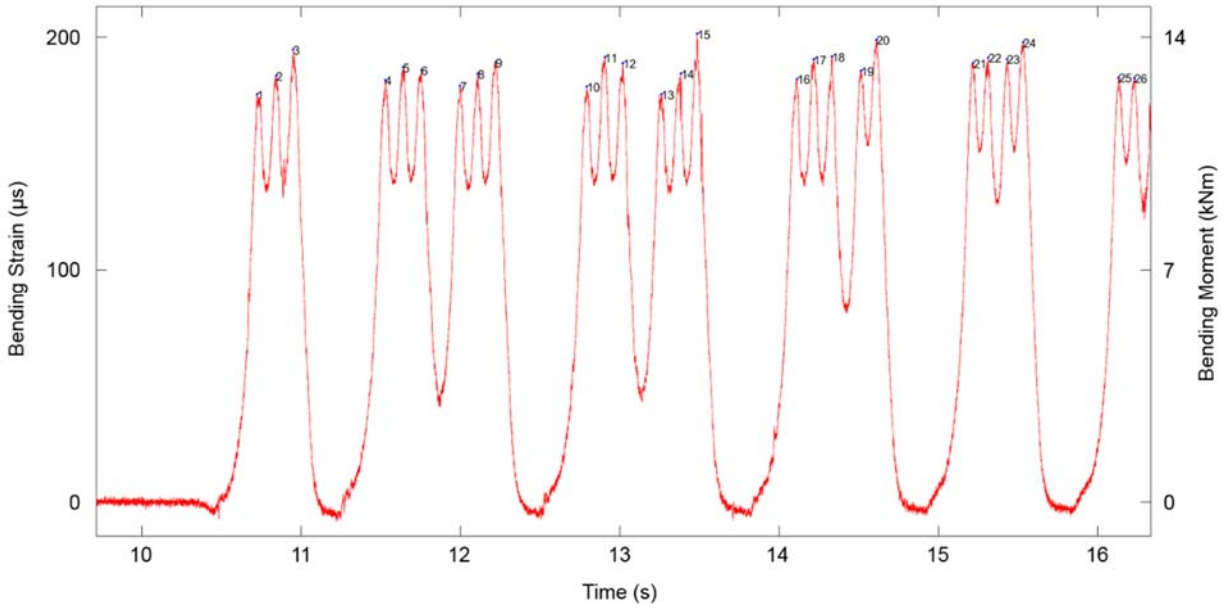

Figure 2.12: Typical crosstie center strain signal and moment captured under the passage of a loaded HAL freight train.

2.4 Results

The instrumentation described in this chapter has proven to be robust, as only one surface strain gauge at this specific HAL freight site has been damaged over of the two-year time frame in which the field site has been operational and there have been no fatigue-related challenges with or failures of the strain gauges. Over the course of the site's functionality approximately 295 million gross tons (MGT) (267 million gross metric tons) of HAL freight traffic was

accumulated by the crossties. The other field sites have experienced similar performance successes in terms of instrumentation robustness, with minimal instrumentation-related failures.

For the purpose of the analysis described in this chapter, a total of 150 train passes containing over 80,000 individual axle passes were collected during the ten-day period from 30 December 2016 to 8 January 2017. I then analyzed the bending moments induced by loaded axles from the signals of the center and rail seat strain gauges (Gauges A, C, and E) mounted on all 10 crossties. The bending moment percent exceeding distribution for the aforementioned 150 trains demonstrate the variability associated with consecutive train passes (Figure 2.13). These distributions are also shown in comparison to the AREMA recommended design limits for both rail seat positive and center negative cracking, effectively showing the moment that would need to be exceeded before a crack propagates to the first line of prestressing steel (AREMA, 2016).

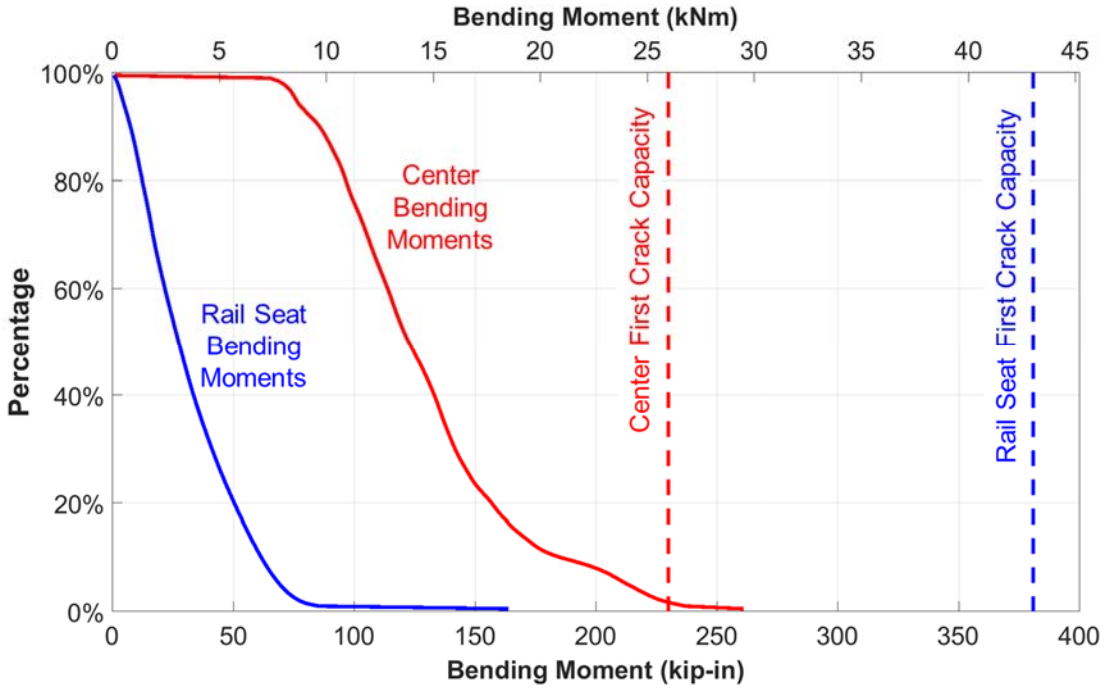

Figure 2.13: Distribution of center and rail seat bending moments for each axle/wheel of all trains captured over a ten-day period in late 2016 and early 2017.

2.4.1 Overview of Measured Bending Moments and Selected Findings

The distribution of the crosstie's average bending moments was largely below the AREMA recommended design limits (indicated by the vertical black dashed lines in Figure 2.13), especially at the rail seats, as their average moment values were less than one-third of the 300 kip-in (33.9 kNm) limit that AREMA recommends for crosstie flexural design (AREMA, 2016). This means that AREMA recommendations might overestimate the flexural demand at the crosstie rail seat section (AREMA, 2016).

Compared to rail seat moments, average center bending moments were closer to the AREMA recommended value of 201 kip-in (22.7 kNm), with the moments for Crosstie 4 exceeding the AREMA recommended value, indicating that center bending could be more demanding than rail seat bending (AREMA, 2016). This agrees with the previous survey, which suggested that center cracking of concrete crossties was more commonly seen in the field (Van Dyk, 2014).

To best visualize the distribution of measured bending moments of each crosstie, box-and-whisker plots were developed for each crosstie (Figure 2.14). The top line of the box represents the 75th percentile bending moment (Q3). The middle line is the median bending moment. The bottom line of the box represents the 25th percentile bending moment (Q1). The interquartile range (IQR), found as Q3 minus Q1, can provide an estimate of the variability of the data set – the greater the IQR, the higher the variability. The upper whisker is the limit for upper outliers, which are defined as data points greater than Q3 plus 1.5 times the IQR. Similarly, the lower whisker is the limit for lower outliers, which are defined as data points smaller than Q1 minus 1.5 times the IQR (or Q1 – 1.5IQR) (Ott and Longnecker, 2008).

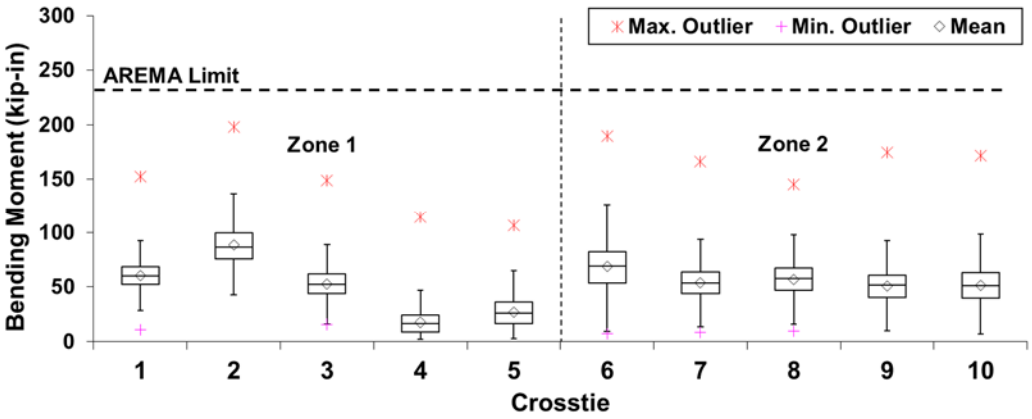

(a) Gauge A - Rail Seat Positive Bending Moment

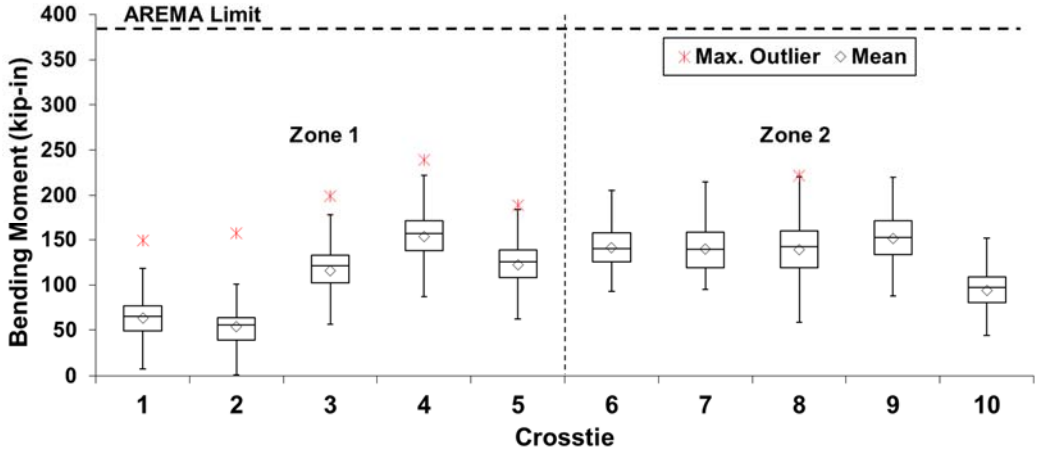

(b) Gauge C - Center Negative Bending Moment

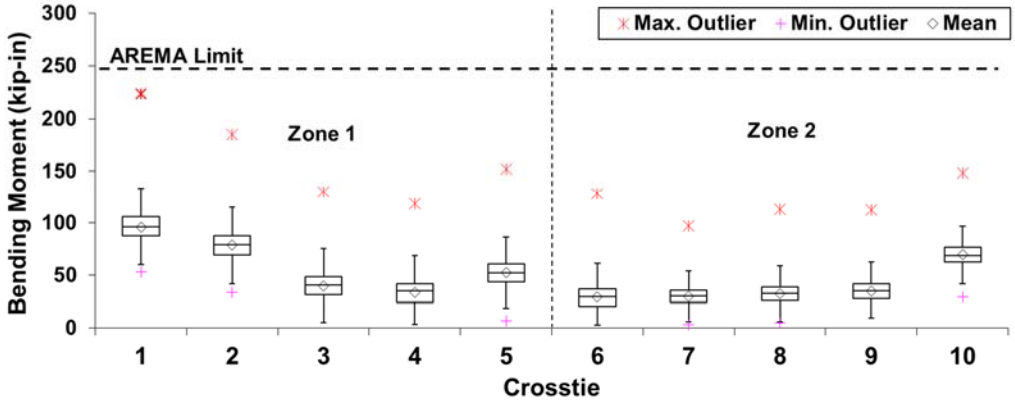

(c) Gauge E - Rail Seat Positive Bending Moment

Figure 2.14: Field data showing the variability of bending moments at three critical concrete crosstie locations on a HAL freight railroad.

Crosstie 4's bending moment values suggest that the crosstie could have experienced a crack to the first level of prestress wires, entering into a range of flexural demand that this instrumentation technology may not be reliable in recording, as discussed earlier in this chapter. This cracking was visually confirmed during a subsequent site visit. The behavior of Crosstie 4 led to the conclusion that, while the overall behavior of crossties was such that the flexural demands were below the design limits, it is evident that the flexural demands can exceed design capacity in certain circumstances. These circumstances likely arise after settlement at the rail seats has generated a "center bound" condition that places greater demand on the crosstie's center section. This condition can be predicted using the methodology introduced in this chapter, and can be mitigated through track maintenance (i.e. tamping of ballast under the crosstie to regain uniform support).

Although a crosstie is cracked, potentially even below the first level of prestress, laboratory experimentation has shown that adequate residual capacity remains and Crosstie 4 is likely to function normally for the foreseeable future (César Bastos, 2016). When excluding Crosstie 4 for the aforementioned reasons, the probability of exceedance of the AREMA recommended practice value for center moment design was calculated as less than 0.5%.

To address the support condition question that led to the deployment of this instrumentation (Figure 2.14), bending moment magnitudes for both crosstie centers and rail seats are quite variable from crosstie-to-crosstie, providing validation and quantification of our assumption of the variability in crosstie support conditions. The standard deviation of average rail seat bending moments and center bending moments are 16.6 kip-in (1.86 kNm) and 25.0 kip-in (2.82 kNm), respectively. This probably indicates that center bending is more sensitive (i.e. variable) to support conditions than rail seat bending.

The maximum values of center bending moments are closer to the AREMA design recommendations than the maximum rail seat bending moments (Figure 2.14a and b) indicating that the factor of safety for rail seats (i.e. design value divided by the field readings) is less than the factor of safety at the crosstie center. This is of specific interest to the railway infrastructure design community, given that AREMA (2016) might overestimate the flexural demand on rail seats and that the design protocol could be better balanced to have similar safety factors for both critical design areas; the rail seat and the crosstie center.

2.5 Conclusions

The concrete surface strain gauge instrumentation methodology and deployment I describe in this chapter successfully measured the bending strains and resulting moments experienced by a wide range of rail traffic types operating in the United States. In this chapter, I demonstrated their utility in quantifying crosstie-to-crosstie variability in a HAL freight railroad revenue service deployment. The effectiveness of surface-mounted concrete strain gauges in measuring crosstie bending behavior yielded the following conclusions:

- Bending moments experienced by concrete crossties varied from crosstie-to-crosstie. This was demonstrated in this chapter with respect to a HAL freight railroad application, showing bending moments at the crosstie center that ranged from 0 kip-in (0 kNm) to 202 kip-in (22.8 kNm) and similar results have been noted in prior research (Wolf, 2015a; Wolf et al., 2015; Wolf et al., 2015; Gao et al., 2016).
- Accumulated freight tonnage plays a role in the flexural demands on concrete crossties, but while the measured moments were quantified correctly, the connection between the two is not as clear as hypothesized. The effects of tamping (i.e. re-establishing the substructure /

ballast under the crosstie) was clearly shown, supporting prevailing guidance on its usefulness at preventing center binding (Gao et al., 2016). Specifically, crosstie center bending moments were observed to decrease by 63% after tamping.

CHAPTER 3: QUANTIFICATION OF RAIL TRANSIT WHEEL LOADS & DEVELOPMENT OF IMPROVED DYNAMIC & IMPACT FACTORS

3.1 Introduction

In this chapter I introduce the concept of modal variability in peak wheel-rail loads, given its criticality as an input to field bending moment magnitude. The focus is on rail transit loadings because of the limited amount of research on the of field loading environment for rail transit modes (Table 1.4). I recorded data and evaluated loads from light, heavy, and commuter rail transit properties and studied variations in the load distributions.

While it is well known that moving wheels produce higher loads than the same wheel at rest (Hay, 1982; Kerr, 2003), predicting the totality (i.e. combined static, dynamic, and impact) of the loading environment at the wheel-rail interface is non-trivial. This is because the total load is not necessarily linearly related to the vehicle's static load. Furthermore, the degree of non-linearity and overall variability may differ for different types of rail transport.

Developing accurate models for predicting dynamic and wheel impact load factors is critical to the efficient design of railway track structures and components given that load factors may be inconsistent for different types of track infrastructure and rolling stock. The current method of assessing a constant impact factor of three for concrete crosstie design as described by AREMA (2016), and use of a wheel load dynamic factor of 0.33 to account for speed as described by Talbot and documented by Hay (1953) and Kerr (2003) is overly simplistic and is likely inaccurate. I recorded extensive wheel-rail input data on rail transit systems over a

several-year period. These data allowed me to generate empirical relationships reflective of the current loading environment.

For the heavy axle load (HAL) freight railroad operating environment, research has been conducted to quantify the load at the wheel-rail interface (Harrison et al. 2006; Stratman et al., 2007; Van Dyk, 2014; Van Dyk et al., 2017). Relatively little comparable work has been conducted on rail transit systems, although commuter rail systems have been studied when their rolling stock operates on infrastructure owned by freight or intercity passenger rail operators (Van Dyk, 2014; Lin et al., 2017). It is generally thought that wheel treads on rail transit rolling stock are more uniform than railroad freight car wheel treads, due to more frequent wheel trueing and other forms of vehicle and track maintenance in the transit environment. Consequently, they may be expected to generate lower dynamic and impact loads.

Beyond static load and speed, which are widely considered to be the most critical variables, total wheel-rail interface loads are shown to be influenced by: wheel diameter, the portion of static load representing unsprung mass, irregularities in the track structure, track maintenance conditions, and a variety of other vehicle and track characteristics (Doyle, 1980; Sadeghi and Barati, 2010; Van Dyk et al., 2016). All of the aforementioned factors are expected to vary when comparing rail transit operations with HAL freight railroads, further emphasizing the need for research to quantify rail transit load factors.

3.1.1 Types of Loads

The railway track loading environment includes the application of static, quasi-static, dynamic, and impact loads (Van Dyk et al., 2014). The static load is the load of the rail vehicle at rest and the quasi-static load is a low frequency oscillation applied over the static weight (Leong and Murray, 2008), which is the combined static load and effect of the static load at

speed (Standards Australia, 2003; Knothe and Stichel, 2013). Dynamic loads are due to the high-frequency effects of wheel/rail interaction, considering track component response and involving inertia, damping, stiffness, and mass. Impact loads that often create the highest loads in the track structure, are generated by track and wheel irregularities.

The distinctions between static, dynamic, and impact loads, their potential implications on the health of the track structure, and the ability to predict their magnitude have been discussed previously (Doyle, 1980; Van Dyk et al., 2014). In this chapter I will briefly discuss rail transit static and dynamic loads and then describe an approach used to quantify the totality of the track loading environment at the wheel-rail interface.

3.1.1.1 Static Loads

Lin et al. (2017) conducted a data collection and processing effort to quantify static rail transit rolling stock wheel loads. They presented graphical results (Figure 3.1) for most of the rolling stock used on light, heavy, and commuter rail transit properties in the United States. The terms AW0 and AW3 are from the American Public Transportation Association (APTA) and represent defined rail transit wheel loading conditions. AW0 loads are the static loads for as-delivered, ready to operate vehicles and AW3 loads represent the AW0 load with an additional "live load" of 6 passengers / square meter. The AW3 load is typically referred to as the "crush" load of a vehicle, and is considered to be the most representative load to use for the design of the track superstructure and its components (Lin et al., 2017). These data are useful for developing a baseline to compare the additional loads that are applied due to dynamic and impact forces. Additionally, they illustrate the variety in the three most common rail transit modes' axle loads,

and the infeasibility of designing components and systems that are globally optimal to all three modes.

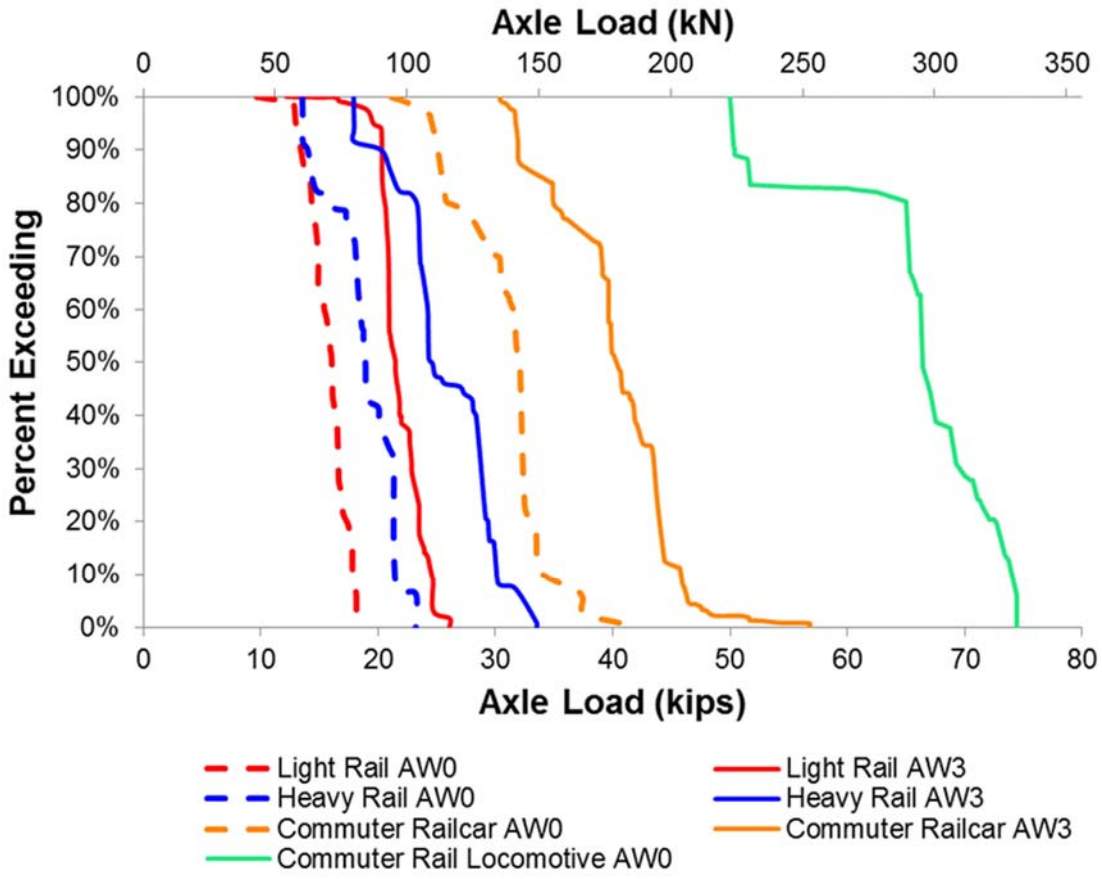

Figure 3.1: Light rail, heavy rail, and commuter rail static axle load percent exceeding distribution (modified from Lin et al., 2017).

3.1.1.2 Dynamic and Impact Loads

Over the previous half-century, over a dozen methods have been developed to predict dynamic loads, which have been summarized in prior research by Doyle (1980) and Van Dyk (2014). A subset of these methods was empirically generated using field data from their respective modes of rail transport. These predictive methods include a variety of track loading, health, and rolling stock design factors, as documented by Van Dyk et al. (2017). Much of the prior research has focused on the evaluation of dynamic impact load factors for HAL freight

trains (Van Dyk, 2014; Van Dyk et al., 2014; Van Dyk et al., 2017), partially due to the widespread deployment of wheel impact load detectors (WILD) on HAL freight railroad corridors in North America.

Despite the large number of methods and equations generated to predict dynamic loading conditions, researchers have noted that most methods substantially overestimate the magnitude of loads imparted into the track structure for HAL freight applications (Van Dyk, 2014; Van Dyk et al., 2017). Additionally, many of the prediction tools also overestimate the loads in the rail transit loading environment, leaving room for further refinement given sufficiently large and accurate data sets (Sadeghi and Barati, 2010; Sadeghi, 2012).

The prediction of impact loads, and its incorporation into design, is comparatively simple. Impact loads are incorporated into recommended design practices for concrete crossties as a 200% increase over the static load, i.e. three times the static load (AREMA, 2016).

3.1.1.3 Revised Dynamic and Impact Load Factors

Use of most of the dynamic factors mentioned above is restricted to a specific operating environment, thereby limiting their utility and breadth of application. Because these factors have been developed over many years in different regions of the world, they may not accurately reflect the operating conditions found in North America, especially for rail transit applications. Additionally, prior research has shown that the impact factor of three may overestimate the flexural demands required under revenue service train operation (Van Dyk et al., 2017; Edwards et al., 2018a).

To improve the prediction of input loads at the wheel-rail interface, and address a key step in the process of executing mechanistic design for track components as outlined by Van Dyk

et al. (2013), I am developing revised predictive equations based on field data. Given that design of rail infrastructure requires knowledge of the total loading that is expected, the loading factors in this chapter account for static, dynamic, and impact loads. Additional consideration will be given to dynamic loads and the need to relate wheel-rail load to speed.

To generate revised formulae inclusive of both dynamic and impact loads, focused field instrumentation was deployed, and WILD data were used to compare actual loading data to predicted dynamic loads and impact factors. These data were collected or obtained for light, heavy, and commuter rail transit systems.

3.2 Data Collection Methodologies

Wheel loading data can be obtained using commercially available systems that are present within many HAL rail corridors or by installing new, focused, instrumentation that records a subset of the data provided by the commercial systems. The two methods are discussed in the sections below.

3.2.1 Wheel Impact Load Detector (WILD) Data

A WILD consists of rail-mounted strain gauges installed over a series of ballast cribs that are oriented in a manner that records vertical rail strain that can be related to wheel loads (Harroson et al. 2006; Van Dyk, 2014) (Figure 3.2). A typical WILD site is about 50 feet (15 meters) in length, with cribs instrumented at various intervals to record a single wheel's rotation five times, recording peak impact and average forces at a data collection rate of up to 25,000 Hertz (Stratman et al., 2007; Canadian National, 2011). There are over 35 unique outputs obtained from a WILD (Van Dyk, 2014), but this chapter will primarily use nominal and peak load data.

Using an algorithm that analyzes variability among strain gauges along the site, average (or *nominal* as they are referred to by the WILD manufacturer) forces are filtered from the peak loads to obtain an estimate of static wheel load (Van Dyk, 2014). This is not a true static wheel load given the dynamic environment in which the measurements are recorded, thus the nominal load obtained from the WILD overestimates the typical static loading. This overestimation is acceptable for the current research given that recent field data have failed to support prevailing, empirically-derived relationships between speed and wheel load intended to estimate dynamic load factors (Van Dyk et al., 2014; Van Dyk et al., 2017). The peak wheel load is simply the highest recorded measurement from the strain gauges along the length of the WILD. While the WILD has typically been used by infrastructure and rolling stock owners to identify poorly-performing wheels, it has also proven to be a practical means of producing reliable wheel load data that is useful to rail infrastructure researchers and rail industry practitioners (Wiley and Elsaleiby, 2007; Elsaleiby, 2014; Van Dyk, 2014; Van Dyk et al., 2014; Quirós-Orozco, 2018).

Figure 3.2: Wheel Impact Load Detector (WILD) on Amtrak's Northeast Corridor at Edgewood, MD; used to capture the commuter rail train loads in this chapter.

WILD sites are constructed on tangent track with concrete crossties, typically with premium ballast, and well-compacted subgrade to reduce sources of load variation within the

track structure due to track geometry and support condition irregularities (Van Dyk, 2014). Although loads experienced at other locations along the railway network may have higher magnitudes due to track geometry and support deviations, these data still provide relevant loading information and are useful in deriving equations for the expected loading environment (Van Dyk et al., 2013).

3.2.2 Focused Loading Environment Instrumentation

Specifically-designed, focused, strain gauge instrumentation was deployed to collect wheel-rail interface input loads on rail transit systems that did not have WILDs. Weldable 350-ohm half-bridge shear strain gauges (Figure 3.3) were applied to the web of the rail to create vertical load circuits with the same configuration used at a single crib of a WILD (Figure 3.4).

Figure 3.3: Weldable half-bridge shear strain gauge (left) and loading frame used to calibrate gauges by relating strain to known system input load (right).

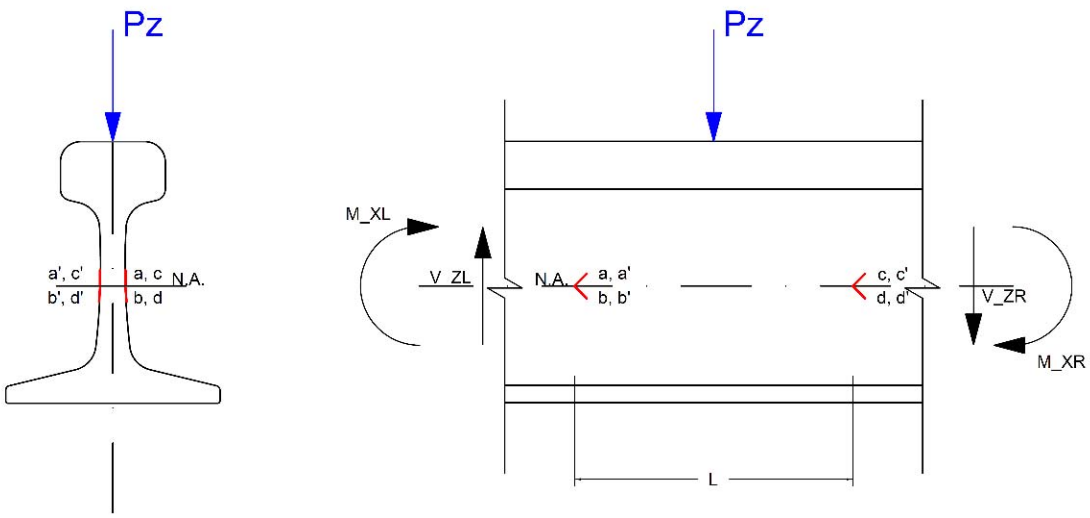

Figure 3.4: Vertical strain gauge orientation for field testing (strain gauges for quantifying lateral load were also deployed, but are not shown due to the scope of this chapter).

Installation of strain gauges required welding gauges to the rail using a portable strain gauge welding unit. This process involved first grinding the web and base of the rail to remove rust and expose pure metal, then clamping a ground wire to the base of the rail, and lastly placing the strain gauge and using the welding electrode to send current through the material, welding the strain gauge to the rail.

A Delta Frame (Figure 3.3) uses a hydraulic cylinder to apply loads to calibrate the strain gauge instrumentation installed on the rail via application of vertical loads of up to 20,000 lbf (88.9 kN). Vertical loads are applied using an upward facing steel triangular frame with loads applied in the center of the bottom side of the frame and reacting off the rail at the two bottom corners (Figure 3.3). Vertical load and strain are collected simultaneously throughout the calibration process, providing the opportunity to relate future strain readings obtained from the instrumentation to the vertical wheel load that generated them.

3.2.3 Interpretation of Data and Generation of Results

Given that the data presented in this chapter were acquired using related but distinct instrumentation methodologies, some clarification on the data collection differences is warranted. WILD sites collect data over as many as 25 consecutive cribs to measure the full revolution of the wheel, whereas the UIUC-deployed instrumentation collects data at a single crib and does not record the full rotation of a wheel. While the method has the limitation of being unable to determine whether the peak load from a wheel was obtained during a given train pass, it records every train pass on a captive rail transit system over long periods of time (one year). This volume of data helps to reduce variability and obtain readings from the entire circumference of a wheel.

3.3 Data Analysis

3.3.1 Comparison of Impact Factor Curves

The evaluation of rail transit wheel-rail interface input loading conditions was performed using data from three rail transit field sites in the United States;

- Light Rail Transit - St. Louis MetroLink at Fairview Heights, Illinois, hereafter referred to as “MetroLink”,
- Heavy Rail Transit – Metropolitan Transportation Authority (MTA) New York City Transit Authority (NYCTA) at Far Rockaway, New York, hereafter referred to as “NYCTA”, and
- Commuter Rail Transit - Maryland Area Regional Commuter (MARC) at Edgewood, Maryland, hereafter referred to as “MARC”.

The first two sites (MetroLink and NYCTA) used focused instrumentation described in Section 3.2.2 and the latter is a WILD site owned by Amtrak. For data collected from instrumentation on MetroLink and NYCTA there were not enough instrumented cribs to record and estimate the nominal wheel load as in a full WILD site. For these sites, the AW0 weight provided in the Federal Transit Administration (FTA) National Transit Database (FTA, 2013) is used as the nominal load. The measured loads were then used for the 'peak' load, which is divided by the nominal AW0 weight to obtain the load factor. As-delivered wheel loads were supplied by MetroLink and were used for the nominal loads in lieu of AW0 loads at the MetroLink site, given the need to better account for wheel-to-wheel nominal load variability of the light rail vehicles (LRVs). These assumptions are conservative with respect to its estimation of impact load factors given that the actual weight of the railcar could be as high as its AW3 load, depending on passenger loading.

A histogram of peak wheel loads for each rail transit mode (Figure 3.5) reveals the variety in input loads as measured in the field, and further emphasizes the disparity in loading when only nominal loads are used (Figure 3.1). Additionally, when plotting the total (dynamic and impact) load factors for each rail transit mode (Figure 3.6), it is evident that the distributions of impact factors for the three rail transit systems are distinct. These reflect the unique relationships that describe the total loading environment that is applied above the static (AW0) loads.

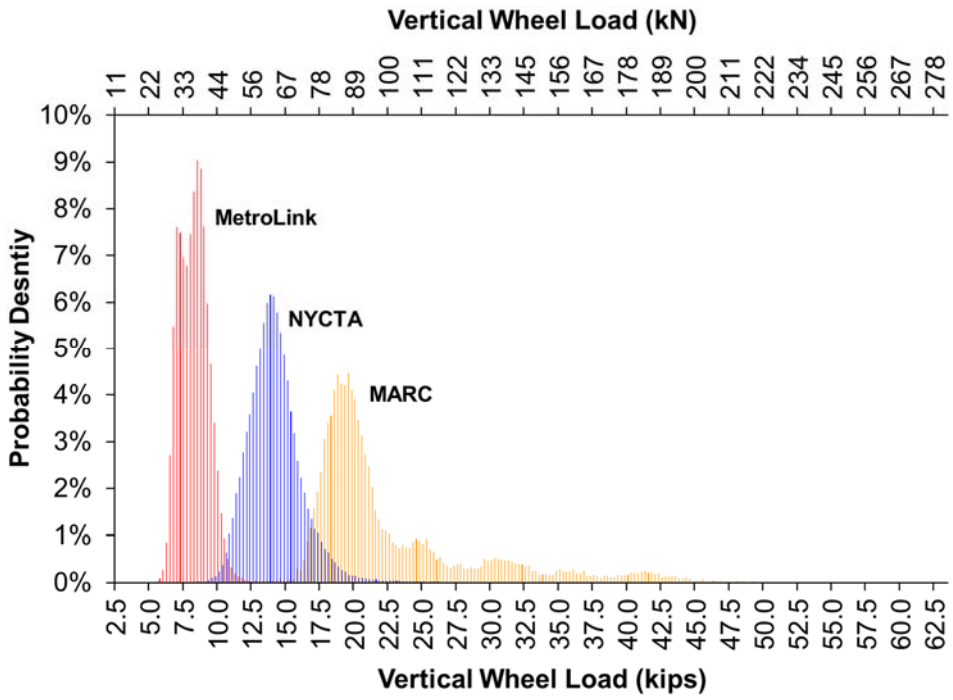

Figure 3.5: Histogram showing distribution of vertical wheel-rail loads from three rail transit systems (MetroLink, NYCTA, and MARC).

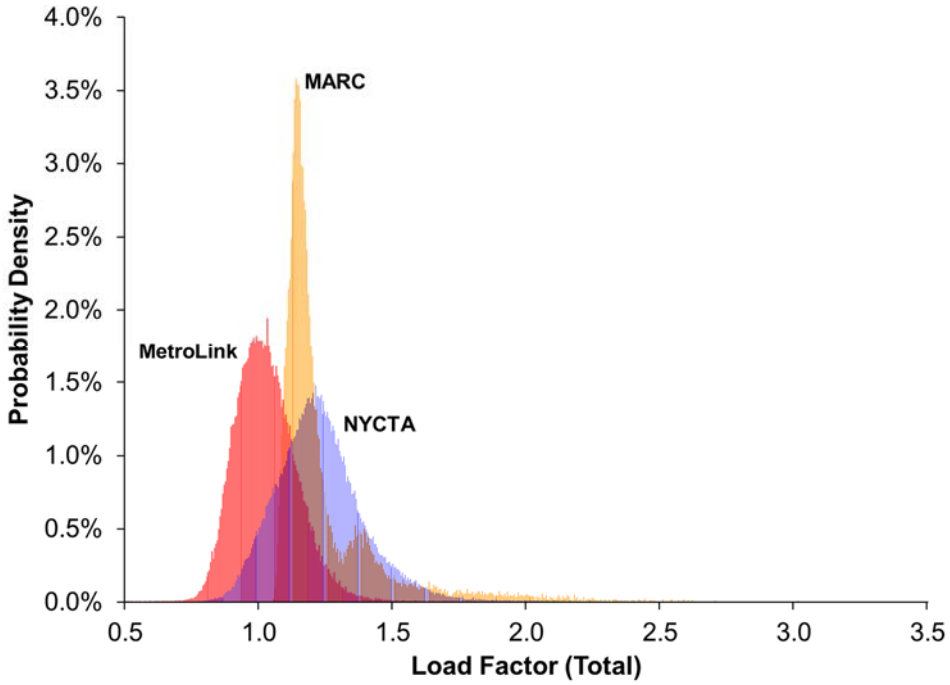

Figure 3.6: Histogram showing distribution of dynamic and impact load (total load) factors from three rail transit systems (MetroLink, NYCTA, and MARC).

The MetroLink distribution, and to a lesser extent the NYCTA distribution, raise questions given the presence of impact factors that are less than 1.0 indicating a dynamic load that is lower than static. This is not reasonable, and based on conversations with MetroLink's mechanical maintenance leadership, can be attributed to several factors. First, MetroLink operates a closed system and has an aggressive wheel truing maintenance program. This reduces the range between static and dynamic loads and thus the expected impact factor. Additionally, each wheel on a MetroLink's LRV has a unique, as-delivered weight associated with it. Weights vary among axles, and between wheels on a single axle, due to the placement of mechanical devices on the LRV. The data collected in the field are processed using the MetroLink-supplied wheel weights and known direction of travel for each train. These loadings, however, may not be reflective of the current weight due to minor changes in the arrangement of equipment on the LRV. For NYCTA, the field site is located on curved track, resulting in varying loads on the high and low rail. Nevertheless, when taken as a whole, data in Figure 3.6 demonstrate that on all three systems the measured load factors were well below the AREMA assumed value of 3.0. This is true even when a safety factor is applied to account for the aforementioned concerns related to the MetroLink data.

I also used descriptive statistics to compare the three distributions of impact factors and to determine how they differed (Table 3.1).

Table 3.1: Descriptive statistics comparing rail transit impact factor data

Statistic	Units	MARC	MetroLink	NYCTA
Sample Size	Number	28,920	62,472	131,062
Range	Load Factor	2.997	1.537	4.652
Mean	Load Factor	1.258	1.023	1.229
Variance	(Load Factor)^2	0.057	0.013	0.037
Standard Deviation	Load Factor	0.240	0.115	0.192
Coefficient of Variation	Decimal Percent	0.190	0.112	0.156
Standard Error	Load Factor	0.001	0.000	0.001
Skewness	Unitless	3.284	0.616	2.437
Excess Kurtosis	Unitless	15.038	1.469	17.537

In comparing the three distributions, the means were found to be similar between MARC (1.26) and NYCTA (1.23), but the variance and skewness were notably higher for the MARC data. Additionally, the standard deviations were quite different, as would be expected based on visual inspection of the plotted data. These statistics show that the three distributions are unique, and cannot be accurately represented using a single distribution. A single impact factor estimate cannot adequately reflect these differences.

Additional statistical tests were used to evaluate the null hypothesis that the impact factor data for the three rail transit modes do not differ (e.g. distribution function) (Press et al., 2002). The Kolmogorov-Smirnov (K-S) test was used to make pair-wise comparisons of each of the three modes. All of the K-S p-values were zero, indicating that the null hypothesis that the three distributions are the same can be rejected. All three types of rail transit systems surveyed had unique impact factor distributions. This dissimilarity has important implications for track component design and the need for different factors for each mode.

3.3.2 Distribution Fitting and Quantification of Goodness of Fit

The focus of this research is to develop generalized relationships to fit the distributions of impact factors for the three rail transit modes, in order to estimate the percentage of loads to be included when selecting future impact factors. This evaluation was made using the distribution fitting feature in the commercially available software EasyFit (by MathWave Technologies), which is able to determine the most appropriate distribution(s) for a set of continuous data using approximately 65 typical distributions (e.g. log-logistic, Gamma, normal, Weibull, etc.) for comparison and fitting purposes.

In addition to the K-S test, the Anderson-Darling statistical procedure was used to compare the distribution of load factors for each transit system to common distributions. The Anderson-Darling method is particularly useful for this application given that it increases the power of the K-S statistic to investigate the tails of the distribution and produces a weighted statistic (Darling, 1957; Press et al., 2002). This is important given the criticality of the tail of the impact-factor distribution in selecting a value for the design of track components. The Anderson-Darling procedure is dicussed in greater detail in Section 6.4.2 in conjunction with its use in quantifying best fit relationships to describe field bending moment data.

The best-fit (optimal) impact factor distribution was selected using the Anderson-Darling criteria, and was plotted with each rail transit impact factor field data set (Figure 3.7). Of particular interest is how the tails are fitted (shown in greater detail in Figure 3.8) for the maximum 0.10% of impact factors. The extreme values for impact loads also show significant scatter for the MARC commuter rail loading environment. It is likely that this greater variability is due to recorded data from multiple cribs at the WILD location.

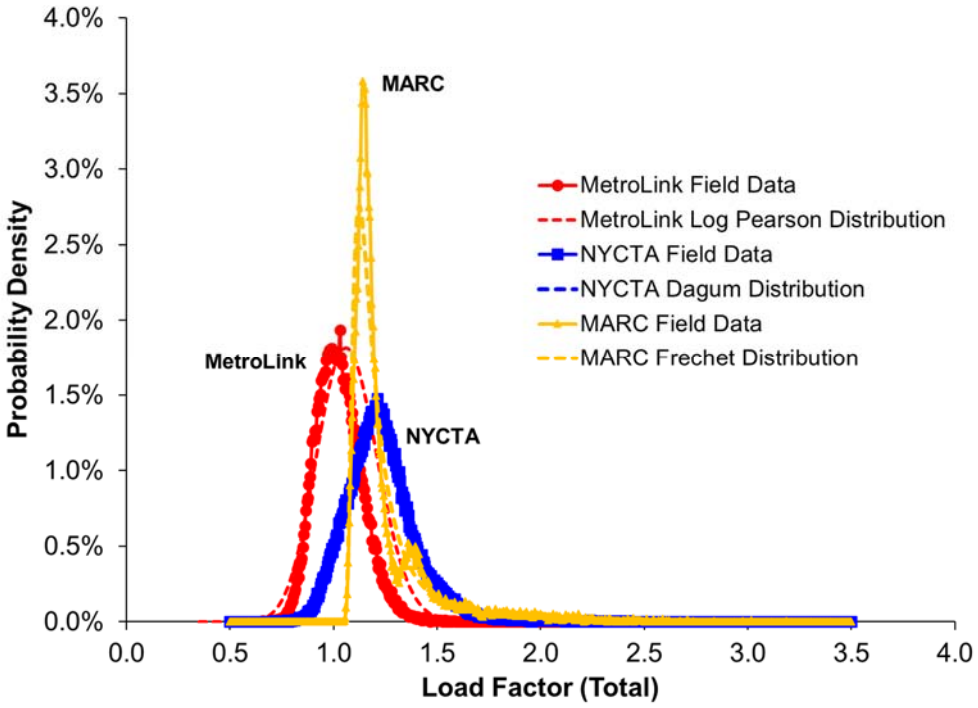

Figure 3.7: Total Load Factors for from three rail transit systems (MetroLink, NYCTA, and MARC) and overlay of best-fit distributions.

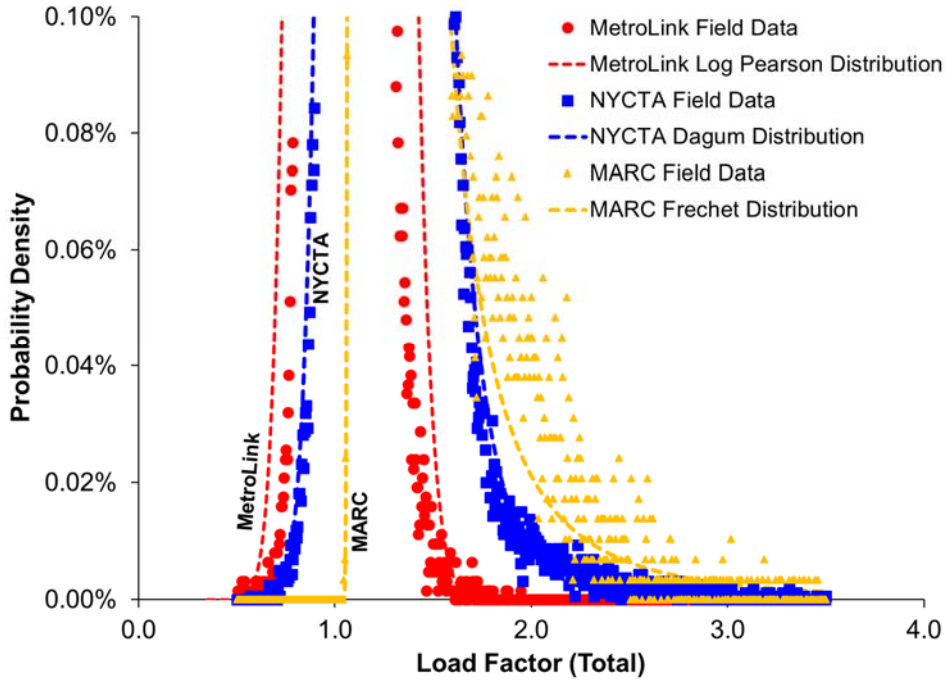

Figure 3.8: Extreme values (highest 0.10%) of total load factors for three rail transit systems (MetroLink, NYCTA, and MARC) and overlay of best-fit distributions.

Goodness-of-fit rank-order values for the K-S method and Anderson-Darling were summarized for the three rail transit modes (Table 3.2). Based on these results it is evident that the three distributions' tails are best fit using a variety of different functions, with little overlap among the generalized distributions. This further illustrates that the variables affecting total load factor were unique for each rail transit mode.

Table 3.2: Ranking of goodness of fit comparisons of rail transit impact factor distributions using K-S & Anderson-Darling methods (sorted by Anderson-Darling MetroLink ranking)

	Kolmogorov-Smirnov			Anderson-Darling		
Distribution	**MARC**	**MetroLink**	**NYCTA**	**MARC**	**MetroLink**	**NYCTA**
Log-Pearson 3	14	2	25	44	1	37
Pearson 6 (4P)	7	5	11	4	2	9
Lognormal (3P)	11	6	12	8	3	11
Pearson 6	26	7	16	23	4	14
Pearson 5	28	3	15	24	5	12
Dagum (4P)	24	13	1	22	7	1
Pearson 5 (3P)	2	4	10	2	8	10
Gamma (3P)	22	12	20	14	13	17
Dagum	35	15	6	54	14	5
Burr (4P)	10	17	4	12	15	3
Log-Logistic (3P)	6	19	3	5	17	2
Beta	31	18	14	13	18	13
Burr	12	21	2	13	19	4
Gen. Extreme Value	3	1	9	3	20	8
Frechet (3P)	1	38	38	1	37	34

The generalized distributions that provided the best fit as ranked by the Anderson-Darling criteria for each of the three modes were as follows; Log Pearson for MetroLink (Equation 3.1), Dagnum for NYCTA (Equation 3.2), and Frechet for MARC (Equation 3.3). These distributions are shown in Figure 3.7 and Figure 3.8, along with a histogram of the field data, and the generalized distributions are given by Equations 3.1, 3.2, and 3.3. Equations 3.4, 3.5, and 3.6

provide the specific distributions representing the data for MetroLink, NYCTA, and MARC, respectively, by inclusion of distribution parameters that best fit the data.

Despite the large number of common distributions checked, the p-values for all data except MetroLink do not allow rejection of the null hypothesis using $\alpha = 0.05$. The Anderson-Darling rejection critieria were not met for any of the three distributions shown, thus the distributions are all considered to be different than the sample data. Specifically, the equations allow for furture calculations of impact loads considering different percentile loading conditions (e.g. designing to the 99th percentile load). This type of calculation is an integral part of a probabalistic or mechanistic design process.

Log Pearson Distribution

$$F(x) = \frac{\Gamma_{(\ln(x)-\gamma)/\beta}(\alpha)}{\Gamma(\alpha)} \tag{3.1}$$

Dagum Distribution

$$F(x) = \left(1 + \left(\frac{x-\gamma}{\beta}\right)^{-\alpha}\right)^{-k} \tag{3.2}$$

Frechet Distribution

$$F(x) = \exp\left(-\left(\frac{\beta}{(x-\gamma)}\right)^{\alpha}\right) \tag{3.3}$$

MetroLink Best Fit

$$F(x) = \frac{\Gamma_{(\ln(x)+1.593)/0.0076}(211.83)}{\Gamma(211.83)} \tag{3.4}$$

NYCTA Best Fit

$$F(x) = \left(1 + \left(\frac{x - 0.55114}{0.6611}\right)^{-7.2334}\right)^{-0.95689} \quad (3.5)$$

MARC Best Fit

$$F(x) = \exp\left(-\left(\frac{0.14201}{(x - 1.0094)}\right)^{1.9514}\right) \quad (3.6)$$

In addition to the previous analysis of load factors, I have also summerized the rail transit datasets by their percentile vertical loads (Tables 3.3 and 3.4) and their dynamic or impact load factors (Table 3.5). MetroLink had both a lower load *and* lower impact factor than either NYCTA or MARC. While this is expected due to the corresponding static wheel loads, the lower impact or dynamic load factor was not necessarily expected. These values could also be used to estimate the percentage of loads that would be covered by a given design factor.

Table 3.3: Percentiles of rail transit vertical loads in kips

		Percentile						
Mode	**Mean**	**10%**	**50%**	**75%**	**90%**	**95%**	**97.5%**	**99.5%**	**100%**
MetroLink	8.1	6.8	8.1	8.8	9.5	9.9	10.2	11.2	18.6
NYCTA	14.0	11.7	13.8	15.0	16.4	17.5	18.6	24.0	59.3
MARC (Nominal)	18.1	15.1	16.7	17.7	26.8	30.7	35.2	38.0	41.1
MARC (Peak)	22.7	17.5	20.1	24.4	32.2	37.8	41.5	46.7	64.6

Table 3.4: Percentiles of rail transit vertical loads in kN

		Percentile						
Mode	**Mean**	**10%**	**50%**	**75%**	**90%**	**95%**	**97.5%**	**99.5%**	**100%**
MetroLink	36.1	30.1	36.2	39.3	42.2	43.9	45.6	49.8	82.6
NYCTA	62.3	51.9	61.3	66.6	72.9	77.8	82.8	106.6	263.9
MARC (Nominal)	80.7	67.1	74.2	78.7	119.1	136.6	156.5	168.9	182.9
MARC (Peak)	100.8	78.1	89.3	108.5	143.1	168.1	184.4	207.9	287.4

Table 3.5: Percentiles of total load factors from rail transit systems

		Percentile							
Mode	**Mean**	**10%**	**50%**	**75%**	**90%**	**95%**	**97.5%**	**99.5%**	**100%**
MetroLink	1.02	0.89	1.01	1.09	1.17	1.22	1.27	1.39	1.94
NYCTA	1.23	1.03	1.21	1.32	1.44	1.54	1.64	2.11	5.21
MARC	1.26	1.10	1.17	1.28	1.50	1.76	1.99	2.47	4.04

While further study is warranted as to why the impacts are lower for MetroLink's LRVs, I surmise that differences in the suspension system of the trucks, wheel health, resilient (i.e. sandwich composite) wheel construction, and track health and degradation rates play a role in reducing these impacts compared to the other two systems. These factors are also noted in many of the aforemented dynamic load factor equations summarized by Doyle (1980) and Van Dyk (2014).

3.4 Development of Improved Speed Factor

To determine the influence of speed on the vertical loads imparted into the track structure, an accurate measurement of speed was needed for each vertical load reading. Speed is provided as a direct output of WILD systems and speeds from trains passing instrumented locations were calculated using the time between measured loads and known axle spacing. Using the speed and wheel load data, loads were categorized into 5 mph (8 kph) speed bins for UIUC-installed instrumentation, and 10 mph (16 kph) bins for the WILD data. Bins with more than 20,000 data points were subdivided until no bin contained more than 20,000 data points. Each speed bin was analyzed to find several relevant percentiles (e.g. 90th, 95th, 99th, and maximum) of wheel loads.

Wheel load data were next used to estimate the effect of speed using an approach similar to Van Dyk (2017). The Talbot equation slope (Hay, 1953; Talbot, 1980; Kerr, 2003) was

modified to minimize the sum of percent exceeding and root mean square deviation for each rail transit dataset. The change in dynamic factor due to the aggregate factors experienced in the field on the three systems surveyed can be expressed in the three equations shown in Table 3.6.

Table 3.6: Summary of impact factor equations for prediction of light, heavy, and commuter rail transit wheel loads as a function of speed and wheel diameter

Rail Transit Mode	Total Load Factor Equation	
	SI Units	US Customary Units
Light	$1 + 0.067\frac{Speed\ (kph)}{Wheel\ Diameter\ (cm)}$	$1 + 0.105\frac{Speed\ (mph)}{Wheel\ Diameter\ (inches)}$
Heavy	$1 + 0.323\frac{Speed\ (kph)}{Wheel\ Diameter\ (cm)}$	$1 + 0.510\frac{Speed\ (mph)}{Wheel\ Diameter\ (inches)}$
Commuter	$1 + 0.198\frac{Speed\ (kph)}{Wheel\ Diameter\ (cm)}$	$1 + 0.313\frac{Speed\ (mph)}{Wheel\ Diameter\ (inches)}$

Based on the slopes of these three lines, it is evident that the wheel health and track maintenance vary for each mode. The MetroLink data displayed the lowest slope (Figure 3.9), thus the least influence of speed on wheel-rail loads. This factor of 0.067, roughly 20% of the Talbot factor, may indicate that the dynamic factor for light rail can be considerably reduced from its current value of 0.33. The NYCTA data, on the other hand, tend to indicate that a higher dynamic factor is required to adequately account for increased loads that vary as a function of speed.

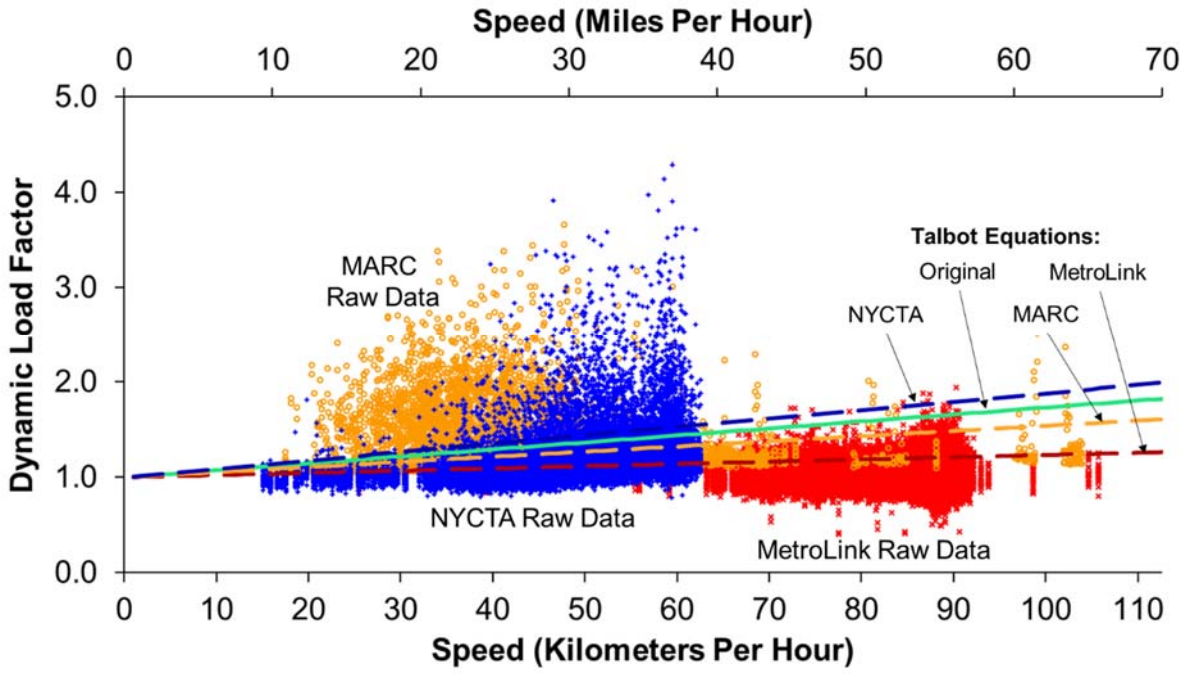

Figure 3.9: Raw data and predictive curves generated from field data from three rail transit modes.

3.5 Conclusions

In this chapter I quantify the aggregate effect of speed and other vehicle and track irregularities to generate accurate dynamic and impact load factors for rail transit systems. Specifically, the following conclusions can be drawn:

- Total load factor distributions for the three rail transit systems significantly differed, demonstrating that unique, specific, load factors are needed to adequately represent the existing wheel loads on rail transit infrastructure and improve design of the critical components that make up the track structure. All distributions indicate that the current AREMA impact factor of three should be reduced, possibly by as much as half.
- Existing dynamic load factors were analyzed, and the Talbot approach to estimating dynamic loading due to speed and wheel diameter was found to be quite conservative,

with the light rail transit loading environment being over-estimated by a factor of three. Conversely, heavy rail transit factors were underestimated by approximately 50%. Finally, commuter rail transit factors matched the Talbot prediction quite well.

- For a given mode, in the absence of field data related to the track loading environment, the selection of an appropriate load factor should be based on knowledge of a particular system's track and rolling stock maintenance practices.
- Focused load-related field instrumentation can be deployed to answer system-specific loading questions within a given rail transit mode. The relatively modest effort required to install instrumentation and process data from such an installation could provide significant returns on investment with respect to mechanistically designing track components.

CHAPTER 4: QUANTIFICATION OF RAIL TRANSIT CONCRETE CROSSTIE FIELD BENDING MOMENTS

4.1 Background and Introduction

In this chapter I present results from a field study quantifying flexural demands on concrete crossties on both light rail transit (LRT) and heavy rail transit (HRT) systems. The research described in this chapter uses the surface strain measurement methodology described in Chapter 2 to obtain bending moments.

Prestressed concrete crossties are commonly used in rail transit applications due to their improved ability to maintain track gauge and higher reliability that reduces the time needed for track maintenance activities (Zeman, 2010; Van Dyk, 2014; McHenry and LoPresti, 2016). While useful input data for the mechanistic design of concrete crossties in heavy axle load (HAL) freight systems were documented in earlier research efforts (Edwards et al., 2017a) (Chapter 2), additional effort is required to generate a robust dataset for rail transit loads, bending moments, and displacements.

The majority of North American design practices used for rail transit are borrowed from HAL freight railroad engineering, thus the potential for incorrect and inefficient application of these standards exists. I am addressing this potential inefficiency (over-design) through a research effort aimed specifically at rail transit infrastructure funded by the US DOT Federal Transit Administration (FTA), with the objective of mechanistically designing track components based on actual field loading conditions.

Most of the overly-conservative rail transit crosstie designs have demonstrated reasonable service lives to date. However, challenges can emerge from concrete crossties that have been over-designed with unnecessarily high levels of prestress, contributing to brittle failures (Windisch, 1970). Additionally, striving for concrete with excessively high levels of compressive strength (in excess of 10,000 psi) could also contribute to premature failures of crossties (Gettu et al., 1990) and necessitate the use of premium (and more costly) mixture designs. Finally, prestress forces have been known to generate bursting stresses around wires or strands that leads to cracking at the ends of crossties (Mayville et al., 2014). Reducing these stresses would prevent at least a portion of this type of failure. While the extent of these concerns remains to be quantified, there is an economic benefit to designing and manufacturing crossties that are optimally sized in terms of the component itself and the equipment needed to install crossties.

While the design of prestressed, precast monoblock crossties has many different facets (e.g. material selection, economic impact, overall performance criteria, etc.), which are addressed in Chapter 1, the flexural design is considered to be the most critical design element given its linkage to the structural integrity of the crosstie. Beyond quantifying bending moment magnitude, which could be incorporated into future mechanistic designs (Van Dyk et al., 2013), both researchers and practitioners are interested in understanding the variability in flexural demands among crossties in order to plan and prioritize tamping operations. Additionally, variability in temperature can affect bending moments (Wolf et al., 2016b).

In this chapter, I quantify the seasonal variation in bending on rail transit systems. Flexural reserve capacity (i.e. ratio between crosstie design capacity and moment observed) and seasonal variability of moments have the potential for being more pronounced in the rail transit

loading environment due to the ratio between the average wheel loads and flexural resistance of crossties being lower than that seen in the HAL freight railroad operating environment. In other words, seasonal and other sources of variation that are independent of load may be more critical in rail transit applications than has been observed in HAL freight service (Wolf, 2015a; Wolf et al., 2016b), due to the distinctly different loading magnitudes, yet relatively similar sectional properties of the crossties.

To address crosstie flexural reserve capacity quantification, crosstie-to-crosstie variability, and seasonal variation of moments, concrete surface strain gauge instrumentation was deployed in the field on both LRT and HRT systems. This method was previously developed, deployed, and validated by Edwards et al. (2017c) and was described in Chapter 2. This method has proven useful in answering similar questions for HAL freight applications (Edwards et al., 2017c).

4.2 Instrumentation Technology

Previous research has used either embedded or surface strain gauges to quantify field bending moments of concrete crossties (Venuti, 1970; Venuti, 1990; Mayville et al., 2014; Kerokoski et al., 2016; Edwards et al., 2017a), which were summarized in Chapter 2. These projects focused almost exclusively on the freight and intercity passenger rail domain, with little mention of rail transit applications.

A minimum sampling rate for rail transit data collection was determined based on the maximum authorized train speed at each field location and the desired data sampling resolution, where the sampling resolution is the distance the train travels between collection of consecutive samples. The sampling resolution desired for the application discussed in this chapter was 0.5

inches (12.7 mm). Based on these requirements, prior experience, and expert recommendation I used a sampling rate of 2,000 Hertz.

4.3 Field Deployment

4.3.1 Example Field Instrumentation Deployment

The specific field tests discussed in this dissertation was conducted at ballasted track field sites on two rail transit systems, St. Louis MetroLink in East St. Louis, IL (hereafter referred to as "MetroLink") and MTA New York City Transit Authority (NYCTA) in Far Rockaway, New York (hereafter referred to as "NYCTA"). Because of the variability in support conditions observed in past field experimentation (Wolf, 2015a; Gao et al., 2016; Edwards et al., 2017c), instrumentation was placed on five consecutive crossties at each field test location (Figure 4.1).

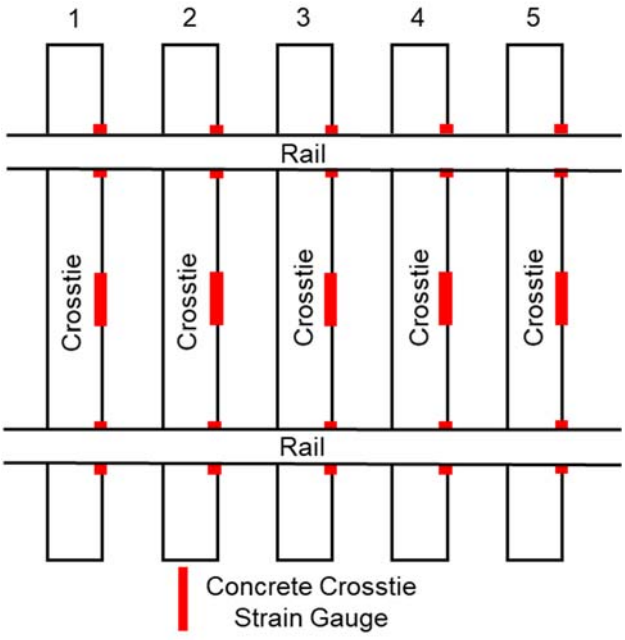

Figure 4.1: Field experimentation site layout with five crossties showing locations of concrete surface strain gauges used in this study.

4.3.2 Instrumentation Deployment on Crosstie

Bending strains at critical locations along the length of the crosstie were measured to quantify the flexural behavior of the crosstie under revenue service train loading. Three strain gauges (labeled A, C, and E) were used on each crosstie, with one applied at each of the two rail seats and one at the center (Figure 4.2). Additional relevant dimensions and properties for the two types of rail transit crossties investigated in this research are shown in Table 4.1, which includes a typical crosstie used in HAL freight service for comparison. All three types of crossties in Table 4.1 use a prestressing tendon that is 0.209 in (5.32 mm) in diameter and similar concrete mixture designs. Specification design capacities in Table 4.1 refer to the transit agency value that must be met or exceeded for flexural strength. Design values are the capacities associated with the unique crosstie designs produced by the manufacturers.

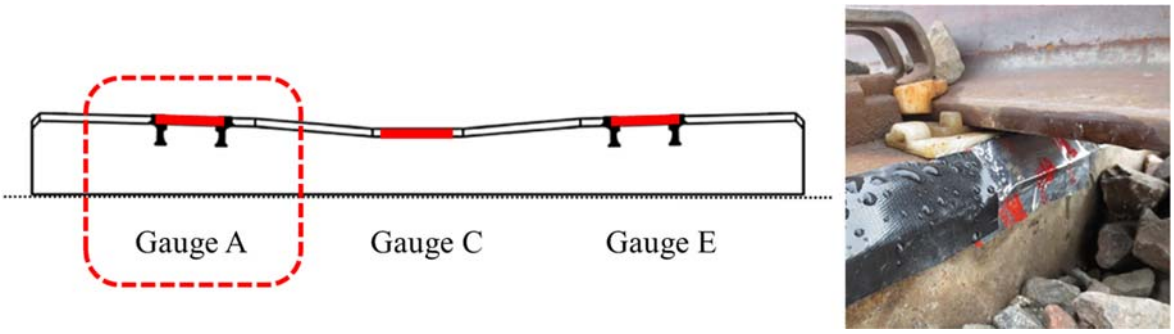

Figure 4.2: Profile view of instrumented crosstie showing locations of strain gauges and image showing example of rail seat with gauge A installed.

Table 4.1: Characteristics of rail transit crossties used in this study and comparison to a typical HAL freight concrete crosstie

Crosstie / System Characteristic			Light Rail (MetroLink)		Heavy Rail (NYCTA)		HAL Freight	
			SI	Imperial	SI	Imperial	SI	Imperial
Static Wheel Loads*	Maximum (AW3)		41.8 to 55.6 kN	9.4 to 12.5 kips	62.9 kN	14.1 kips	35.8 kips	159 kN
	Minimum (AW0)		28.9 to 42.7 kN	6.5 to 9.6 kips	50.6 kN	11.4 kips	Varies	Varies
Crosstie Geometry	Length		2.51 m	8’ 3”	2.59 m	8’ 6”	2.59 m	8’ 6”
	Tie Spacing		0.76 m	30”	0.61 m	24”	0.61 m	24”
Crosstie Prestressing	Number of Wires		12		18		20	
	Jacking Force		31.1 kN	7 kips	31.1 kN	7 kips	31.1 kN	7 kips
	Precompression (Crosstie Center)		10,204 kN/m^2	1.48 ksi	13,858 kN/m^2	2.01 ksi	15,444 kN/m^2	2.24 ksi
Crosstie Design Capacity	Center Negative	Specification	16.3 kN-m	144 kip-in	19.0 kN-m	168 kip-in	26.0 kN-m	230 kip-in
		Design	16.6 kN-m	147 kip-in	21.9 kN-m	194 kip-in	26.0 kN-m	230 kip-in
	Center Positive	Specification	10.5 kN-m	93 kip-in	13.3 kN-m	118 kip-in		
		Design	16.3 kN-m	105 kip-in	14.9 kN-m	132 kip-in	21.0 kN-m	186 kip-in
	Rail Seat Positive	Specification	20.2 kN-m	179 kip-in	28.3 kN-m	250 kip-in	33.9 kN-m	300 kip-in
		Design	25.0 kN-m	221 kip-in	32.0 kN-m	283 kip-in	43.1 kN-m	381 kip-in
	Rail Seat Negative	Specification	12.0 kN-m	106 kip-in	15.6 kN-m	138 kip-in		
		Design	15.4 kN-m	136 kip-in	20.1 kN-m	178 kip-in	24.7 kN-m	219 kip-in

*AW0 loads are the as-delivered, ready to operate static loads and AW3 loads (crush load) represent the AW0 load plus the weight of seated passengers and an additional “live load” of 6 standing passengers / square meter, a common load used for passenger vehicle design.

The process of instrumenting crossties in the field, including the protection of strain gauges, is shown in Figure 4.3 and described in Chapter 2. To relate the field-measured strains to a bending moment, calibration factors were generated using laboratory tests conducted at UIUC's Research and Innovation Laboratory (RAIL) using the processes described in Chapter 2.

Figure 4.3: Crossties instrumented with concrete surface strain gauges and the completed St. Louis MetroLink light rail field experimentation location.

4.4 Data Analysis

To quantify the bending moments concrete crossties experience in revenue service, peaks in the strain gauge signal caused by crosstie bending due to a wheel or axle load must be extracted from the data stream collected at 2,000 Hertz. This was accomplished using a modified version of the "findpeaks" function in MATLAB (2012) that was introduced in Chapter 2. To improve the performance of this function for this application, several of the built-in options were used, and additional modifications were made to the code that was originally developed by Wolf (2015a).

Before the peaks were obtained, the strain signal was zeroed using data captured before the arrival of the first axle, and a linear baseline correction was applied to adjust for any signal

drift over the course of a single train pass. As such, data collection was initiated several seconds prior to the arrival of the leading axle to provide a stable zero point for the crosstie under no applied load. Additionally, the data collection was ended several seconds after the final train axle passed to serve as an end point for the baseline correction. To ensure that the true peaks were being captured by the program, as opposed to false peaks that did not represent the extreme strain reading for a given axle pass, a minimum spacing between the peaks was specified and a minimum value for all peaks was set. Additional detail on filtering and processing of data was previously documented by Edwards et al. (2017c) and is included in Chapter 2.

Figure 4.4 (left vertical axis) shows an example of a typical strain gauge signal for a center gauge for a single MetroLink train pass made up of two, six-axle light rail vehicles (LRVs). The signal was zeroed out and the peaks were numbered in sequence, which were then converted into bending moments using the laboratory moment calibration factors described previously (Figure 4.4, right vertical axis).

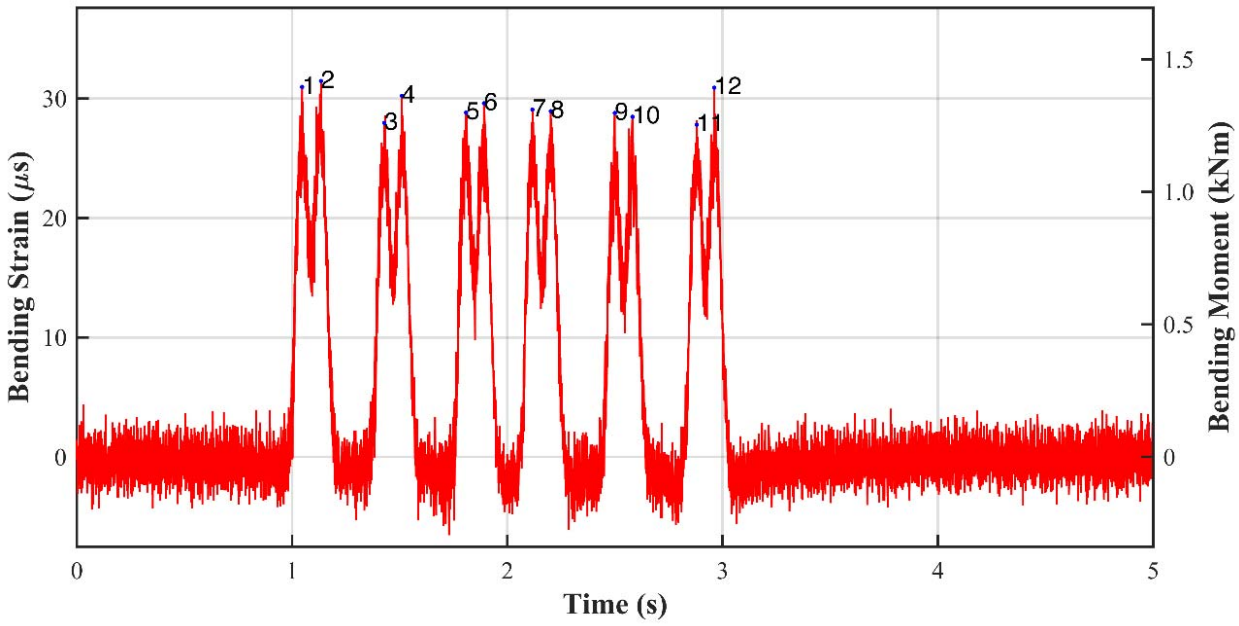

Figure 4.4: Typical crosstie center strain signal and resulting center bending moment captured under the passage of a 12-axle St. Louis MetroLink light rail trainset.

4.5 Results

The instrumentation plan described in this chapter was deployed for approximately one year on each of the two rail transit properties. In total, 27,092 light rail train passes were recorded at the MetroLink site from 18 March 2016 until 19 May 2017 and 11,597 heavy rail train passes were recorded at the NYCTA site between 26 April 2016 and 27 February 2017. For the duration of these deployments, the instrumentation described in this chapter functioned properly. Other field sites have experienced similar successes (Edwards et al., 2017b). Using these data from MetroLink and NYCTA, bending moments induced by loaded axles from the signals of the center and rail seat strain gauges were analyzed.

4.5.1 Magnitude of Bending Moments and Comparison to Design Standards Capacities

The concrete crosstie center negative (C-) bending moment distributions for the trains show both the overall magnitude and variability of moments (Figure 4.5). It is evident that the variability and range associated with NYCTA moments exceeds that of MetroLink, as evidenced by the shallower slope of the NYCTA data. Additionally, similar plots are shown for the rail seat positive bending moments in Figure 4.6, with greater variability and range seen in the NYCTA data. These distributions are also shown in comparison to the specifications and design capacities for both rail seat positive and center negative cracking, which are most commonly based on limits generated using AREMA recommended design practices (AREMA, 2016). These values, as generated using the AREMA (2016), method define a threshold that a bending moment would need to exceed before a crack propagates to the first level of prestress**.**

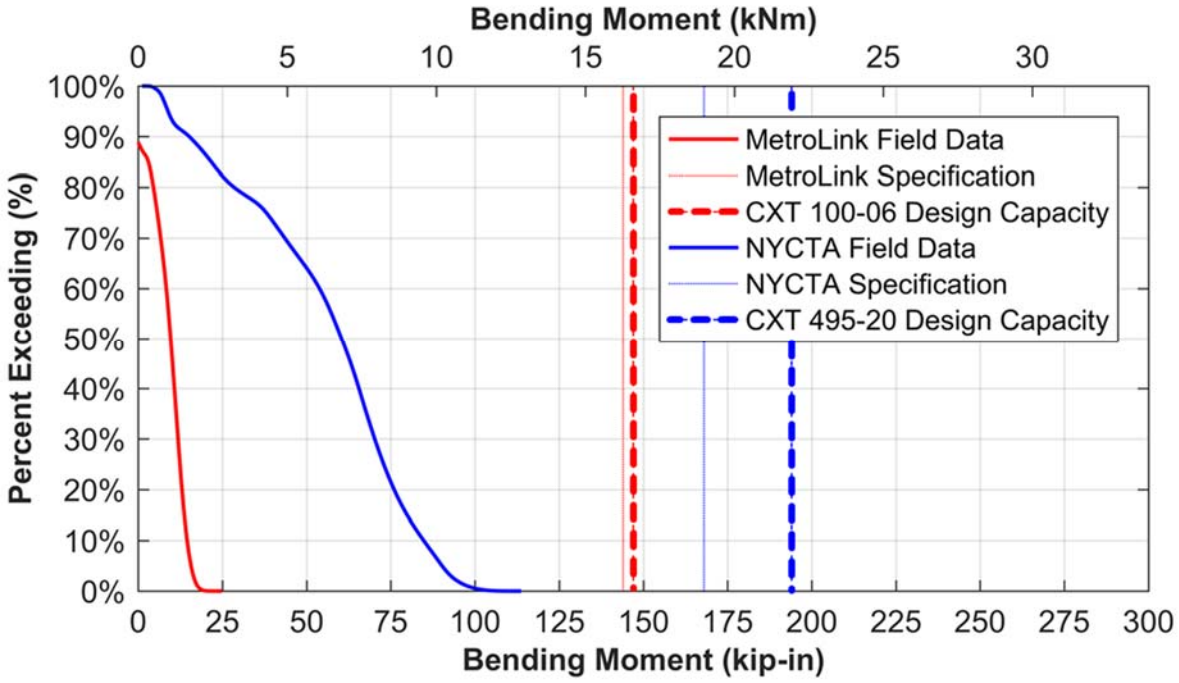

Figure 4.5: Distribution of MetroLink and NYCTA center negative (C-) bending moments for each axle and comparison with design capacity and transit specifications.

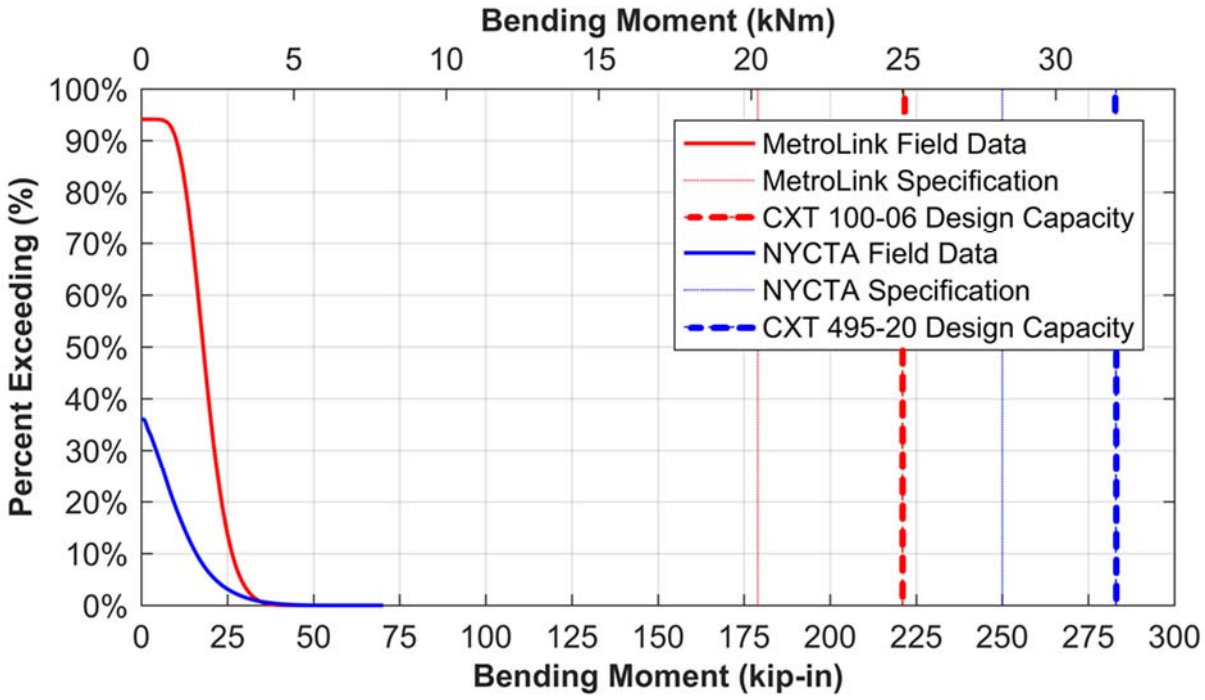

Figure 4.6: Distribution of MetroLink and NYCTA rail seat positive (RS+) bending moments for each axle and comparison with design capacity and transit specifications.

None of the crosstie bending moments recorded reached the specification or design limit (shown by the vertical lines in Figures 4.5 and 4.6). This is especially evident at the rail seats, as the 95th percentile rail seat positive (RS+) moment values were less than 10% of the 179 kip-in (20.2 kNm) and 250 kip-in (28.2 kNm) specification limits for crosstie flexural design for MetroLink and NYCTA, respectively. When combined with high estimates for input wheel loads in design specifications, AREMA (2016) recommendations can overestimate the flexural demand at the crosstie rail seat (Figure 4.6). Compared to rail seat positive (RS+) moments, 95th percentile center negative (C-) bending moments were closer to the specification values, reaching as much as 50% of the 144 kip-in (16.3 kNm) and 168 kip-in (19.0 kNm) values for MetroLink and NYCTA, respectively.

This indicates that center bending conditions may govern the design in terms of factors of safety (AREMA, 2016) (Figure 4.5). This finding is also in agreement with a previous survey of industry experts that suggested that center cracking of concrete crossties was more commonly seen in the field, albeit in HAL freight railroad applications (Van Dyk, 2014). This type of failure may be preferable to infrastructure owners given they are more easily detected through visual inspection.

A measure of reserve capacity was generated by dividing the design capacity of the crosstie at the center or rail seat by the observed field moments at varying percentiles (Table 4.2). Current crosstie designs, even when compared with the maximum bending moments experienced in the field, have a reserve capacity exceeding 3.2 in rail seat positive bending (RS+) for MetroLink and exceeding 1.7 in center negative (C-) bending for NYCTA. These respective reserve capacity factors further increase to 7.6 and 2.1 when considering 95th percentile bending moments.

Table 4.2: Reserve capacity for light rail (MetroLink) and heavy rail (NYCTA) crossties

Bending Moment Percentile	Light Rail		Heavy Rail	
	Center	Rail Seat	Center	Rail Seat
Minimum	-4.9	-3.4	168.5	-2.7
0.10%	-7.9	-5.9	49.4	-4.9
1%	-9.9	-8.1	32.2	-6.1
5%	-18.3	-14.7	21.9	-7.6
10%	-95.9	21.7	12.8	-8.8
90%	10.1	8.4	2.3	17.8
95%	9.4	7.6	2.2	13.2
99%	8.4	6.5	2.0	8.6
99.90%	7.5	5.7	1.9	6.3
Maximum	5.9	3.2	1.7	4.0

Reserve design capacities are consistently higher for MetroLink than NYCTA. There are a variety of factors that likely influence this including the crosstie design and its related assumptions, the input rail seat loads (primarily a function of wheel tread condition and maintenance), and the crosstie support conditions (primarily a function of track quality).

Of additional interest is the fact that positive center moments were recorded on MetroLink and negative rail seat moments were recorded on NYCTA. Negative values of reserve design capacity in Table 4.2 indicate that the "opposite" moment was recorded (e.g. rail seat negative and center positive). While these values are expected to occur infrequently, they do occur, and these data provide insight regarding their occurrence. It is interesting to note that the lowest reserve capacity ratios are found for rail seat negative (RS-) as opposed to rail seat positive (RS+) for NYCTA and for center positive (C+) as opposed to center negative (C-) for MetroLink. These apparent contradictions of conventional thinking are due to the specific support conditions that were present where the instrumentation was deployed, with the MetroLink crossties being well-supported at the rail seat and NYCTA crossties having more

support at the center as evidenced by the high center negative (C-) bending moments. Furthermore, this finding can provide a method for future estimation of support conditions and a process to infer whether center binding is present.

4.5.2 Crosstie-to-Crosstie Moment Variability

A critical question is the extent of variability in bending moments for consecutive crossties. This question has been addressed in earlier work aimed primarily at the HAL freight environment (Edwards et al., 2017c), but no previous research has focused on concrete crossties used in rail transit systems. Figure 4.7 and Figure 4.8 show the distribution of center negative (C-) and rail seat positive (RS+) bending moments, respectively, under MetroLink light rail transit loading for seven crossties and 14 rail seats. Figure 4.9 and Figure 4.10 show the same distributions under heavy rail traffic on NYCTA.

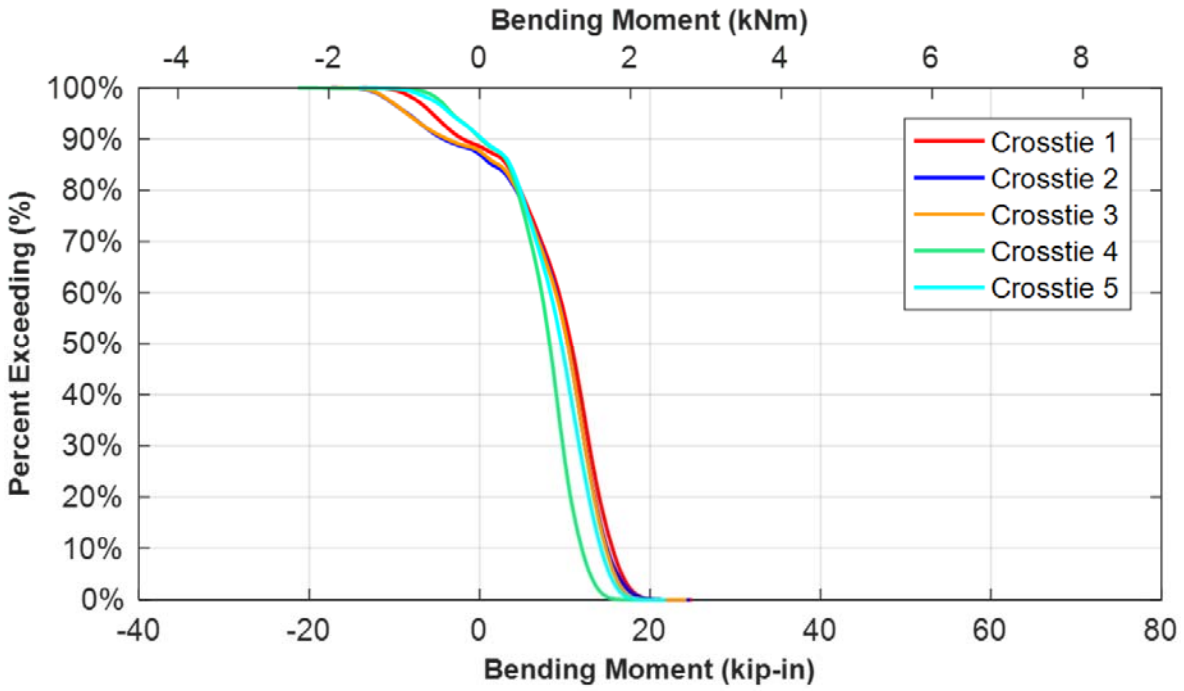

Figure 4.7: Distributions showing crosstie-to-crosstie variability of center negative (C-) bending moments for light rail transit loading on St. Louis MetroLink.

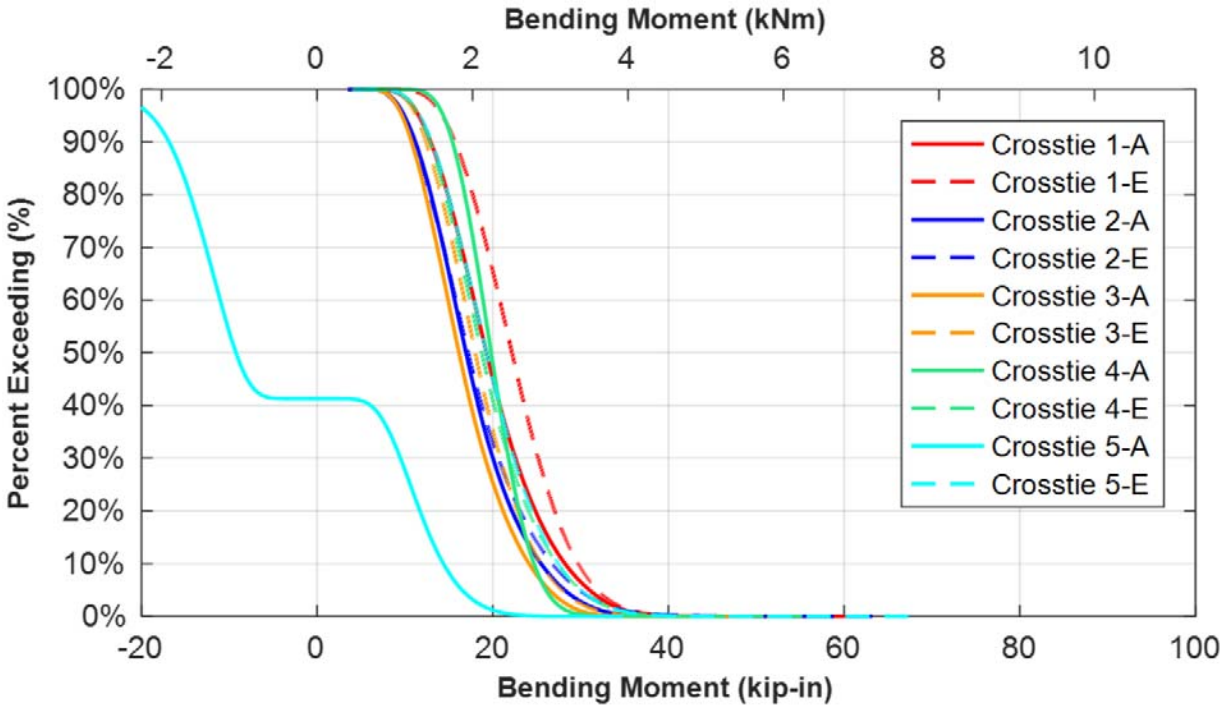

Figure 4.8: Distributions showing crosstie-to-crosstie variability of rail seat positive (RS+) bending moments for light rail transit loading on St. Louis MetroLink.

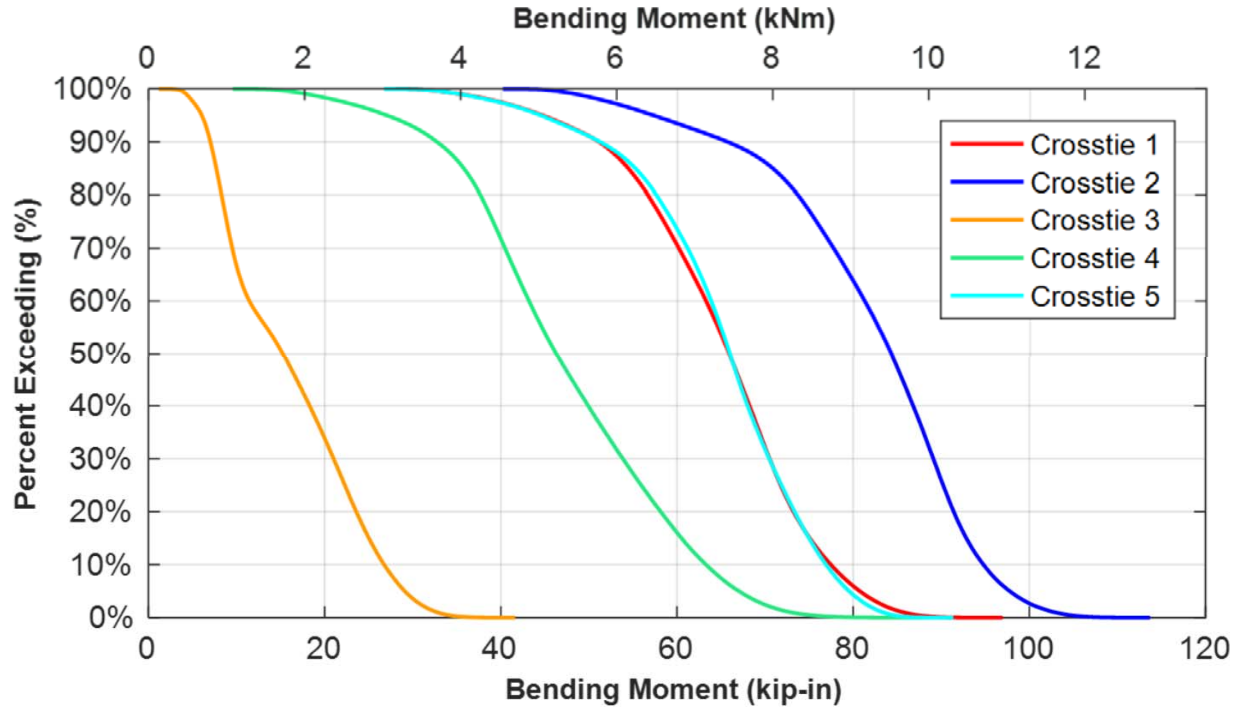

Figure 4.9: Distributions showing crosstie-to-crosstie variability of center negative (C-) bending moments for heavy rail transit loading on NYCTA.

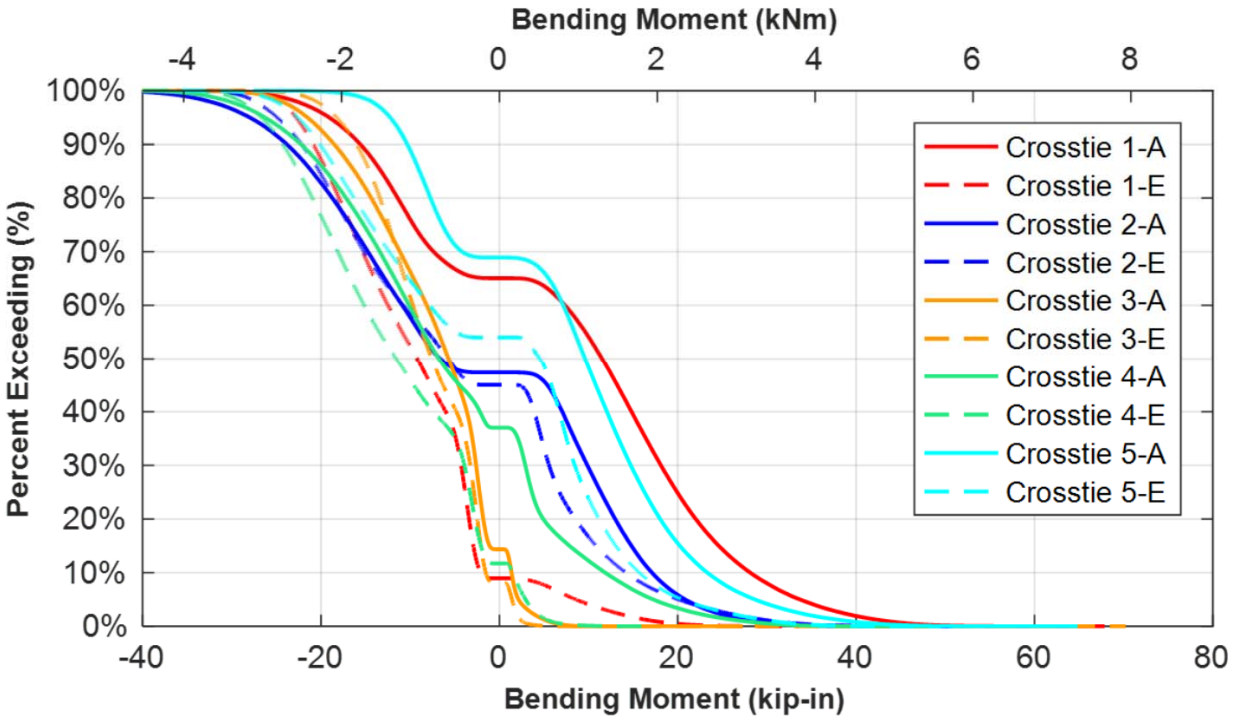

Figure 4.10: Distributions showing crosstie-to-crosstie variability of rail seat positive (RS+) bending moments for heavy rail transit loading on NYCTA.

With the exception of one rail seat's bending moment distribution (Crosstie 5-A), the crosstie-to-crosstie variability of the bending moments experienced on MetroLink were as low as 10%. The variability of the bending moments at both the rail seat (RS+) and crosstie center (C-) were considerably higher at NYCTA, reaching as high as 100% (a factor of 2). This range in variabilities is likely due to different support conditions generated by higher unique track deterioration rates due to the much heavier static railcar axle loads on NYCTA (approximately twice the magnitude of MetroLink). Additionally, the MetroLink track is newer. It was constructed in 2003 and has required little (if any) tamping since construction. Similar variability has been noted around other areas of special trackwork or track transition zones due to the higher loads and corresponding dynamic response of the track structure to these loads (Askarinejad et al., 2013; Zong et al., 2013).

4.5.3 Seasonal Effect on Bending Moments

Temperature-induced curl of the crosstie due to different temperatures on the top and bottom (i.e. a temperature gradient) has been shown to influence the flexural demand placed on the crosstie (Wolf et al., 2016b). Initially, curl was found to change over the course of the day as the temperature gradient changed, which was noted in both laboratory and field settings (Wolf, 2015a). Temperature gradients were also found to vary over the course of the year under HAL freight operations. These changes affected the bending moments induced in the concrete crossties (Wolf, 2015a; Wolf et al., 2016b), a behavior similar to what has been noted in rigid pavement applications (Beckemeyer et al., 2002).

Figure 4.11 shows the seasonal variation of bending moments throughout a year of data collection at MetroLink with single data points representing the average of a train pass over the site. Figure 4.12 shows similar data for NYCTA. For graphical clarity these data represent only one crosstie at each field-testing location, but the crosstie selected was indicative of the overall behavior noted at each site.

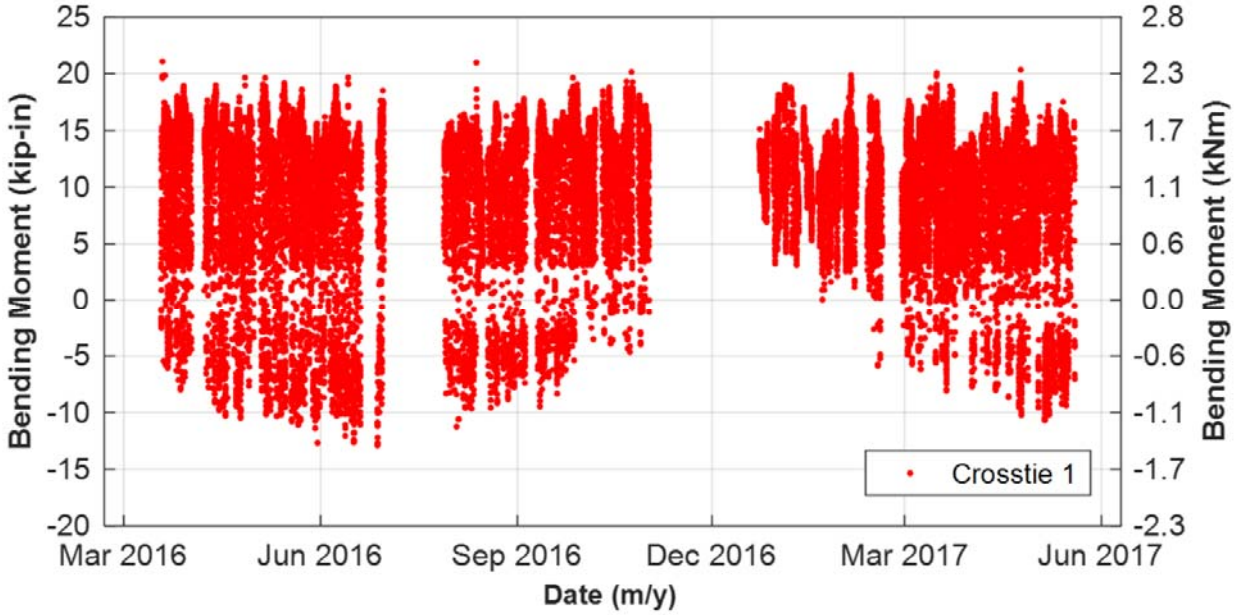

Figure 4.11: Distributions showing seasonal variation of center negative (C-) bending moments for light rail transit loading on St. Louis MetroLink.

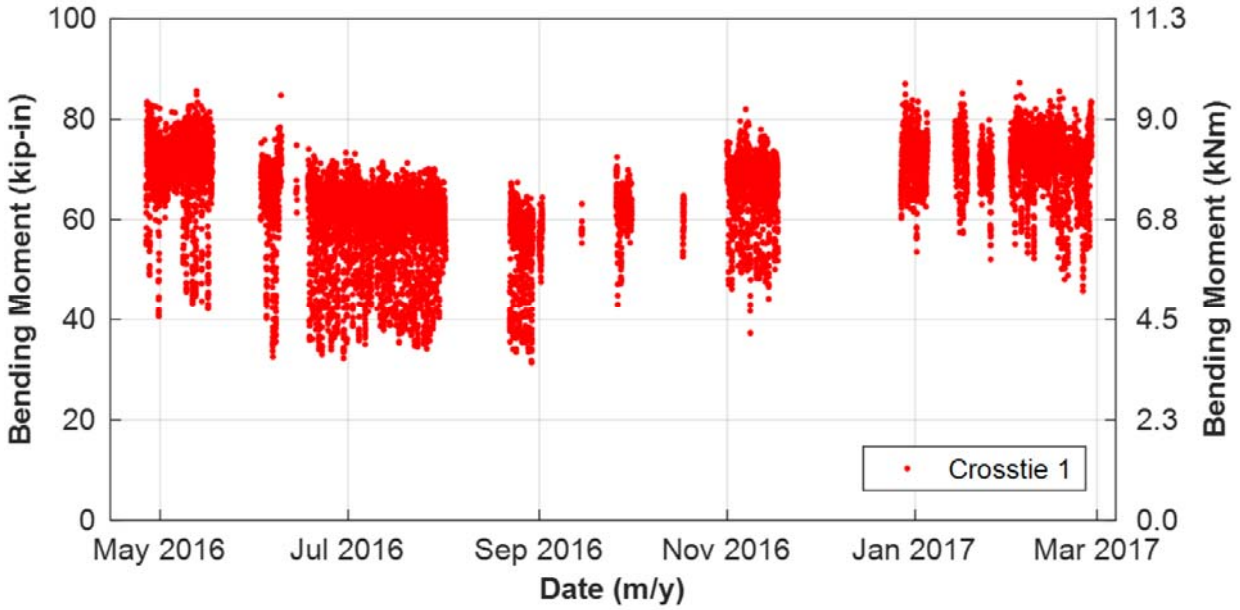

Figure 4.12: Distributions showing seasonal variation of center negative (C-) bending moments for heavy rail transit loading on NYCTA.

Seasonal variation is further demonstrated by extracting the daily average for each of the center gauges on the two rail transit systems, shown in Figure 4.13 and Figure 4.14 for MetroLink and NYCTA, respectively. The variation in absolute bending moment values seen in Figure 4.14 maps to the variability that was seen at the NYCTA field site as discussed above.

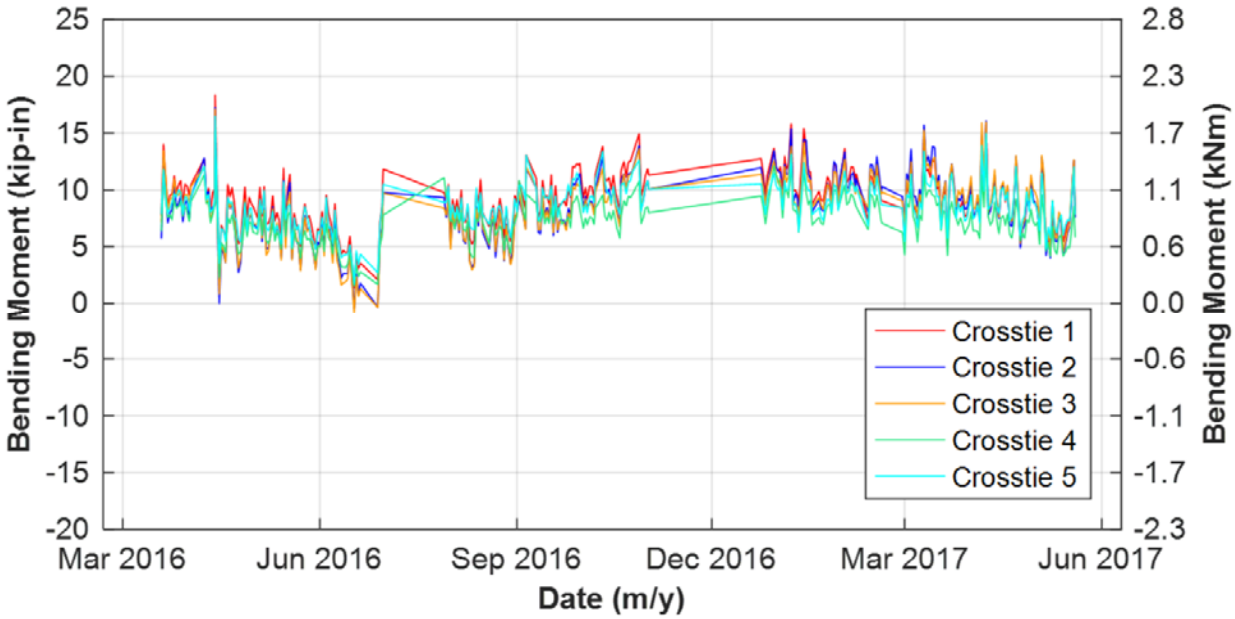

Figure 4.13: Distributions showing crosstie-to-crosstie variability of average train pass center negative (C-) bending moments for light rail transit loading on MetroLink.

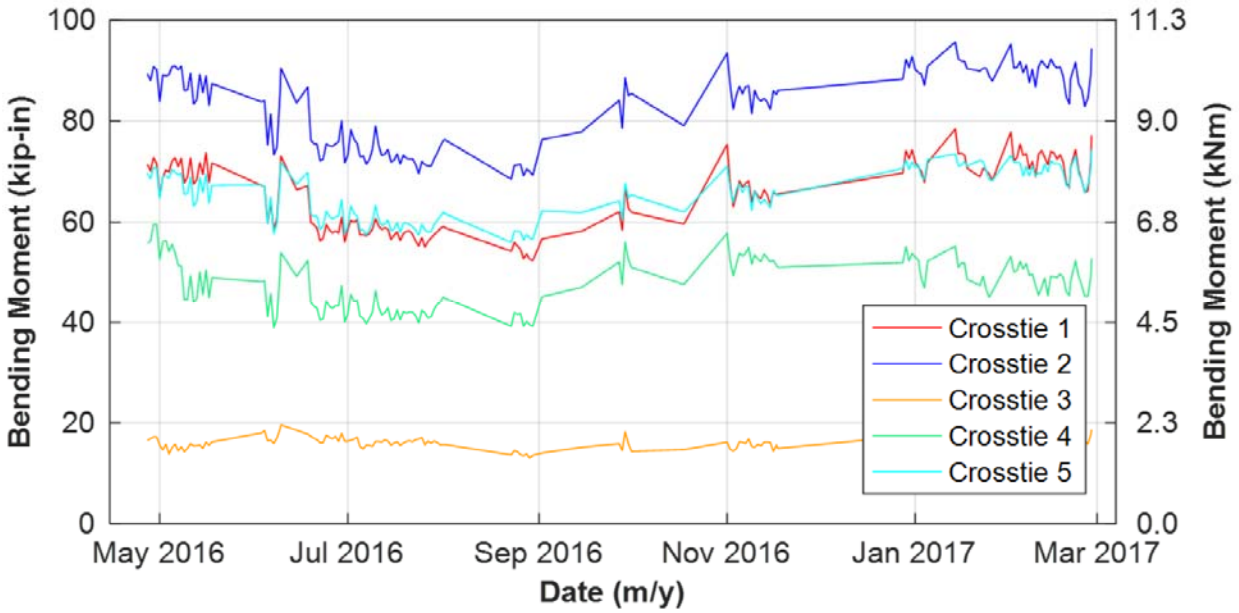

Figure 4.14: Distributions showing seasonal variation of average train pass center negative (C-) bending moments for heavy rail transit loading on NYCTA.

The daily average train pass fluctuations in bending moments ranged by as much as 30 kip-in (3.3 kNm) and 40 kip-in (4.5 kNm) for MetroLink and NYCTA, respectively. Despite these seasonal effects, the fluctuations in center negative (C-) bending moments due to daily temperature fluctuations exceeded seasonal variability by a factor of approximately two.

The data show a modest seasonal trend (Figure 4.13 and Figure 4.14) with higher absolute center negative bending moments occurring during the winter months consistent with the idea that track support is stiffer during cold weather (Hay, 1982; Cai et al., 1994). Additionally, while not investigated in this phase of the research, the physical deterioration of the crosstie is another factor that could affect the long-term flexural behavior of crossties. Temperature-induced curl and bending moment relationships were also documented by Canga Ruiz (2018), albeit over shorter time durations. He observed a change in bending moments of up to 30 kip-in (3.3 kNm) for MetroLink and 40 kip-in (4.5 kNm) for NYCTA (Figure 4.15).

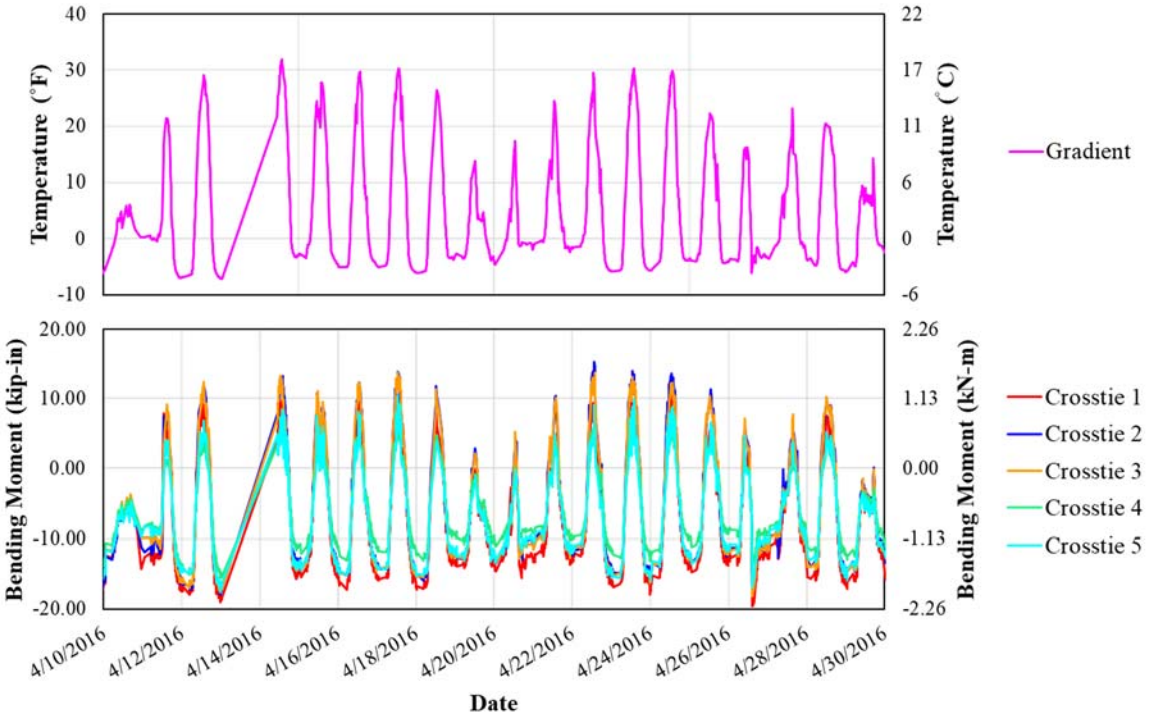

(a) Data from MetroLink

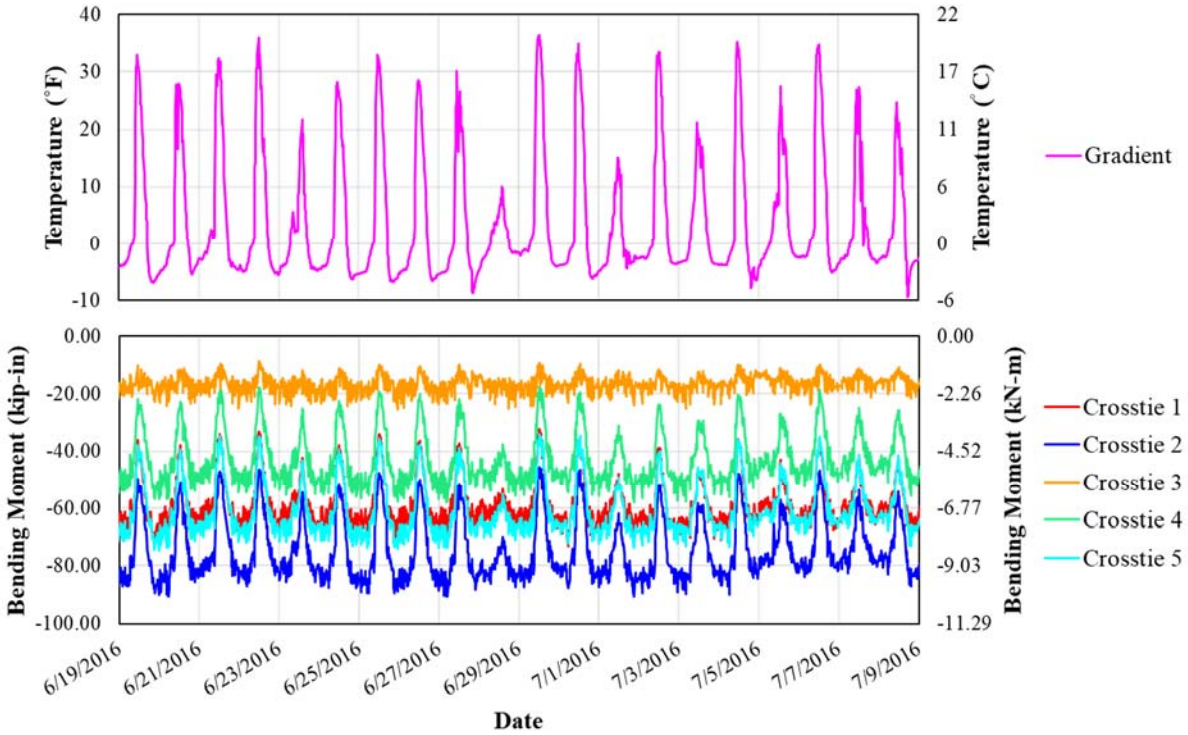

(b) Data from NYCTA

Figure 4.15: Comparison of temperature gradient and center bending moment variation as a function of time (Canga Ruiz 2018).

4.6 Conclusions

Concrete surface strain gauge instrumentation methodology and deployment successfully measured concrete crosstie bending strains and the resulting moments experienced by two rail transit modes in the United States. Through field deployments on MetroLink and NYCTA, were used to answer questions related to crosstie-to-crosstie variability, and the occurrence and magnitude of temperature-induced curl. The following conclusions were drawn from this research:

- The magnitude of maximum center negative bending moments ranged from 25 kip-in (2.8 kNm) on MetroLink to 120 kip-in (13.5 kNm) on NYCTA. Significant residual capacity was found in both systems. Considering the 99th percentile center negative (C-) bending moments, residual load capacities of approximately 6 and 2 were found for light and heavy rail transit systems, respectively.
- Bending moments vary widely from crosstie-to-crosstie. This was demonstrated on a HAL freight railroad, showing bending moments at the crosstie center that ranged from 0 kNm (0 kip-in) to 22.8 kNm (202 kip-in). This is consistent with prior research (Wolf et al., 2015; Wolf, 2015; Gao et al., 2016).
- Temperature-induced curl (e.g. warping of the crosstie due to different temperatures on the top and bottom) has a quantifiable impact on concrete crosstie flexural demand. Curl in concrete crossties was found to change over the course of the day as the temperature gradient changed. These changes affected the bending moments induced in the concrete crossties (Wolf, 2015a; Wolf et al., 2016b), a behavior similar to that which has been noted in rigid pavement applications (Beckemeyer et al., 2002).

CHAPTER 5: DEVELOPMENT OF PARAMETRIC MODEL FOR PREDICTION OF CONCRETE CROSSTIE BENDING MOMENTS

In this chapter I investigate the influence of a variety of predictor variables on the magnitude of concrete crosstie bending moments under revenue service train operations. These effects were explored through instrumentation installed on heavy rail transit (HRT) and heavy axle load (HAL) freight railroad field sites. I analyzed many months of data at each field site, and I quantified the effects of axle load, axle location (i.e. leading or trailing), train speed, ambient temperature, temperature gradient, and crosstie support conditions on the magnitude of both center and rail seat bending moments.

5.1 Background and Problem

As discussed in Chapters 1 and 4, flexural design is considered the most critical design element given its relationship to the structural integrity and long-term performance of the crosstie. Flexural design has largely been based on a static analysis of loads, with the application of estimated, empirically-derived impact factors. As such, it is important to quantify the variability in bending moments associated with load (wheel rail interface input loads) as well as other factors that may influence bending, including crosstie support conditions, axle location within truck, ambient temperature, and temperature gradient between top and bottom of crosstie (Wolf et al., 2016b). If data are available for these variables, a useful means of understanding the relative effect of each on bending moment is multiple linear regression and the generation of a parametric model.

Prior research aimed at understanding variability in the field performance of crosstie bending moment was conducted by Edwards et al. (2017a). Controlled laboratory experimentation in which the support conditions were varied in order to quantify their effect on bending has also been undertaken (César Bastos, 2016). Additionally, the effect of variability in temperature on bending moments has previously been considered (Wolf et al., 2016b; Canga Ruiz, 2018; Edwards et al., 2018b; Canga Ruiz et al., 2019). While all these efforts have provided insight into the influence of individual parameters on crosstie bending moment, none have addressed the relative importance and possible interactions among inputs as they relate to the calculation of bending moments.

To address this, I investigated the sources of bending moment variability using data from New York City Transit Authority (NYCTA) and a HAL freight railroad. Use of rail transit data enabled me to investigate variation in bending moments that are independent of load because of their lower wheel loads as compared to HAL freight service (Wolf, 2015a; Wolf et al., 2016b). This is partly due to the distinctly different loading magnitudes, combined with the similar sectional geometries of the crossties. Additionally, the selection of HAL freight data serves to increase the range of axle loads applied to crossties, providing insight into a broader range of factors that influence crosstie bending than would be possible with a review of rail transit data alone.

By developing a model that explains how critical variables affect bending moments, one can understand how to either improve new designs or adjust current maintenance practices. For example, if temperature gradient is a reliable predictor of flexural demand, future designs and/or maintenance strategies could account for this (assuming causation can be demonstrated in addition to correlation).

5.2 Methodology

5.2.1 Instrumentation Technology and Deployment

Surfaces strain gauges were deployed on concrete crossties using a procedure presented in Chapter 2 and summarized by Edwards et al. (2017c). Data from strain gauges were collected using a National Instruments (NI) compact data acquisition system (cDAQ) (Wolf, 2015a; Edwards et al., 2017c). cDAQ signals from the instrumentation were recorded through a NI LabVIEW virtual instrument (VI). A minimum sampling resolution of 0.5 inches (12.7 mm) and sampling rate of 2,000 Hertz was selected based on: the maximum authorized train speed at both of the field sites, desired data sampling resolution, prior experience, and expert recommendation.

5.2.2 Field Instrumentation Deployment (Site Descriptions)

The data collection discussed in this chapter was conducted on ballasted track locations on NYCTA at Far Rockaway, New York, and a HAL freight railroad in the western United States. Because of the observed variability of support conditions observed in previous field experimentation (Wolf, 2015a; Gao et al., 2016; Edwards et al., 2017a), and knowledge of load dispersion (Hay, 1982; Van Dyk, 2014), data were collected and processed from five consecutive crossties at the HRT field test location and a total of 10 crossties at the HAL freight location (in two five-crosstie zones).

5.2.3 Instrumentation Deployment on Crosstie

Concrete surface strain gauges were oriented longitudinally along the chamfer near the top surface of the crosstie to quantify bending strains at three critical locations along its length (Figure 2.4). The strain gauges (labeled A, C, and E) were used on each crosstie, with one applied at each of the two rail seats and one at the center (Figure 2.4). Additional relevant

dimensions and properties for the specific designs of crossties investigated in this chapter are included in Table 4.1.

5.3 Regression Analysis of Bending Moments

I conducted a regression analysis to understand which predictor variables were most useful in explaining the variability associated with a given response variable (in this case, center or rail seat bending moment). It is important to understand the ultimate objective of a model when determining how to construct it. For my purpose, focusing on concrete crosstie center negative and rail seat positive bending moments, I was interested in the relationships between predictor and response variables and in predicting bending moments. This meant that accurate estimates of the model parameters were of greatest importance. I could tolerate some multicollinearity among the predictor variables that would otherwise be undesirable (Kutner, 2005). Consequently, while investigating the effects of multicollinearity among predictor variables, I did not over-emphasize the need to mitigate their effects. Whenever possible, a smaller, more parsimonious model (i.e. one with fewer predictors) was preferred because it would facilitate simpler implementation of a future field experimentation program to collect necessary data.

There are, however, limitations to the use of regression analysis. First, correlation does not necessarily imply causation between predictor variables and the response variable. Second, it is important to understand that hidden extrapolations may exist, depending on the ranges of predictor variables that were sampled. These should be avoided to ensure that inaccurate inferences are not generated. Finally, broader generalization of these findings beyond the specific field sites surveyed should be undertaken with care for the reasons listed above.

Nevertheless, the utility of regression to investigate the effects of multiple predictors on the center and rail seat flexural demands for concrete crossties has value. The results will inform development of practices to generate mechanistic methods to quantify the flexural response of crossties and ultimately optimize their design.

5.3.1 Model Development

Four models were developed to account for bending moments at center and rail seat for both HRT and HAL freight lines. To address the question of which predictors best explain variability in bending moment data, a subset of a much larger dataset was used to build a model that predicts bending moment. The predictor variables that were considered for initial concrete crosstie bending moment model development are shown in Table 5.1. Different subsets of the predictor variables were used to model the rail seat or center moments, and these initial selections were made using *a priori* knowledge of which values had the ability to physically influence the response variables.

Table 5.1: Units and descriptions for predictor and response variables for development of concrete crosstie center and rail seat bending moment models

	Variables	Notation	Type	Unit	Description
Response	Center Bending Moment	M_C	Quantitative	kip-inches	Center bending moment measured by surface strain guages
Response	Rail Seat Bending Moment	M_{RS}	Quantitative	kip-inches	Rail seat bending moment measured by surface strain guages
Predictor	Vertical Load (one rail)	X_{i1}	Quantitative	kips	Vertical Load at Wheel Rail Interface
Predictor	Total Vertical Load	X_{i2}	Quantitative	kips	Summation of Both Vertical Loads
Predictor	Lateral Load	X_{i3}	Quantitative	kips	Lateral Load at Wheel Rail Interface
Predictor	Speed	X_{i4}	Quantitative	miles / hour	Speed of train at time of loading or moment capture
Predictor	Ambient Temperature	X_{i5}	Quantitative	°F	Temperature at field instrumentation site
Predictor	Temperature Gradient	X_{i6}	Quantitative	°F	Difference between the top of bottom surface of the crosstie
Predictor	Axle Location	X_{i7}	Classification	Binary	1=Leading, 2=Trailing axle on a given railcar's truck
Predictor	Season	X_{i8}	Classification	Binary	1=December-March, 0=Otherwise
Predictor	Crosstie Location	C_{LOC}	Classification	Integer, 10 Total	Identifies Different Crossties
Predictor	Rail Seat Location	RS_{LOC}	Classification	Integer, 10 Total	Identifies Different Rail Seats

A dataset containing a random sample of approximately 5,000 center and rail seat bending moment observations for each rail mode were used as training data to build the two models. An additional 5,000 observations were retained as testing data for each mode and bending moment location. In total there were approximately 9,800 trains processed at NYCTA, with 1,571,000 and 2,027,520 center and rail seat bending moment observations, respectively. For the HAL freight location, approximately 30 HAL freight trains were processed with 460 axles each resulting in 142,600 and 138,000 center and rail seat bending moment observations, respectively. The datasets were sampled in a manner that minimized bias by maximizing the coverage (range of values) for each predictor variable.

Preliminary models considered squared continuous predictor variables and interactions among all continuous predictor variables. The results from the second order model and a model containing both interactions and second order terms provided negligible gains in both the coefficient of multiple determination (R^2) and adjusted coefficient of multiple determination (R_a^2). This also introduced challenges with multicollinearity that limited the utility of the model. Thus, a second order model would not improve the ability to explain variability between predictors and the response variable, so I developed parsimonious first order parametric regressions.

The general form of one such model is shown in Equation 5.1, with the specific predictor variables listed in Table 5.1. The predictors associated with crosstie or rail seat location are separated from the independent predictors, as these vary among the models.

$$y_i = \beta_0 + \sum_{j=1}^{p} (\beta_j x_{ij}) + \sum_{k=p+1}^{p+q} (\beta_k x_{ik}) + \varepsilon_i \tag{5.1}$$

where,
y_i = value of response variable for trial *i*
$x_{i1}, x_{i2}, \ldots, x_{ij}, x_{ik}, \ldots, x_{i(p+k-1)}, x_{i(p+k)}$ = values of predictor variables for trial *i*
p = total number of predictor variables (not reflecting crosstie or rail seat location)
k = total number of predictor variables in the model (for crosstie or rail seat location)
β_0 = regression parameter for the intercept
β_j = regression parameter associated with x_{ij}
ε_i = random error term for trial *i*

Using the HRT and HAL data, SAS® software was used to construct two unique models for each of the two rail transport modes – one for rail seat and another for center bending moments. Using stepwise selection, I determined that all relevant (i.e. predictors related to the measurement under consideration) indicated in Table 5.1 should be included in each of the respective models. For the stepwise selection process to terminate, none of the variables omitted

from the model had an F statistic significant at $\alpha = 0.10$ and all variables remaining in the model were significant at $\alpha = 0.15$, which are commonly accepted values for model development (Kutner, 2005). There were only negligible improvements to the respective model's R^2 values if some of the latter variables were included in the models, indicating models with fewer predictors were probably feasible.

5.3.2 Evaluation of Parameters and Multicollinearity

Of specific interest were the parameter estimates, their standard errors, and the values within the covariance matrix, the latter of which allows for detection of multicollinearity of predictor variables. I discuss the independent development of center and rail seat bending below.

5.3.2.1 Center Bending Moments

Tables 5.2 provides parameter estimates for the full models for HRT and HAL freight center bending moment models along with their respective standard errors. Table 5.3 provides the same data for the reduced model. Visual inspection of the data indicates a large intercept term and relatively large and opposite sign parameter estimates for axle location. The latter result is inconsistent with prior findings demonstrating that leading axles apply greater load (Edwards et al. 2017a, 2017b; Van Dyk et al., 2017).

Table 5.2: Parameter estimates and standard errors for full concrete crosstie center bending moment model

Variable	Units	Heavy Rail Transit		HAL Freight	
		Parameter Estimate	Standard Error	Parameter Estimate	Standard Error
Intercept	kip-inch	-76.920	1.705	-103.564	3.677
Vertical Load	kips	-0.318	0.049	-0.247	0.038
Speed	mph	0.057	0.019	-0.392	0.041
Ambient Temp.	Deg. F	0.290	0.009	0.565	0.031
Temp. Gradient	Deg. F	0.548	0.011	0.496	0.022
Axle Location	1=Lead; 0=Trail	-8.110	0.216	6.089	0.387
Season	Binary (1 = Winter)	2.456	0.333	26.541	1.085
Crosstie 1	1=Crosstie; 0=Not Crosstie	1.073	0.300	-12.659	0.848
Crosstie 2		-15.746	0.305	17.076	0.861
Crosstie 3		46.832	0.303	-43.682	0.872
Crosstie 4		12.229	0.305	-108.784	0.872
Crosstie 5		N/A	N/A	-59.585	0.874
Crosstie 6		N/A	N/A	-37.803	0.856
Crosstie 7		N/A	N/A	-17.192	0.868
Crosstie 8		N/A	N/A	-36.900	0.859
Crosstie 9		N/A	N/A	-36.057	0.851

Table 5.3: Parameter estimates and standard errors for reduced concrete crosstie center bending moment model

Variable	Units	Heavy Rail Transit		HAL Freight	
		Parameter Estimate	Standard Error	Parameter Estimate	Standard Error
Intercept	kip-inch	-52.816	1.311	-79.980	2.180
Vertical Load	kips	-0.456	0.050	-0.233	0.038
Temp. Gradient	Deg. F	0.681	0.011	0.485	0.022
Axle Location	1=Lead; 0=Trail	-8.263	0.236	6.008	0.413
Crosstie 1	1=Crosstie; 0=Not Crosstie	1.081	0.337	-12.367	0.904
Crosstie 2		-15.805	0.343	17.539	0.917
Crosstie 3		46.798	0.340	-43.416	0.928
Crosstie 4		12.183	0.342	-108.076	0.928
Crosstie 5		N/A	N/A	-59.212	0.930
Crosstie 6		N/A	N/A	-37.314	0.912
Crosstie 7		N/A	N/A	-16.627	0.925
Crosstie 8		N/A	N/A	-36.024	0.914
Crosstie 9		N/A	N/A	-35.760	0.906

The covariance matrix revealed that there was minimal multicollinearity of parameters, with the exception of the predictor for season, which was highly correlated with both ambient temperature and temperature gradient. The removal of season increased the mean square error (MSE) from 232 to 250, and R_a^2 decreased from 0.82 to 0.80 for HAL freight. A similar, minimal effect was observed for HRT. As such, season was retained in the model as a predictor variable. Additionally, there was only moderate correlation between speed and vertical load, which was unexpected based on a review of previous literature on the interaction between speed and wheel load (Van Dyk et al., 2017; Edwards et al., 2018a). Finally, given that the inclusion of both speed and temperature in the model did little to improve it, these predictors were removed. No other values in the variance-covariance matrix were significant ($\alpha = 0.05$).

A parsimonious model that excluded speed, ambient temperature, and season was developed (Table 5.3). These three predictor variables showed moderate to high levels of multicollinearity and previous research indicated that they were correlated with other variables already in the model (e.g. relationship between ambient temperature and temperature gradient). Any remaining multicollinearity was related to the classification variables and their interaction with the continuous predictors. Their variance inflation factors were low (always less than two) thus they were not a concern (Kutner, 2005).

Temperature gradient parameter estimates differed by approximately 40% for HRT and HAL freight and were calculated as 0.681°F (0.378°C) and 0.485°F (0.269°C), respectively. Assuming equal magnitude temperature gradients for both locations (but opposite in sign) ranging from -9°F (-5°C) to 38°F (21°C) this results in additional center negative bending moments of up to 26 kip-in (2.9 kNm). For the rail transit crosstie, this additional thermal-induced bending moment is 13% of the center design capacity and 45% of the mean center

flexural demand observed. For HAL freight, a 26 kip-in (2.9 kNm) additional moment represents 21% of the mean flexural service demand observed. Temperature gradient rather than ambient temperature was selected as a predictor given the direct relevance of gradient to the flexural response of the crosstie due to the influence of thermal expansion and crosstie curling.

5.3.2.2 Rail Seat Bending Moments

I developed parameter estimates for HRT and HAL freight rail seat bending moments along with their respective standard errors. The data indicate a negative intercept term. This was not initially expected for rail seat moments because they are generally thought to be positive. Unlike the crosstie center, the parameter estimates associated with axle location were similar for both modes. This is of interest because this is where the load is first transferred into the crosstie. It indicates that the opposite effect observed at the center was either an artifact of the location where the data were collected, or indicative of a dynamic response of the crosstie that is different at the center and rail seat.

A review of the covariance matrix revealed that there was significant multicollinearity of temperature gradient and lateral load and a variety of other combinations. As such, several predictors were removed with the objective of reducing multicollinearity. As in the center bending moment model discussed in the previous section, the removal of season had a minimal effect on the quality of the model predictions. After removal of the aforementioned predictor variables, a significant correlation between lateral load and vertical load remained. Removal of lateral load improved the model, and no values in the covariance matrix were significant ($\alpha = 0.05$).

Again, applying the principal of parsimony, a model was generated that excluded speed, ambient temperature, and season (Table 5.4). These three predictor variables showed moderate to high levels of multicollinearity and were previously identified to be correlated with other variables already included in the model. Like the center bending moment models, the variables retained in the final rail seat bending moment model are vertical load, temperature gradient, and axle location. It is of interest that the temperature gradient has a much larger parameter estimate for HRT (0.58) compared to HAL freight (0.07). As such, temperature gradient was excluded as a predictor for HAL freight (Table 5.4).

Table 5.4: Parameter estimates and standard errors for reduced rail seat bending moment model

Variable	Units	Heavy Rail Transit		HAL Freight	
		Parameter Estimate	Standard Error	Parameter Estimate	Standard Error
Intercept	kip-inch	-9.505	1.150	70.889	1.574
Vertical Load	kips	1.235	0.086	-0.451	0.054
Temp. Gradient	Deg. F	0.582	0.014	Excluded	Excluded
Axle Location	1=Lead; 0=Trail	-13.958	0.286	-3.345	0.216
Rail Seat 1/A1	1=Rail Seat; 0=Not Rail Seat	10.802	0.612	7.354	0.696
Rail Seat 2/E1		-9.476	0.605	-5.350	0.682
Rail Seat 3/A2		-0.520	0.612	-41.209	0.707
Rail Seat 4/E2		-2.495	0.605	-41.234	0.692
Rail Seat 5/A3		-11.928	0.612	-39.768	0.683
Rail Seat 6/E3		-12.028	0.605	-27.268	0.697
Rail Seat 7/A4		-4.319	0.612	1.729	0.687
Rail Seat 8/E4		-13.690	0.605	-23.018	0.683
Rail Seat 9/A5		10.202	0.612	-32.364	0.697

A summary of the final models for both center and rail seat moments is provided in Table 5.5, demonstrating which predictor variables were included in each of the four models previously introduced.

Table 5.5: Comparison of predictor variables for each of the fitted regression models

			Initial Model		Final Model	
Variable	**Notation**	**Unit**	**Center**	**Rail Seat**	**Center**	**Rail Seat**
Center Bending Moment	M_C	kip-inches	●		●	
Rail Seat Bending Moment	M_{RS}	kip-inches		●		●
Vertical Load (one rail)	X_{i1}	kips		●		●
Total Vertical Load	X_{i2}	kips	●		●	
Lateral Load	X_{i3}	kips		●		
Speed	X_{i4}	miles / hour	●	●		
Ambient Temperature	X_{i5}	°F	●	●		
Temperature Gradient	X_{i6}	°F	●	●	●	●*
Axle Location	X_{i7}	Classification	●	●	●	●
Season	X_{i8}	Classification	●	●		
Crosstie Location	C_{LOC}	Classification				
Rail Seat Location	RS_{LOC}	Classification		●		●

*Only in Heavy Rail Transit Model

5.4 Model Validation

Another 5,000 data points were randomly extracted from each dataset to validate the models. The parameter estimates generated when running the final model with these new data were similar to the ones generated with the training dataset and final predictor variables (Tables 5.2 through 5.5). There was agreement between the training and validation parameter estimates and standard errors for crosstie center bending moments. Similar agreement was found for rail seat bending moment testing data but is not included for purposes of brevity (Table 5.6). This was expected due to the large size of the dataset used to generate the model, and its convergence on representation of the total population. Given the similarity of these values, further validation of the model was deemed unnecessary.

Table 5.6: Comparison of parameter estimates and standard errors for model building and model validation data for concrete crosstie center bending moments

Variable	Unit	Heavy Rail Transit				HAL Freight			
		Training Data		Validation Data		Training Data		Validation Data	
		Parameter Estimate	Standard Error	Parameter Estimate	Standard Error	Parameter Estimate	Standard Error	Parameter Estimate	Standard Error
Intercept	kip-inch	-52.816	1.311	-51.340	1.430	-79.980	2.180	-78.650	2.163
Vertical Load	kips	-0.456	0.050	-0.505	0.054	-0.233	0.038	-0.260	0.038
Temp. Gradient	Deg. F	0.681	0.011	0.648	0.012	0.485	0.022	0.481	0.022
Axle Location	1=Lead; 0=Trail	-8.263	0.236	-8.499	0.250	6.008	0.413	6.479	0.414
Crosstie 1	1=Crosstie; 0=Not Crosstie	1.081	0.337	0.831	0.359	-12.367	0.904	-12.131	0.925
Crosstie 2		-15.805	0.343	-15.394	0.357	17.539	0.917	17.807	0.895
Crosstie 3		46.798	0.340	46.356	0.361	-43.416	0.928	-43.757	0.909
Crosstie 4		12.183	0.342	11.807	0.357	-108.076	0.928	-108.330	0.906
Crosstie 5						-59.212	0.930	-60.062	0.907
Crosstie 6						-37.314	0.912	-37.580	0.924
Crosstie 7			N/A			-16.627	0.925	-16.863	0.906
Crosstie 8						-36.024	0.914	-37.850	0.915
Crosstie 9						-35.760	0.906	-36.080	0.932

5.5 Model Functionality and Use

Given proper validation of the parsimonious models as described earlier, they can now be used to predict center bending moments given values for predictor variable coefficients. As discussed above, these predictions should be made with the range of data in mind. In the next two sub-sections I will discuss the prediction of moments, absent consideration of support condition variability, in an attempt to understand the influence of non-support related variables.

5.5.1 Center Moment Prediction

Equations 5.2 and 5.3 facilitate the prediction of center bending moments for the HRT and HAL freight field sites, respectively. The prediction equations are incomplete, given that they do not include a term for support conditions. This factor will be included in the model later and is referred to as R (support **R**eaction). After estimating the regression parameters, the final fitted models are shown in Equations 5.2 and 5.3 for center moment prediction on HRT and HAL freight, respectively, where $\hat{y}_i$ is the expected value of y_i (see Table 5.1 for additional nomenclature of predictor variables).

$$\hat{y}_{HRTcenter} = -52.8 - 0.456x_{i2} + 0.681x_{i6} - 8.263x_{i7} + \mathrm{R} \quad (5.2)$$

$$\hat{y}_{HALcenter} = -79.9 - 0.233x_{i2} + 0.485x_{i6} - 6.01x_{i7} + \mathrm{R} \quad (5.3)$$

5.5.2 Rail Seat Moment Prediction

Equations 5.4 and 5.5 facilitate the prediction of rail seat bending moments for HRT and HAL freight, respectively. These equations follow the same general form as Equation 5.2, and do not include a term for rail seat location.

$$\hat{y}_{HRTrailseat} = -9.51 - 1.23x_{i1} + 0.582x_{i6} - 14.0x_{i7} + \mathrm{R} \quad (5.4)$$

$$\hat{y}_{HALrailseat} = -79.9 - 0.451x_{i1} - 3.34x_{i7} + \mathrm{R} \quad (5.5)$$

5.5.3 Crosstie Support Effects

Crosstie or rail seat location was used as a proxy for support condition, as prior research has indicated significant variation in support among crossties (Wolf, 2015a; Edwards et al., 2017c, 2018b). To build on these findings, parameter estimates generated in the two models I developed provide another method for quantifying variability. For HRT, parameter estimates for crossties range from -16 kip-in (1.8 kNm) to 47 kip-in (5.3 kNm) and those that are thought to have poorer support are negative (Table 5.3 and Figure 5.1). For HAL freight, parameter estimates for crossties that are thought to have poor support range from -108 kip-in (12.2 kNm) to -36 kip-in (4.1 kNm) (Table 5.3 and Figure 5.1). The disparity among crosstie location

parameters signifies the differences in support conditions in the two modes and their relative contribution to center negative bending moment.

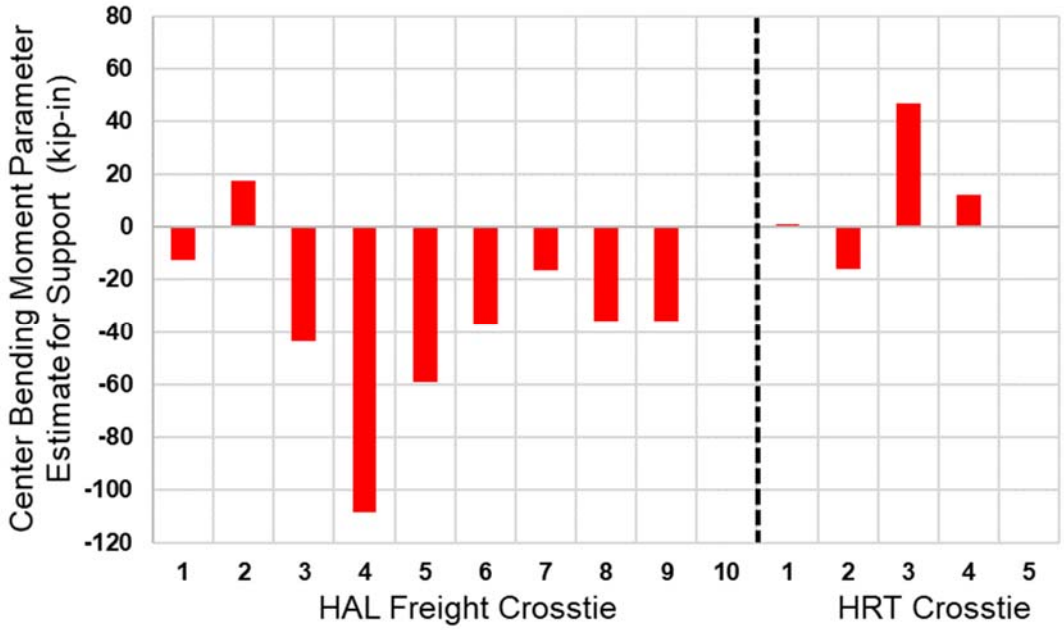

Figure 5.1: Comparison of parameter estimates for crosstie location for use in the prediction of crosstie center bending moments.

The disparity is also seen among rail seats (Figure 5.2). Support condition parameter estimates for negative rail seat moments range from -14 kip-in (4.6 kNm) to 11 kip-in (1.2 kNm) for HRT and -41 kip-in (4.6 kNm) to 7 kip-in (0.8 kNm) for HAL freight. These range of parameter estimates for rail seat support are lower than center support. This is due to support at the rail seat having less influence on rail seat bending than variations in support at the crosstie center. The latter drives high bending moments due to the comparatively long moment arm from the center of the crosstie to the point of load application, which is the rail seat.

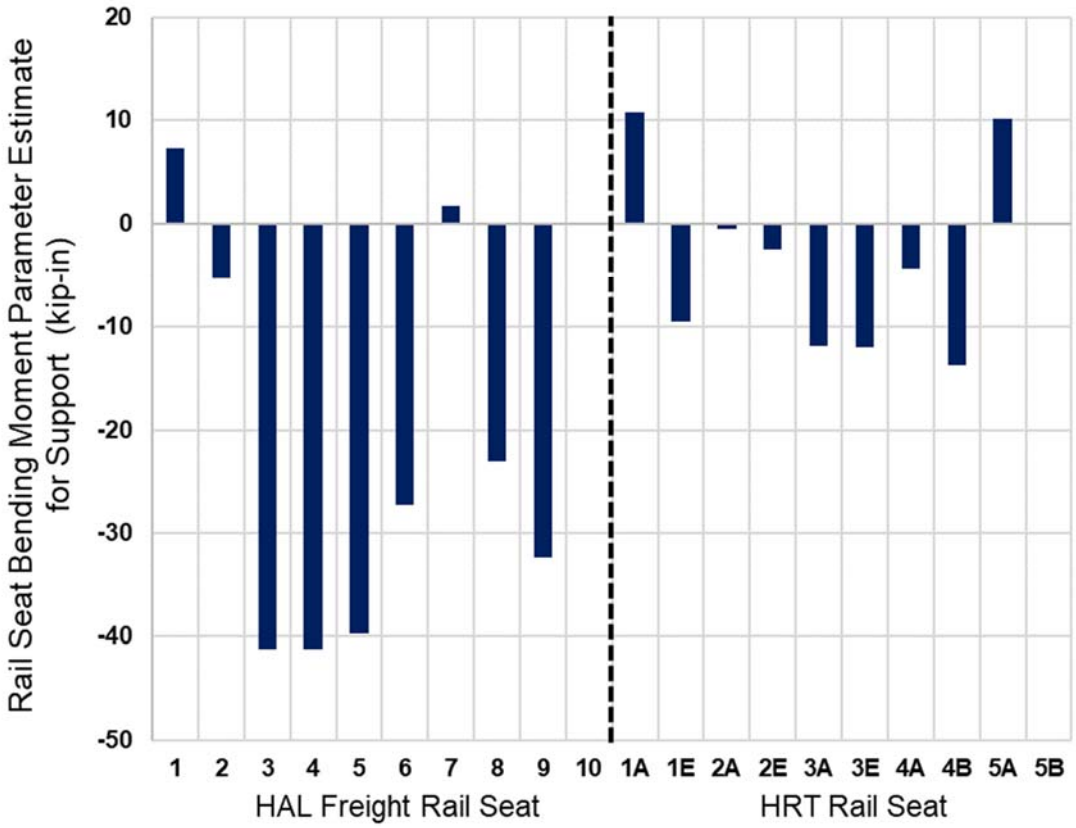

Figure 5.2: Comparison of parameter estimates for rail seat location for use in the prediction of crosstie center bending moments.

Figures 5.1 and 5.2 indicate the significant influence that support condition has on crosstie bending. Focusing on the objective of the research described in this chapter (model development) and absent *a priori* knowledge of how the crosstie is supported, it is difficult to assign estimates to a parameter that relates to crosstie or rail seat location. One possibility is to assume general groupings and categories of the aforementioned predictors for crosstie location, assuming that the subset of crossties and rail seats tested are representative of the broader set of support conditions likely to be encountered. Using this approach, Table 5.7 provides low, average, and high values for the range of possible support conditions. These values can be added to Equations 5.2 through 5.5 to include the effect of support condition.

Table 5.7: Constants proposed for use in the prediction of rail seat and center moments to include the influence of support condition variability

Rail Mode	Symbols	Center Negative			Rail Seat Positive		
		Low	Average	High	Low	Average	High
Heavy Rail Transit	R_{HRC-}, R_{HRRS+}	46.80	0.00	-18.81	-13.69	0.00	10.80
HAL Freight	R_{HALC-}, R_{HALRS+}	17.54	-35.76	-108.00	-41.23	-5.35	7.35

5.5.4 Explanation of Variability

To use the model to explain the variability between predictor variables and response variables, the change in bending moments was plotted for both center and rail seat locations for both field locations (Figures 5.3 and 5.4). The sensitivity of center bending moments to predictor variables representing load, temperature gradient, and axle location is quite low compared to the influence of support condition. The intercept values for both modes and moments are also plotted using solid horizontal lines, and the first crack flexural capacity for both modes is shown using a dashed horizontal line. Reviewing the results in comparison to the various capacities provides insight on the relative magnitude of each of the predictor variable's influence.

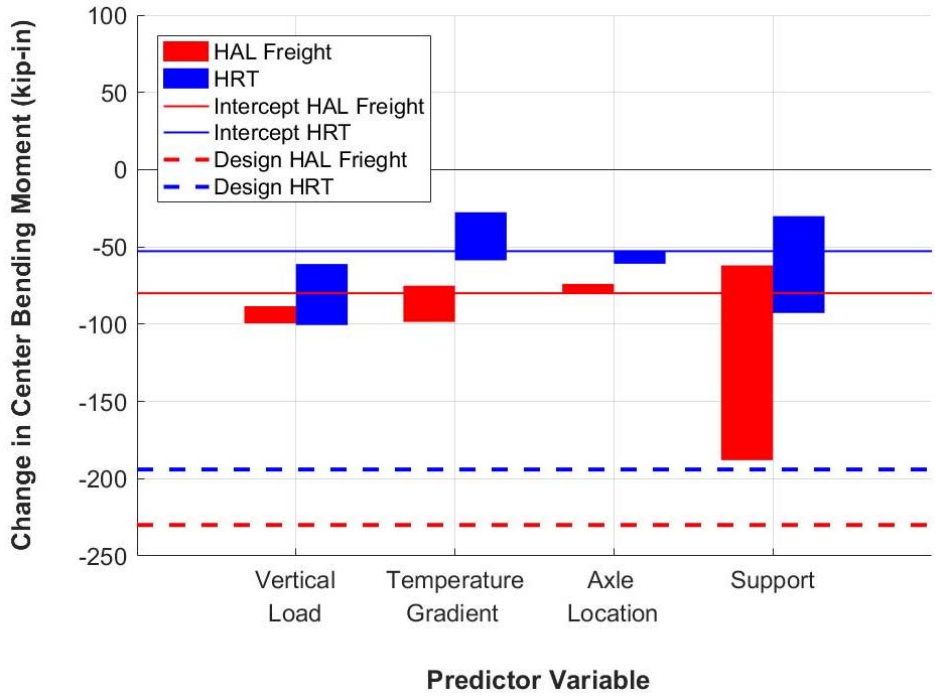

Figure 5.3: Sensitivity of center bending moments to changes in predictor variables.

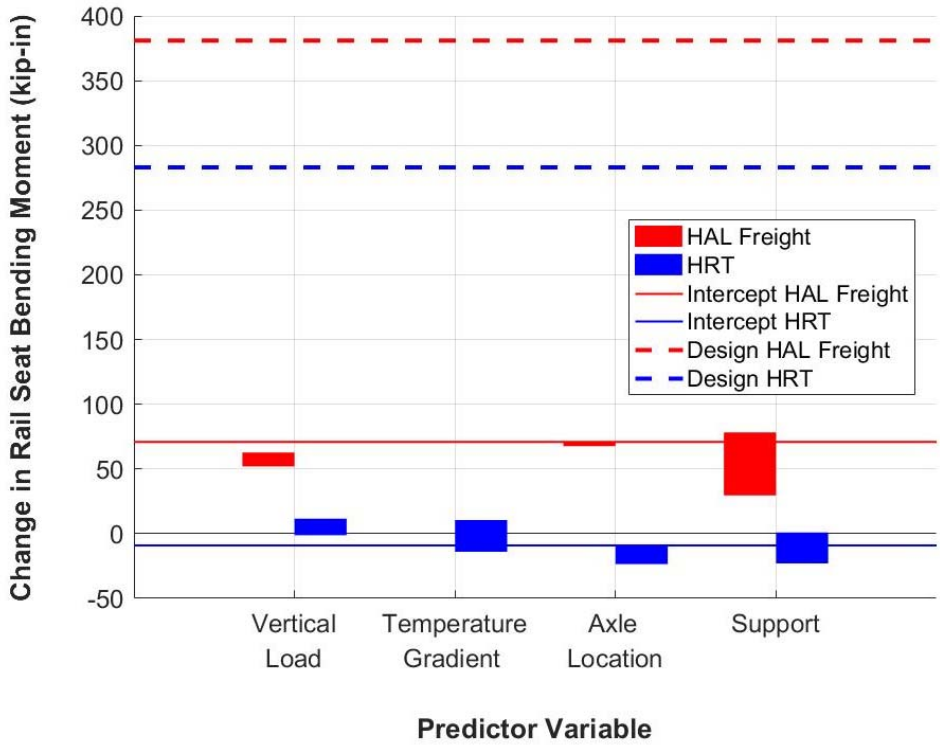

Figure 5.4: Sensitivity of rail seat bending moments to changes in predictor variables.

For the rail seat region, the sensitivity of bending moments to predictor variables load, temperature gradient, and axle location is similar in magnitude to the influence of support condition (Figure 5.4). This aligns with earlier conclusions related to the different moment arms and resulting sensitivities of support conditions at the crosstie center and rail seat regions.

5.6 Conclusions

The installation of concrete surface strain gauge instrumentation on HRT and HAL freight railroad concrete crossties was successful in measuring bending strains and resulting moments at both the center and rail seat. Data were used to generate four distinct multiple linear regression models for prediction of moments to understand the interaction and influence of key parameters.

For center bending moment prediction, I identified an opposite effect of axle location on center bending moment for HAL and HRT. The magnitude of the center bending moment variation due to axle location is likely due to the response time of the crosstie as it receives load and reacts in bending. The opposite effect for the two modes is most likely due to different support conditions present at the two sites. The effects of vertical axle load and train speed are minimal, which is unexpected based on prevailing design standards (AREMA, 2016). Previous work by Wolf et al. (2016) on the effect of temperature was extended in this study and its effects were significant, especially at the crosstie center. The effect is similar in both rail transport modes studied, and provides a useful metric for considering the effect of temperature differentials on concrete crosstie bending moments. The effect of train speed and axle load was much less pronounced at the center than expected.

A notable finding with respect to rail seat moment prediction is the minimal influence of support conditions, limited sensitivity to wheel-rail interface vertical load, and that temperature gradient was unnecessary for generating an accurate model of rail seat bending for HAL freight.

For both center and rail seat bending moments, the predictor that describes the most variability is crosstie or rail seat location, which is considered a proxy for support condition. This finding builds on prior research demonstrating the importance of adequate support for crossties to reduce bending moment demand.

Equations 5.2 through 5.5 in combination with Table 5.7 provide a means of predicting center and rail seat field bending moments for HRT and HAL operations. Future work should aim to develop more generalized models that facilitate broader application of the findings in this study. Specifically, this research suggests the need to consider temperature gradient in the design of crossties (Canga Ruiz et al., 2019). This research also indicates the variability and influence of support conditions on the flexural response of the crosstie and its implication to maintenance practices. Finally, additional research on the effect of axle location on crosstie center flexural demand was identified.

CHAPTER 6: PROBABALISTIC APPROACH TO THE DESIGN OF CONCRETE CROSSTIE FLEXURAL STRENGTH

6.1 Background

In this chapter, I develop and demonstrate a novel, probabilistic method for the analysis and design of concrete crosstie flexural strength based on field bending moment data. The method was applied to case studies on heavy rail transit (HRT) and heavy axle load (HAL) freight infrastructure to demonstrate its validity for crosstie design optimization under two different rail transport systems.

As discussed earlier in this dissertation, the flexural design of concrete crossties is widely considered as the most critical design element, given its direct relationships to the structural integrity and long-term performance of the crosstie. To date, flexural design is based largely on a static analysis of loads, with the application of empirically-derived impact factors that vary widely in the international railway engineering community. The primary input into methods for the flexural design of crossties is the rail seat load, which is considered in conjunction with assumed crosstie support conditions. Quantification of these values has been challenging from an experimental standpoint, thus assumptions are made related to increase in wheel load over static (i.e. dynamic and impact loading), percentage of wheel load transferred to the rail seat under the point of load application, and expected support conditions for both center and rail seat regions.

Prevailing international concrete crosstie design practices are deterministic in nature. They rely on load factors to ensure conservatism in design that covers the probabilistic nature of

both the loading (demand) and the capacity of crossties. Additionally, there are no known design practices that incorporate empirical field bending moment data, largely due to the scarcity of these data and the challenges associated with interpolation and extrapolation of field results to the variety of applications in which concrete crossties are used.

In the United States, exceptions to the normal method of design include the preliminary application of structural reliability analysis (SRA) to light rail transit crossties as presented by Canga Ruiz (2018) and research aimed at using field data and other best practices to design the next generation of concrete crossties for Amtrak's Northeast Corridor (NEC) (Quirós-Orozco et al., 2018). Additionally, reliability analysis methods were developed at the University of Wollongong in Australia (Remennikov et al., 2012). The methodologies I present in this Chapter extend this preliminary work to a broader set of data from additional rail transport modes and development of a framework for both the analysis of existing crosstie designs and design of future crossties using a probabilistic approach based on SRA methods.

6.2 Introduction

Documentation of the need for concrete crosstie structural design optimization in the United States can be found as early as 1970 (RMSA), coinciding with their initial installation. Prior research into the structural design of railway crossties has been conducted by Remennikov et al (2012) using a probabilistic approach, Wakui and Okuda (1997) and Murray (2015) using a limit state approach, and Harris et al. (2011) using more traditional optimization methods. Remennikov et al (2012) presents an approach that infers rail seat loads, and resulting flexural demands, from Wheel Impact Load Detector (WILD) data. This process is the most robust concrete crosstie design method proposed to date; considering both field loading and design

capacity in a probabilistic manner. The inference of rail seat loads from WILD data, however, leaves room for error. Results from field experimentation have shown substantial variability in the percentage of wheel load that is transferred to the rail seat beneath the point of load application (Edwards et al., 2017a, 2017b). This research also found that even small gaps (less than ¼ in.) between the crosstie and ballast can result in wide variability in applied rail seat loads and bending moments. Controlled laboratory experimentation varying support conditions and quantifying their impact on bending has also been undertaken to demonstrate how bending moment demand is sensitive to support conditions (César Bastos, 2016; César Bastos et al., 2017). Research has also shown that variability in temperature can affect bending moments in the field (Wolf et al., 2016b; Canga Ruiz, 2018; Edwards et al., 2018b; Canga Ruiz et al., 2019), which is another factor that is not considered in a method that relies solely on input loading at the wheel rail interface to calculate flexural demand.

Bending moment variability is due to a variety of factors (predictor variables) that relate to the stiffness of the track structure and the uniformity of ballast beneath the crosstie. The effect of these predictor variables was investigated in previous research described in Chapter 5. Regardless, the topic of bending moment variability warrants additional research to holistically quantify moments under a variety of operating and loading conditions.

The relationship between wheel loads and rail seat loads, and thus bending moments, is non-linear, as shown by Prause and Kish (1978) and more recently by Quirós-Orozco (2018). This finding further demonstrates the importance of using bending moment data as the primary input into a design process for concrete crossties and not being reliant on functional relationships between wheel loads and bending moments.

6.3 Probabilistic Design

The concept of probabilistic design was proposed by Kalay and Samuels (2002) in the context of reducing the "stress state of the railroad." Stress state reduction lends itself to a probabilistic analysis their proposed approach viewed changes to rolling stock gross rail load and wheel condition and track infrastructure design in terms of its impact on either the stress (i.e. demand) or strength (i.e. capacity) of the system.

More specifically, the flexural design of concrete railway crossties lends itself to a probabilistic approach. This method is well developed and documented in the literature (Ang and Tang, 2006) and has been frequently applied in the realm of structural design (Soares, 1997; Elishakoff, 2017). The field of SRA continues to evolve (Frangopol et al., 1997; Der Kiureghian, 2008; Steenbergen et al., 2013) and provides a viable method for assessing the design of many types of structural elements, including crossties, further substantiating the need for, and feasibility of, a probabilistic design approach.

There has been no comprehensive application of SRA methods to concrete crosstie design using bending moments as the input for generating a demand model, although a preliminary analysis by Canga Ruiz (2018) was undertaken to demonstrate the viability of such an approach for light rail transit. The significant body of research conducted by Remennikov et al. (2012) is the most robust probabilistic undertaking of track component design to date. Beyond the aforementioned research related to concrete crossties, there has been limited probabilistic consideration of the analysis of the track substructure and its behavior (Lee, 2013) with some application to the performance of rail steel, albeit in terms of risk assessment and not design, per se (Jamshidi et al., 2017).

The best input into an SRA or probabilistic design methodology for the flexural capacity of concrete crossties are field data representative of the actual flexural demands. Such a methodology has been developed (Edwards et al., 2017c) and deployed by researchers at UIUC to answer a variety of engineering questions related to crossties and the field moment demands placed on them (Wolf et al., 2016a; Canga Ruiz, 2018; Edwards et al., 2018b; Quirós-Orozco et al., 2018). This method is documented and demonstrated in Chapters 2 and 4.

After a preliminary application of SRA methods to validate the need for a more optimized design approach, I propose a probabilistic methodology using data from both an HRT property and a HAL freight railroad. The selection of flexural response data from both HRT and HAL freight sources was due, in part, to the distinctly different loading magnitudes yet similar crosstie cross-sectional properties, facilitating an interesting comparison between the concrete crosstie designs and their expected loading conditions.

The application of probabilistic design and SRA for the analysis and design of concrete crossties is interesting from an academic standpoint for several reasons. First, large variation in loading conditions are generated by a variety of different types of railroad rolling stock and a wide range of wheel conditions and resulting impact loads. Second, the occurrence of both positive and negative bending at the rail seat and center cross sections due to differing crosstie support conditions is of interest and is largely absent from other prestress concrete applications. Finally, the availability of large quantities of reliable demand data collected using field instrumentation is unique (described in Chapters 2, 4, and 5).

6.4 Part I - Analysis

As an initial step toward concrete crosstie probabilistic design, and to quantify the potential value in pursuing such a method, I first undertake a quantitative evaluation of the center flexural capacity of existing crosstie designs using SRA methods similar to what was demonstrated by Canga Ruiz (2018) for another rail transit mode. There is a difference between the design specification value and actual flexural capacity of a crosstie. This difference represents an internal safety factor that concrete crosstie manufacturers apply to ensure that even their "weakest" crossties exceed the specified design value specified by the end user to minimize rejection of product due to inadequate flexural capacity. Additionally, a portion of this differential may be due to the discrete nature of key inputs in the crosstie design and manufacturing process (e.g. an integer number of wires can be used, finite grades of prestressing steel, etc.) Beyond this safety factor, results from previous field experimentation have indicated that there is significant excess design capacity (actual capacity exceeding service demand), highlighting the need for optimization of crossties and the selection of a probabilistic design method (Wolf et al., 2016a; Edwards et al., 2017c, 2018b; Quirós-Orozco et al., 2018). This is especially true for rail transit crossties (Edwards et al., 2018b).

Current design standards use only deterministic parameters for both the demand and capacity of concrete crossties (Figure 6.1A). The demand is augmented with dynamic and impact factors to increase the static bending moment. The capacity is augmented by applying safety factors to account for variability in this deterministic application. The specific values used to incorporate variability and estimate capacity and demand will be discussed in later sections, but are often derived through trial and error, occasionally supported by experimental results.

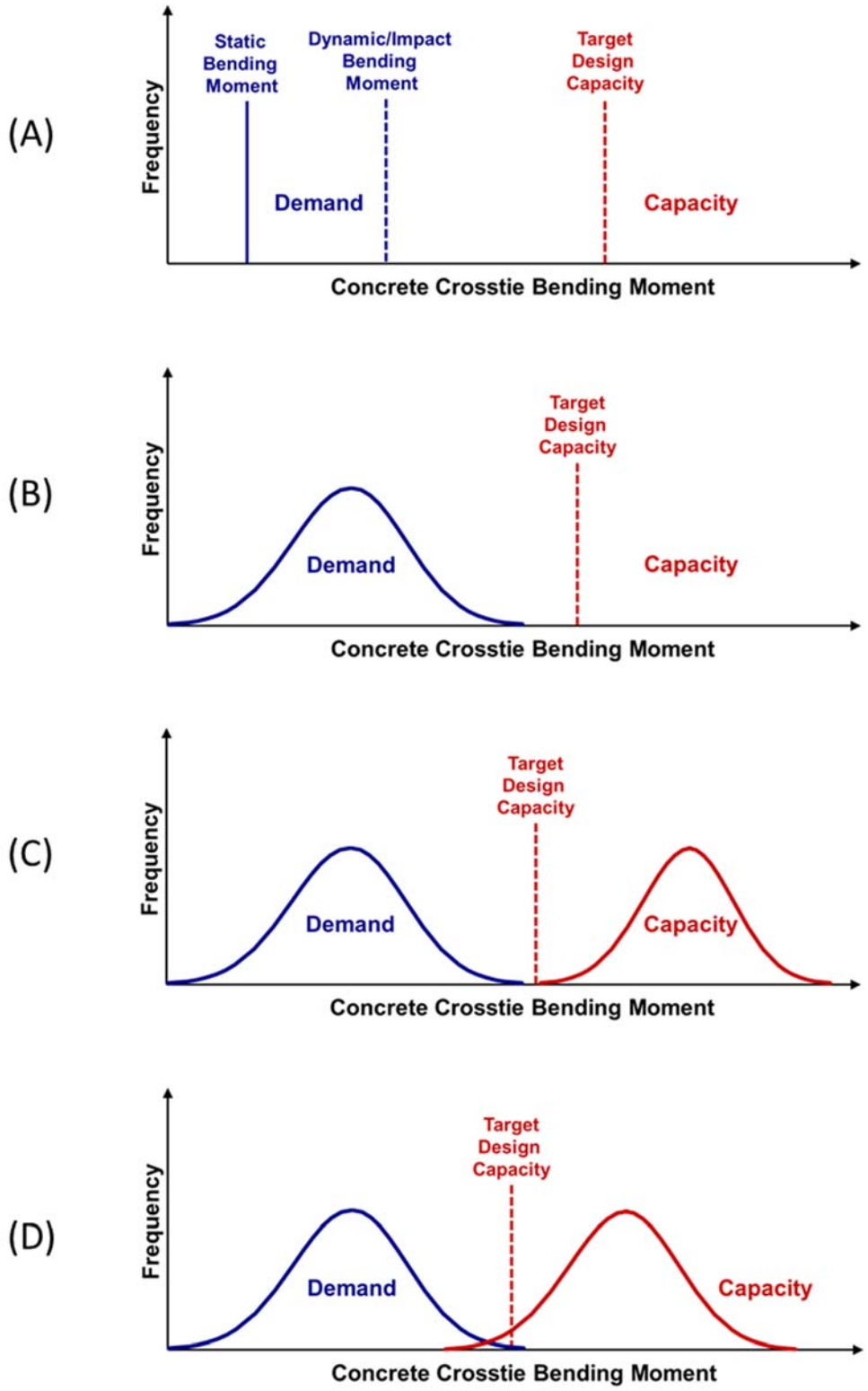

Figure 6.1: Qualitative representation of design considerations for concrete crossties; (A) deterministic scenario with no consideration of probability, (B) probabilistic (and empirical) demand curve, (C) some reserve capacity as demonstrated by probabilistic design, and (D) some acceptance of risk using probabilistic design.

When interpreting field bending moments, and generating quantitative numbers for residual design capacity, previous research has only considered a constant, deterministic value for the design capacity of the crosstie (Edwards et al., 2017c, 2018b) (Figure 6.1B). This is a simplification of a more detailed approach that considers a statistical distribution of capacities for manufactured products and their inherent variability. This is a mature topic that has received considerable study (Radford, 1922). This probabilistic distribution is shown for two scenarios; one in which there is excess (residual) capacity indicating that the system has the potential for being optimized (Figure 6.1C) and an optimized scenario that considers some level of risk acceptance (Figure 6.1D).

Additionally, from the standpoint of the concrete crosstie manufacturer, the specification bending moment values are the "demand." This would indicate that only the right half of Figure 6.1C is the primary focus of the crosstie manufacturer. Having the design process driven by the end user allows a more holistic incorporation of probabilistic design principles that encompass both the demand on, and capacity of, the component (Figure 6.1D).

The vertical lines in Figure 6.1 indicate the current, deterministic, manner by which design capacities are discussed in practice and in the literature, specified by end users, and used for the evaluation of residual bending capacity (or lack thereof). For the probabilistic design method proposed in this chapter, I will use the metric of bending moment, measured in kip-inches (kNm) given it is the most widely used metric to quantify the "strength" of concrete crossties. Additionally, I will use probability density functions (PDFs) as the primary means of visualizing bending moment data.

In addition to macro-level probabilistic considerations between a demand and capacity curve for a given crosstie, there are also considerations among capacity curves that must be

understood (Figure 6.2). There are multiple distributions that are reflective of the capacity of a crosstie from when it is produced until it is removed from service. First, prior to manufacture, there is a singular deterministic capacity that is specified by the end user. To ensure that the crossties are manufactured to meet or exceed the stated end-user capacity, a manufacturer will increase the average capacity to ensure the left-hand tail of the capacity distribution does not penetrate below the manufacturer's design capacity. Doing so would result in rejection of product and attendant cost and loss of revenue by the manufacturer. Additionally, given the time-dependent nature of concrete strength growth, the final capacity of the crosstie is typically far greater than the manufacturers' design capacity or the target (specification) capacity. These applied safety factors and their variation make the capacity modeling non-trivial. For my research, I will use the target design capacity (specification value) and consider its probabilistic distribution. This is due in part to the final objective of this work, which is an optimized design capacity that is practical for use by industry.

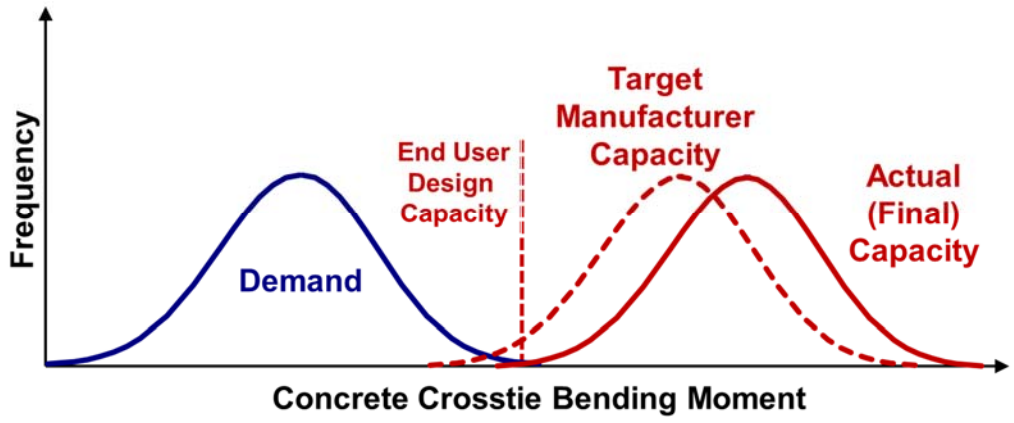

Figure 6.2: Qualitative representation of the probabilistic capacity-related design considerations for concrete crossties.

6.4.1 Development of Demand Model

The first element in the SRA process employed in this research is the assessment of concrete crossties to obtain reliable field data that represent the flexural demands placed on concrete crossties. These data need to be collected at both the center and rail seat sections given that both regions are critical sections that warrant independent design analysis using a sectional method (César Bastos, 2016).

6.4.1.1 Instrumentation Technology – Concrete Surface Strain Gauges

To quantify crosstie bending moments, concrete surface strain gauges were deployed in the field during revenue service train operation. This method was previously developed, deployed, and validated under heavy axle load (HAL) freight (Edwards et al., 2017c) and rail transit applications (Edwards et al., 2018b) (discussed in Chapter 2).

6.4.1.2 Instrumentation Deployment on Crosstie

Concrete surface strain gauges were oriented longitudinally along the chamfer near the top surface of the crosstie to quantify bending strains at three critical locations along the length of the crosstie. The strain gauges (labeled A, C, and E) were applied to each crosstie, with one at each of the two rail seats and one at the center (Figure 4.1).

Table 6.1: Characteristics of HRT and HAL freight railroad loading conditions and crosstie structural geometric properties for the locations considered in this study

Crosstie / System Characteristic			Heavy Rail Transit		HAL Freight	
			SI	US Cust.	SI	US Cust.
Static Wheel Loads	Maximum (AW3)*		62.9 kN	14.1 kips		
	Minimum (AW0)*		50.6 kN	11.4 kips		
	Loaded 286k Car				159 kN	35.8 kips
	Empty 286k Car (Approx.)				36.7 kN	8.25 kips
Crosstie Geometry	Length		2.59 m	8’ 6”	2.59 m	8’ 6”
	Tie Spacing		0.61 m	24”	0.61 m	24”
Crosstie Prestressing	Number of Wires		18		20	
	Jacking Force		31.1 kN	7 kips	31.1 kN	7 kips
	Precompression (Center)		13,858 kN/m^2	2.01 ksi	15,444 kN/m^2	2.24 ksi
Crosstie Cracking Moment	Center Negative	Specification	19.0 kN-m	168 kip-in	26.0 kN-m	230 kip-in
		Design	21.9 kN-m	194 kip-in	26.0 kN-m	230 kip-in
	Center Positive	Specification	13.3 kN-m	118 kip-in	N/A	N/A
		Design	14.9 kN-m	132 kip-in	21.0 kN-m	186 kip-in
	Rail Seat Positive	Specification	28.3 kN-m	250 kip-in	33.9 kN-m	300 kip-in
		Design	32.0 kN-m	283 kip-in	43.1 kN-m	381 kip-in
	Rail Seat Negative	Specification	15.6 kN-m	138 kip-in	N/A	N/A
		Design	20.1 kN-m	178 kip-in	24.7 kN-m	219 kip-in

*AW0 loads are the as-delivered, ready to operate static loads and AW3 loads (crush load) represent the AW0 load plus the weight of seated passengers and an additional “live load” of 6 standing passengers / square meter, a common load used for passenger vehicle design.

Additional relevant dimensions and properties for the specific designs of crossties investigated are shown in Table 6.1. Further information on the deployment of instrumentation is described in Chapters 2 and 4 and have been published by Edwards et al. (2017c). Table 6.1 also includes the owner-provided “specification” value that must be met or exceeded to avoid crosstie cracking. Design values represent the first crack capacities associated with the unique crosstie designs that are supplied by the crosstie manufacturers.

To relate the field-measured strains to center and rail seat bending moments, calibration factors were generated through laboratory experimentation at UIUC's RAIL per the methods described in Chapter 2 and documented by Edwards et al. (2017).

6.4.1.3 Field Instrumentation Deployment

The field instrumentation and data collection discussed in this chapter were conducted on ballasted HRT track locations on the New York City Transit Authority (NYCTA) at Far Rockaway, NY (hereafter referred to as "HRT") and a high-density mainline HAL freight railroad location in the western United States (hereafter referred to as "HAL freight"). Because of the observed variability of support conditions observed in past field experimentation (Wolf, 2015a; Gao et al., 2016; Edwards et al., 2018b), and knowledge of load dispersion (Hay, 1982; Van Dyk, 2014), data were collected and processed from multiple consecutive crossties, with a minimum of five crossties at both field installations, as discussed in Chapter 4.

6.4.2 Findings

A dataset containing a random sample of approximately 5,000 center and rail seat bending moment observations for each rail mode were used to generate the four demand models (center and rail seat models, for both rail modes). These data were extracted from a larger set containing approximately 1,571,000 and 2,027,520 HRT center and rail seat bending moment observations, respectively. For the HAL location, data were extracted from a sample of approximately 142,600 and 138,000 center and rail seat bending moment observations. These data were also used in Chapter 5 for the development of a parametric model for prediction of center and rail seat bending moments.

Additionally, prior research documented in Chapter 5 provided confidence that the data set is representative of the population. Figure 6.3 shows raw data for rail seat and center bending moments for HRT and Figure 6.4 provides the same data for HAL freight systems.

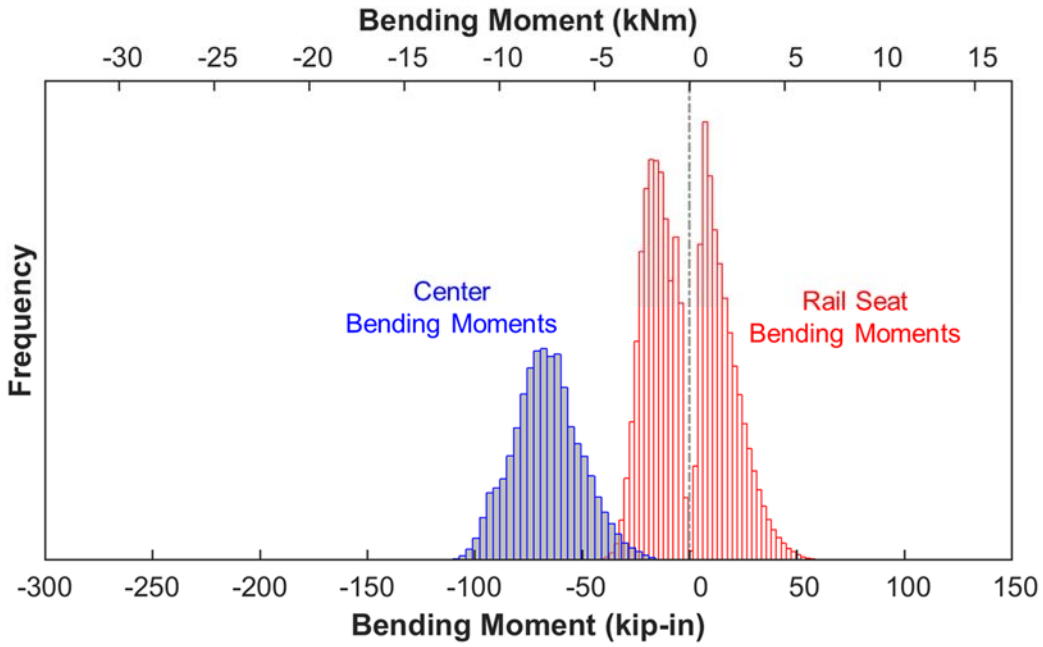

Figure 6.3: Histogram of raw data of crosstie rail seat and center bending moments used to generate demand models for HRT.

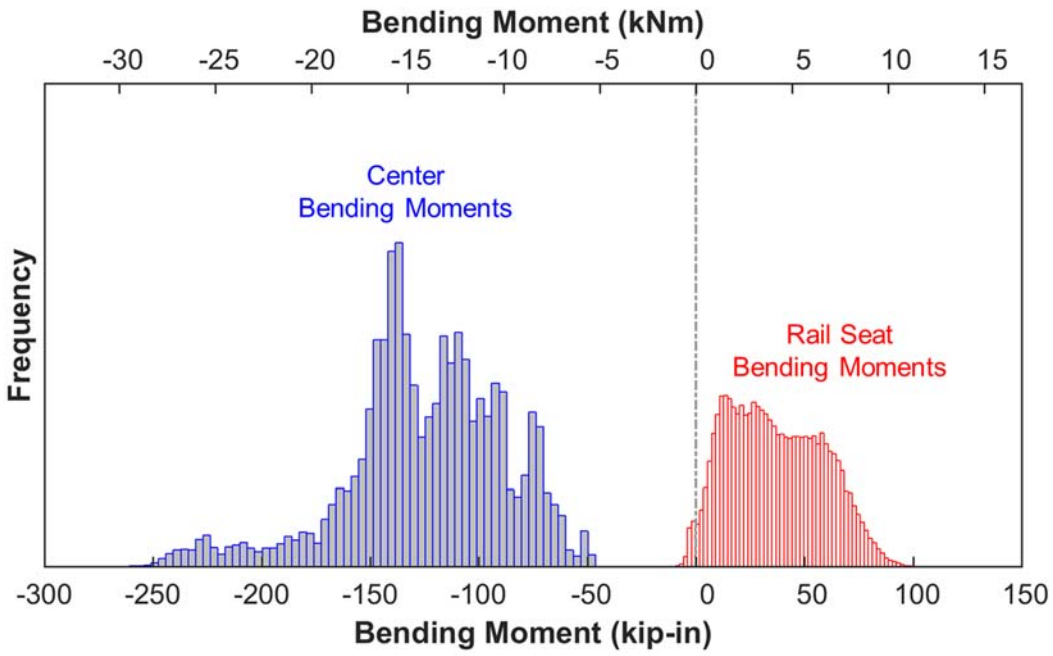

Figure 6.4: Histogram of raw data of crosstie rail seat and center bending moments used to generate demand models for HAL freight.

The bi-modal nature of the HRT rail seat bending moment data (Figure 6.3) is due to the methods used to filter the data. Given that most rail seat bending moments were close to zero, peak extraction from the data stream is challenging, and very small negative or positive values are selected instead of zero, as it is highly unlikely that zero moment is produced when the wheel is directly above a rail seat. The magnitude of the rail seat moments is negligible compared to any reasonable design capacity, thus the primary weakness of this form of data extraction is the subsequent visual representation of the data and depiction of two modes that are not actually present in the field.

As expected, the demand placed on HAL crossties is greater than that which is placed on HRT crossties, both at the center and rail seat regions. This is mostly driven by the large difference in wheel loads (Table 6.1). It should also be noted that bending moments are induced that are opposite to what is commonly expected (i.e. center positive and rail seat negative

bending), which require special attention and analysis (as will be discussed later) and provide a unique loading scenario that is atypical of most previous SRA applications.

To develop bending moment demand distributions and establish fitted curves for further analysis, data were analyzed in MATLAB and the commercially available software EasyFit (by MathWave Technologies). EasyFit considers 65 of the most common distributions (e.g. log-logistic, Gamma, normal, Weibull, etc.) for comparison and fitting purposes, and was also used in Chapter 3 for the analysis of wheel-rail interface loads and their distributions. In summary, EasyFit facilitates the estimation of parameters for fitted PDFs and cumulative distribution functions (CDFs). To evaluate the adequacy of the fit of the selected distributions both the Kolmogorov-Smirnov (K-S) and Anderson-Darling tests were employed. The Anderson-Darling procedure is based on calculation of its test statistic, given by Equation 6.1.

$$A^2 = -n - \sum_{i=1}^{n} \frac{2i-1}{n} \left[\ln\left(F(Y_i)\right) + \ln\left(1 - F(Y_{n+1-i})\right) \right] \tag{6.1}$$

Where;
A^2 = Anderson-Darling test statistic
n = Number of data points in sample
i = i^{th} sample when the data is sorted in ascending order
Y_i = Individual data points, ordered
F = Cumulative distribution function of the specified distribution

As compared to the K-S test, the Anderson-Darling test has advantages that are applicable to the engineering questions being considered here. The Anderson-Darling method is especially useful for this application because it increases the power of the K-S statistic to investigate the tails of the distribution and produces a weighted statistic (Darling, 1957; Press et al., 2002; Engmann and Cousineau, 2011). Additionally, there is evidence that the Anderson-

Darling test can detect very small differences in the goodness of fit for distributions, even for large sample sizes such as what are used for this research (Engmann and Cousineau, 2011).

As is the case with wheel-rail interface loading data (see Chapter 3), focusing on the tail is important given our application for the design of future railway track infrastructure components. The best-fit (optimal) distribution was then selected using the Anderson-Darling criteria, with priority given to distributions that are more commonly recognized, and of a lower order (e.g. avoidance of three or four parameter models). The rank ordered results, sorted by Anderson-Darling are presented in Tables 6.2 and 6.3 for HRT and Tables 6.4 and 6.5 for HAL freight, respectively.

Table 6.2: Ranking of common distributions by goodness of fit for HRT center bending moment distributions using the K-S and Anderson-Darling tests

	Anderson-Darling		Kolmogorov-Smirnov	
Distribution	**Parameter**	**Rank**	**Parameter**	**Rank**
Gen. Gamma (4P)	1.83	1	0.0194	7
Johnson SB	1.88	2	0.0179	5
Burr (4P)	2.13	3	0.0164	2
Burr	2.18	4	0.0166	3
Beta	2.24	5	0.0190	6
Normal	2.86	6	0.0235	14
Weibull (3P)	2.99	7	0.0201	10
Weibull	3.21	8	0.0198	9
Error	3.34	9	0.0263	15
Kumaraswamy	3.35	10	0.0209	11
Gen. Logistic	3.89	11	0.0168	4
Log-Logistic (3P)	4.02	12	0.0196	8
Lognormal (3P)	5.86	13	0.0306	16
Gen. Extreme Value	7.17	14	0.0224	12
Logistic	7.89	15	0.0232	13
Gamma (3P)	8.70	16	0.0359	19
Erlang (3P)	10.31	17	0.0405	21
Pearson 6 (4P)	11.96	18	0.0414	22
Chi-Squared (2P)	12.56	19	0.0425	23
Nakagami	14.02	20	0.0308	17
Hypersecant	18.37	21	0.0377	20
Gamma	26.86	22	0.0457	24
Pearson 6	27.81	23	0.0555	27
Gen. Gamma	29.20	24	0.0575	28
Erlang	33.27	25	0.0545	26
Rice	34.74	26	0.0754	34
Laplace	46.71	27	0.0643	29
Log-Logistic	47.50	28	0.0664	32
Inv. Gaussian	49.75	29	0.0500	25
Lognormal	54.86	30	0.0766	35
Cauchy	60.93	31	0.0792	37
Fatigue Life	62.51	32	0.0841	41
Log-Gamma	68.34	33	0.0838	40
Gumbel Min	71.85	34	0.0661	31
Fatigue Life (3P)	77.36	35	0.0919	42
Inv. Gaussian (3P)	78.56	36	0.0923	43
Pert	96.70	37	0.0783	36
Pearson 5	98.57	38	0.1008	44
Pearson 5 (3P)	117.31	39	0.1086	45
Gumbel Max	120.92	40	0.0825	38

Table 6.3: Ranking of common distributions by goodness of fit for HRT rail seat bending moment distributions using the K-S and Anderson-Darling tests

	Anderson-Darling		Kolmogorov-Smirnov	
Distribution	**Parameter**	**Rank**	**Parameter**	**Rank**
Error	36.82	1	0.0689	6
Pert	37.57	2	0.0663	4
Beta	42.72	3	0.0711	7
Kumaraswamy	44.84	4	0.0739	9
Triangular	47.33	5	0.0728	8
Weibull (3P)	49.67	6	0.0745	10
Gen. Gamma (4P)	50.71	7	0.0825	11
Gen. Extreme Value	54.57	8	0.0847	12
Gamma (3P)	54.70	9	0.1031	21
Fatigue Life (3P)	58.39	10	0.1052	23
Inv. Gaussian (3P)	58.82	11	0.1048	22
Lognormal (3P)	60.81	12	0.1029	19
Frechet (3P)	61.52	13	0.1120	25
Pearson 5 (3P)	62.58	14	0.1004	17
Pearson 6 (4P)	63.32	15	0.1023	18
Dagum (4P)	68.01	16	0.1185	27
Chi-Squared (2P)	69.40	17	0.0916	13
Normal	70.98	18	0.0936	14
Log-Logistic (3P)	72.21	19	0.1075	24
Rayleigh (2P)	74.79	20	0.0994	16
Burr (4P)	74.81	21	0.1211	28
Error Function	76.66	22	0.1029	20
Johnson SB	88.62	23	0.0664	5
Gen. Logistic	93.88	24	0.0990	15
Gumbel Max	100.21	25	0.1228	29
Logistic	117.42	26	0.1148	26
Erlang (3P)	147.98	27	0.1677	34
Hypersecant	159.95	28	0.1302	30
Cauchy	179.07	29	0.1390	31
Gumbel Min	207.21	30	0.1534	32
Laplace	240.76	31	0.1555	33
Gen. Pareto	431.96	32	0.0600	2
Wakeby	431.96	33	0.0600	1
Power Function	512.85	34	0.2333	35
Exponential (2P)	687.58	35	0.2833	36
Phased Bi-Exponential	775.58	36	0.3217	37
Uniform	864.28	37	0.0620	3
Levy (2P)	1269.20	38	0.4575	38
Phased Bi-Weibull	6054.00	39	0.6086	40
Student's t	8153.00	40	0.4770	39

Table 6.4: Ranking of common distributions by goodness of fit for HAL Freight center bending moment distributions using the K-S and Anderson-Darling tests

	Anderson-Darling		Kolmogorov-Smirnov	
Distribution	**Parameter**	**Rank**	**Parameter**	**Rank**
Burr	14.77	1	0.0513	9
Gen. Logistic	16.56	2	0.0540	17
Log-Logistic (3P)	17.66	3	0.0578	22
Pearson 5 (3P)	17.97	4	0.0532	16
Gen. Gamma	18.09	5	0.0496	4
Gamma	18.16	6	0.0497	5
Lognormal (3P)	18.22	7	0.0531	15
Gen. Extreme Value	18.32	8	0.0503	7
Fatigue Life (3P)	18.51	9	0.0528	14
Log-Pearson 3	18.84	10	0.0518	10
Gamma (3P)	18.93	11	0.0525	11
Johnson SB	18.94	12	0.0528	13
Erlang	19.27	13	0.0569	21
Gen. Gamma (4P)	19.28	14	0.0526	12
Beta	19.53	15	0.0512	8
Weibull (3P)	22.43	16	0.0610	25
Kumaraswamy	22.69	17	0.0614	26
Dagum (4P)	24.97	18	0.0563	20
Logistic	26.53	19	0.0452	2
Chi-Squared (2P)	26.71	20	0.0600	23
Lognormal	26.95	21	0.0678	28
Nakagami	27.30	22	0.0648	27
Error	27.45	23	0.0498	6
Fatigue Life	27.97	24	0.0683	30
Log-Logistic	28.84	25	0.0800	34
Inv. Gaussian	28.95	26	0.0684	31
Hypersecant	31.32	27	0.0545	18
Frechet (3P)	31.69	28	0.0704	32
Log-Gamma	34.07	29	0.0755	33
Normal	34.13	30	0.0678	29
Rayleigh (2P)	40.17	31	0.0606	24
Inv. Gaussian (3P)	43.46	32	0.0821	36
Gumbel Max	43.68	33	0.0810	35
Pearson 6	44.91	34	0.0824	37
Rice	45.99	35	0.0492	3
Pearson 5	47.07	36	0.0844	39
Pert	47.21	37	0.0904	41
Weibull	51.98	38	0.0555	19
Laplace	56.10	39	0.0824	38
Erlang (3P)	61.55	40	0.0908	42

Table 6.5: Ranking of common distributions by goodness of fit for HAL Freight rail seat bending moment distributions using the K-S and Anderson-Darling tests

	Anderson-Darling		Kolmogorov-Smirnov	
Distribution	**Parameter**	**Rank**	**Parameter**	**Rank**
Pert	12.69	1	0.0379	6
Beta	13.04	2	0.0379	7
Triangular	13.41	3	0.0301	4
Kumaraswamy	15.27	4	0.0421	9
Error	17.97	5	0.0358	5
Gen. Gamma (4P)	19.93	6	0.0452	12
Weibull (3P)	20.63	7	0.0414	8
Burr (4P)	21.77	8	0.0448	11
Gen. Extreme Value	24.31	9	0.0432	10
Gamma (3P)	27.22	10	0.0552	20
Fatigue Life (3P)	29.33	11	0.0547	18
Lognormal (3P)	30.40	12	0.0532	17
Rayleigh (2P)	30.60	13	0.0471	14
Pearson 6 (4P)	31.24	14	0.0521	16
Pearson 5 (3P)	31.25	15	0.0519	15
Frechet (3P)	32.52	16	0.0609	22
Chi-Squared (2P)	36.93	17	0.0551	19
Log-Logistic (3P)	40.24	18	0.0575	21
Normal	41.20	19	0.0657	24
Johnson SB	47.48	20	0.0161	1
Erlang (3P)	51.20	21	0.0833	27
Gen. Logistic	53.06	22	0.0645	23
Inv. Gaussian (3P)	56.42	23	0.0755	25
Gumbel Max	70.68	24	0.0777	26
Logistic	77.09	25	0.0873	28
Hypersecant	109.20	26	0.1028	29
Cauchy	129.20	27	0.1227	32
Laplace	167.57	28	0.1275	33
Gumbel Min	193.20	29	0.1220	31
Phased Bi-Weibull	240.23	30	0.1162	30
Phased Bi-Exponenti	273.81	31	0.1869	34
Wakeby	344.47	32	0.0191	2
Power Function	417.54	33	0.2052	35
Gen. Pareto	490.64	34	0.0242	3
Exponential (2P)	601.09	35	0.2473	36
Uniform	883.49	36	0.0466	13
Levy (2P)	1145.50	37	0.4448	37
Dagum (4P)	5323.90	38	0.6639	39
Error Function	6492.60	39	0.5718	38
Student's t	27256.00	40	0.9403	40

Table 6.6 summarizes the best fit for each of the data sets collected, as ranked by the Anderson-Darling test criteria. The majority of the best-fit models contained three and four parameters. Specifically, Table 6.6 contains the distribution types, PDF functions, and parameter estimates for each model.

Table 6.6: Descriptions for best fit demand models, with equations and parameters

System	Location	Distribution	Function	Parameters
Heavy Rail Transit	Center	Generalized Gamma	$f(x) = \frac{k(x-y)^{k\alpha-1}}{\beta^{k\alpha}\Gamma(\alpha)} \exp(-((x-y)/\beta)^k)$	k = 5.3321 α = 31.136 β = 240.79 γ = -391.69
	Rail seat	Error	$f(x) = c_1\sigma^{-1}exp(-\lvert c_0 z\rvert^k)$	k = 4.046 σ = 17.949 μ = -0.48365
HAL Freight	Center	Burr	$f(x) = \frac{\alpha k \left(\frac{x-y}{\beta}\right)^{\alpha-1}}{\beta\left(1+\left(\frac{x-y}{\beta}\right)^{\alpha}\right)^{k+1}}$	k = 1.7615 α = 4.9579 β = 142.25
	Rail seat	Pert	$f(x) = \frac{1}{B(\alpha_1,\alpha_2)} \frac{(x-a)^{\alpha_1-1}(b-x)^{\alpha_2-1}}{(b-a)^{\alpha_1+\alpha_2-1}}$	m = 31.413 a = -10.311 b = 104.91

While the "best" fit distribution is most useful for modeling the flexural demand of a specific transit or HAL freight railroad system, a more general distribution for representing the data is useful for widespread application of the demand curves and the broader probabilistic methodology described in this chapter. This is due in part to the fact that distributions with more than two parameters are likely overfitting the existing field demand data to reflect the specific attributes of a given rail transit system. As such, and as shown in Table 6.7, the selection of a

Weibull distribution for center moments and a normal distribution for rail seat moments is reasonable for both HRT and HAL freight.

Table 6.7: Descriptions for simplified demand models, with equations and parameters

System	Location	Distribution	Function	Parameters
Heavy Rail Transit	Center	Weibull	$f(x) = \frac{k}{\lambda}\left(\frac{x}{\lambda}\right)^{k-1} e^{\left(-\frac{x}{\lambda}\right)^k} \; when \; x \geq 0$	$k = 4.783$ $\lambda = 72.324$
	Rail seat	Normal	$f(x) = \frac{1}{\sigma\sqrt{2\pi}} \exp(-\frac{(x-\mu)^2}{2\sigma^2})$	$\sigma = 17.803$ $\mu = -0.42$
HAL Freight	Center	Weibull	$f(x) = \frac{k}{\lambda}\left(\frac{x}{\lambda}\right)^{k-1} e^{\left(-\frac{x}{\lambda}\right)^k} \; when \; x \geq 0$	$k = 3.494$ $\lambda = 138.94$
	Rail seat	Normal	$f(x) = \frac{1}{\sigma\sqrt{2\pi}} \exp(-\frac{(x-\mu)^2}{2\sigma^2})$	$\sigma = 36.74$ $\mu = 21.71$

These two distributions were selected due to widespread knowledge of their use. Additionally, the normal distribution is reflective of the uniform expected rail seat bending moments. Weibull distributions were generated in the context of engineering and fatigue analysis and excel at representing extreme events (Weibull, 1951), an attribute of the center bending moment data that must be considered. The selected distributions are overlaid on the histograms of raw data in Figures 6.5 and 6.6. Note that the overlap in the distributions for HRT (Figures 6.3 and 6.5) are referring to two locations of bending moments, not overlapping demand and capacity curves that would be indicative of a failure.

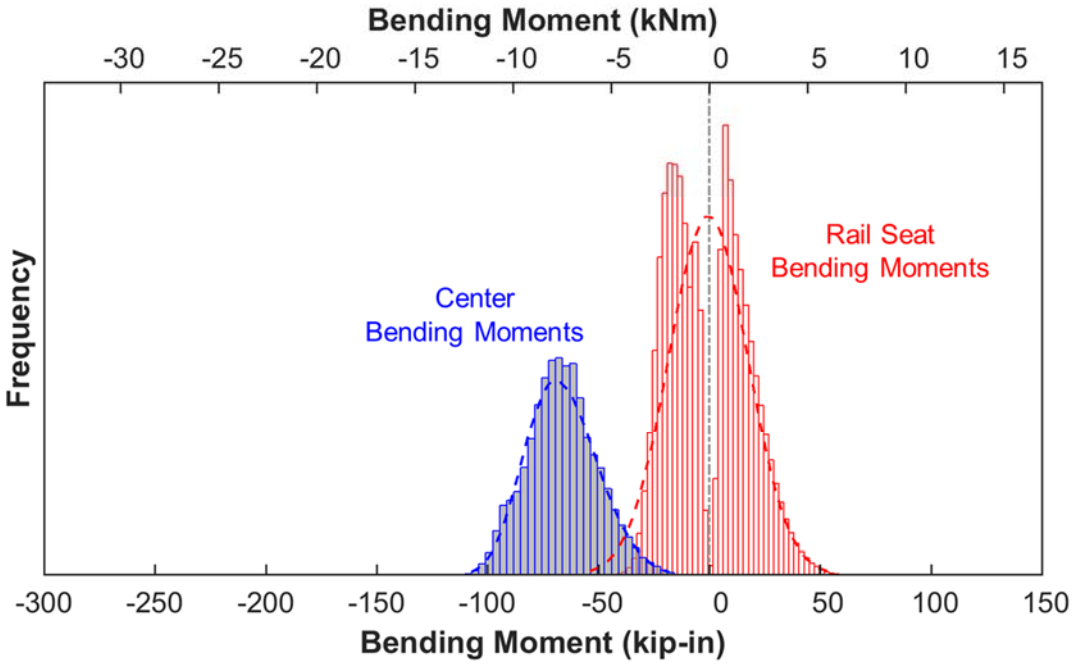

Figure 6.5: Fitted PDFs overlaid on raw data of crosstie rail seat and center bending moments used for demand models for HRT.

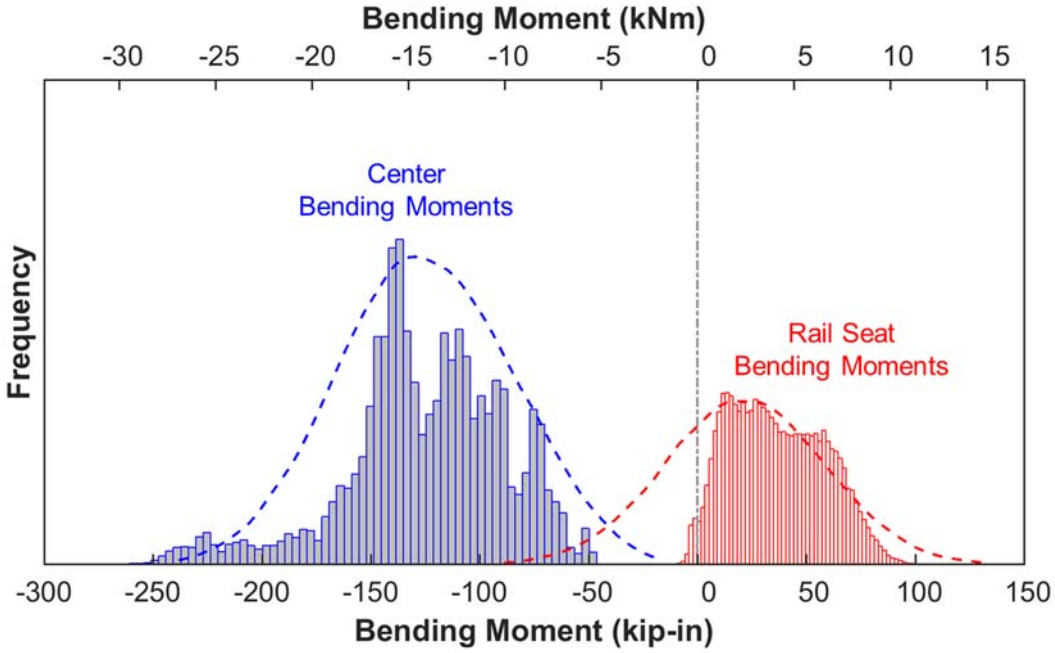

Figure 6.6: Fitted PDFs overlaid on raw data of crosstie rail seat and center bending moments used for demand models for HAL freight.

To improve the demand model, data collected at discrete field sites could be extrapolated to consider a variety of other support conditions that could be present over the entire railway network. Such an extrapolation was documented by Quirós-Orozco et al. (2018) in conjunction with the redesign of Amtrak's concrete crosstie for the NEC. The study of support condition variability is non-trivial, and the cost of obtaining a holistic understanding of an entire rail corridor would be substantial. For purposes of this research, the demand curves listed above will be used.

There is also a time dependency in the demand curve. Factors influencing this are initial construction loads (e.g. ballast trains on track with no ballast layer that may be placed on a crowned sub-ballast) and the time and tonnage dependent deterioration of track support conditions. Other than hand calculations to confirm the former, and pilot projects to quantify the latter (Wolf, 2015a), these factors are largely unquantified and require separate study.

6.4.3 Generation of Capacity Model

6.4.3.1 Method

Most prestressed concrete crossties in the United States are designed as Class U (uncracked) members using the American Concrete Institute (ACI) Building Code Requirements for Structural Concrete and Commentary, ACI 318-14 (2014). Their flexural capacity is defined based on first crack, typically occurring at the extreme tensile fiber (e.g. top center of crosstie in center bending). This is similar to what AREMA MRE, Chapter 30 (2016) states except that AREMA requires a crack to penetrate to the first level of prestressing from the tensile surface of the crosstie.

As such, the total stresses at the extreme tensile fiber cannot exceed the modulus of rupture (f_r) of the concrete (Equation 6.2), an empirically derived limit that provides an indirect

measure of concrete's tensile capacity. The three terms in Equation 6.2 (also presented as Equation 1.1) represent precompression, the internal moment caused by the eccentricity of prestressing, and the external moment due to passing wheel/axle loads.

$$-\frac{F_{se}}{A_c} - \frac{F_{se}(e)c}{I_c} + \frac{M_c c}{I_c} \leq f_r \tag{6.2}$$

Where:
f_r = modulus of rupture of concrete (ksi) [0.627 ksi for f_c' of 8 ksi]
M_c = center negative bending moment (kip-in)
F_{se} = effective prestressing force (after losses) (kips)
A_c = cross-sectional area (in^2)
I_c = section moment of inertia (in^4)
e = eccentricity of prestress centroid (in.)
c = distance from neutral axis to extreme fiber (in.)

For concrete with a compressive strength (f_c') of 7 ksi (typical for concrete crossties) the value for f_r is 0.627 ksi according to Table 24.5.4.1 in ACI 318-14 (2014). The strength of a prestressed concrete member is typically governed by cracking at the tensile surface, not crushing in the compression region due to the manner in which it is loaded (e.g. uniform load or two distributed rail seat loads). McNeely and Lash (1963) suggests use of distributions for f_r with a standard deviation of 8.5% based on experimental results from split tensile tests on cylindrical specimens.

Compared to the tensile strength, the crushing limit for concrete is much higher, on the order of 4.2 ksi for concrete with a compressive strength (f_c') of 8 ksi according to ACI 318-14 (2014). Literature also indicates that the fatigue life of concrete should be considered, but the inclusion of concrete fatigue criteria into this largely static design process and evaluation is challenging (ACI, 1997). In general, fatigue limits are more conservative than the $0.6f_c'$ limit,

and are recommended in the range of $0.2f_c'$ to $0.4f_c'$ (ACI, 1997). This does not seem reasonable with respect to the present application, thus no additional reduction of concrete's compressive strength will be considered for fatigue.

The limit state values for both tensile and compressive strength of concrete specified by ACI 318-14 (2014) and used in this dissertation are conservative. This is especially true for compressive strength, which is reduced by 40%. Future research should include a sensitivity analysis in which the strength reduction factors are varied within reasonable ranges based on data from prior experimentation.

To align with conventional mechanics terminology, compressive stresses are characterized as negative, and tensile stresses are positive. Additionally, the negative second term in Equation 6.2 ($\frac{F_{se}(e)c}{I_c}$) indicates that the eccentricity induced by the prestress produces compression in the top of the crosstie that is used to counteract a positive bending moment. The stresses listed in Equation 6.2 can also be represented graphically for the case of center negative bending (Figure 1.3).

The critical stress-related value that must be quantified in order to identify when the structural member will fail, is the bending moment, as indicated earlier. Equation 6.3 is generated by solving Equation 6.2 (also presented as Equation 1.2) for the cracking moment that would indicate that the total stresses in the tensile surface equal the modulus of rupture (f_r), which defines the maximum moment capacity at first crack at a given section.

$$M_{cr} = \frac{I_c}{c_{tens}}\left(f_r + \frac{F_{se}}{A_c} + \frac{F_{se}(e)c_{tens}}{I_c}\right) \tag{6.3}$$

Where:
M_{cr} = cracking moment (kip-in)
c_{tens} = distance from neutral axis to extreme tensile fiber (in)

For brevity, only the crosstie center region was considered when providing a background to prestressed crosstie design, and the tensile (top) surface will be the location of greatest attention. The rail seat flexural considerations are similar, although limited by tension on the bottom surface of the crosstie as a result of positive bending moments. The "minor" bending moments, rail seat negative and center positive, are also considered using this same method but with minor modifications listed below.

The proposed process will generally follow a procedure in which limit state functions define the boundary between failure and functionality of a component. This represents the location in which the capacity and demand model cancel each other as shown in Equation 6.4.

$$g(\boldsymbol{x}) = C(\boldsymbol{x}) - D(\boldsymbol{x}) \tag{6.4}$$

Where:
x = the vector of random variables;
C(**x**) = the capacity model;
D(**x**) = the demand model.

Thus, when the limit state function has a negative result, failure occurs, as the induced demand exceeds the provided capacity of the concrete crosstie. The probability of failure is based on the likelihood of the demand (C(**x**)) being greater than the capacity (D(**x**)), as indicated by the overlap of the two curves. This methodology facilitates evaluation of current designs, and can also be applied to development and optimization of future designs. For reference, earlier probabilistic design literature has referred to the curves using the terms of resistance (R) and load effect (Q) (Szerszen and Nowak, 2003).

As a part of this application of the SRA methodology, limit state equations for each of the critical design cross sections were derived, that map to the stress level at top and bottom fibers of the crosstie based on AREMA (2016) and ACI 318 (2014). These equations define the transition

of the component from functional to failed. Failure is defined as "cracked." Equations 6.5 and 6.6 represent the top and bottom fiber stresses at the center cross section, respectively.

$$g_1(\boldsymbol{x}) = 7.5\sqrt{f_c'} + \frac{P_i}{A_{center}} + \frac{P_i\, y_{t_{center}}}{I_{center}} - \frac{M_{field}\, y_{t_{center}}}{I_{center}} \tag{6.5}$$

$$g_2(\boldsymbol{x}) = 0.6f_c' - \frac{P_i}{A_{center}} + \frac{P_i\, y_{b_{center}}}{I_{center}} - \frac{M_{field}\, y_{b_{center}}}{I_{center}} \tag{6.6}$$

Similarly, Equations 6.7 and 6.8 represent the stresses at top and bottom respectively, at the rail seat cross sections.

$$g_3(\boldsymbol{x}) = 0.6f_c' - \frac{P_i}{A_{rail\ seat}} + \frac{P_i\, y_{t_{rail\ seat}}}{I_{rail\ seat}} - \frac{M_{field}\, y_{t_{rail\ seat}}}{I_{rail\ seat}} \tag{6.7}$$

$$g_4(\boldsymbol{x}) = 7.5\sqrt{f_c'} + \frac{P_i}{A_{rail\ seat}} + \frac{P_i\, y_{b_{rail\ seat}}}{I_{rail\ seat}} - \frac{M_{field}\, y_{b_{rail\ seat}}}{I_{rail\ seat}} \tag{6.8}$$

Additionally, there are four more equations (Equations 6.9 - 6.12, $g_5(\boldsymbol{x})$ through $g_8(\boldsymbol{x})$) that represent the lesser bending moments that can be induced at the center (positive) and rail seat (negative).

$$g_5(\boldsymbol{x}) = 7.5\sqrt{f_c'} + \frac{P_i}{A_{center}} - \frac{P_i\, y_{b_{center}}}{I_{center}} - \frac{M_{field}\, y_{b_{center}}}{I_{center}} \tag{6.9}$$

$$g_6(\boldsymbol{x}) = 0.6f_c' - \frac{P_i}{A_{center}} - \frac{P_i\, y_{t_{center}}}{I_{center}} - \frac{M_{field}\, y_{t_{center}}}{I_{center}} \tag{6.10}$$

$$g_7(\boldsymbol{x}) = 0.6f_c' - \frac{P_i}{A_{rail\ seat}} - \frac{P_i\, y_{b_{rail\ seat}}}{I_{rail\ seat}} - \frac{M_{field}\, y_{b_{rail\ seat}}}{I_{rail\ seat}} \tag{6.11}$$

$$g_8(\boldsymbol{x}) = 7.5\sqrt{f_c'} + \frac{P_i}{A_{rail\ seat}} - \frac{P_i\, y_{t_{rail\ seat}}}{I_{rail\ seat}} - \frac{M_{field}\, y_{t_{rail\ seat}}}{I_{rail\ seat}} \tag{6.12}$$

6.4.3.2 Results

Equations 6.5 – 6.12 are then used as limit state functions for a first order reliability method (FORM) analysis to generate reliability indices (Zhao and Ono, 1999). To solve the problem using FORM, a MATLAB (2012) toolbox created by the University of California Berkeley for SRA topics (*Struct Saf 2006*) to conduct the simulation was used (Der Kiureghian et al., 2006).

The factors considered in the analysis are listed in Table 6.8, along with the type of distribution and its simple statistics. Concrete compressive strength was obtained from prevailing concrete crosstie specifications. Compressive strength distribution characteristics were obtained by a review of relevant literature (Bartlett and MacGregor, 1999; ACI, 2002; Mertol et al., 2008; Remennikov et al., 2012; Nowak and Collins, 2013; Rakoczy and Nowak, 2013; Rakoczy and Nowak, 2014). The jacking force value of 7 kips (75% of prestressing steel ultimate capacity) and resulting losses were estimated based on the ACI 318-14 (2014) assumption of 15% total losses and a reasonable standard deviation associated with the process of stressing wires and its inherent complexity.

Table 6.8: Random variables used in concrete crosstie flexural capacity models

Variable	Symbol	Distribution	Units	Mean	Standard Deviation
Concrete compressive strength	f_c'	Lognormal	ksi	7	1.05
Jacking force	P_e	Normal	kips	7	0.42
Prestressing losses	loss	Lognormal	%	15	3.00

To provide a graphical output of an aggregate capacity curve that can be compared to the field demand curve, Monte Carlo Simulation (MCS) was used. Using MCS, the distribution of possible flexural capacities was generated by using approximately 10,000 iterations that can be considered representative of the "population". The method by which data were selected within the MCS was direct sampling. This method is appropriate given the fact that the input variables are all independent and there is no correlation among them. Beyond this graphical representation generated using MCS, FORM, and second order reliability methods (SORM) are considered to be more accurate methods to execute an SRA (Frangopol et al., 1997; Zhao and Ono, 1999). Due to the linear nature of this work, SORM does not improve the results (Canga Ruiz, 2018), thus FORM was deemed appropriate and reliable.

Figure 6.7 through Figure 6.10 present graphical results from the MCS of the two crosstie designs under consideration, showing both rail seat and center sectional results for both positive and negative bending moment applications. To represent the field data, Wiebull and normal distributions were chosen (Table 6.2).

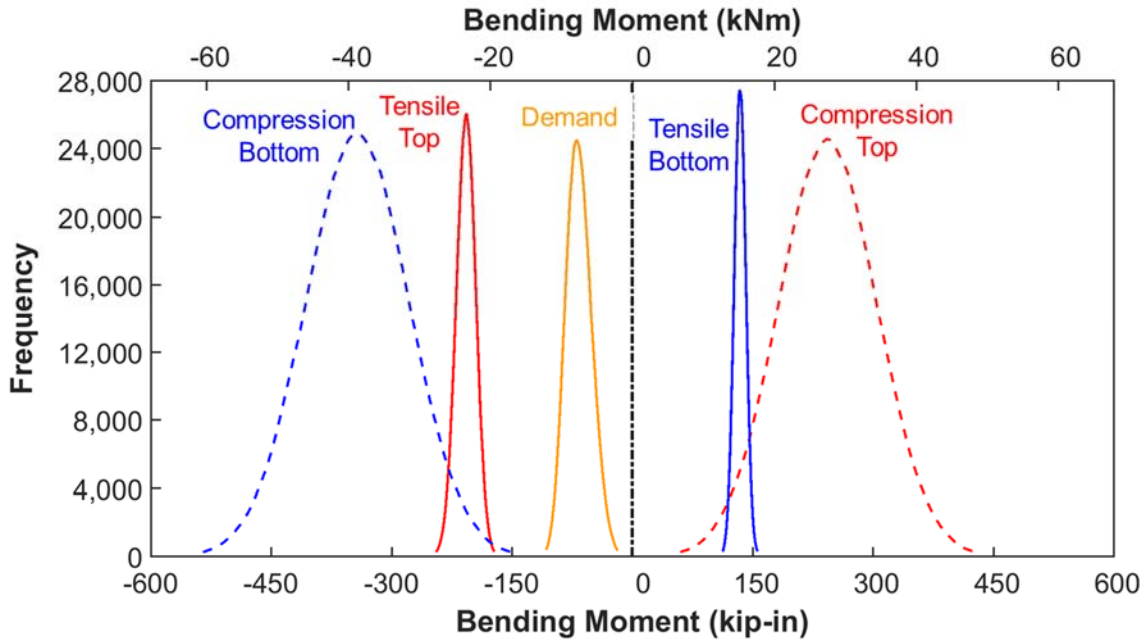

Figure 6.7: Results from MCS of crosstie center bending moments for HRT.

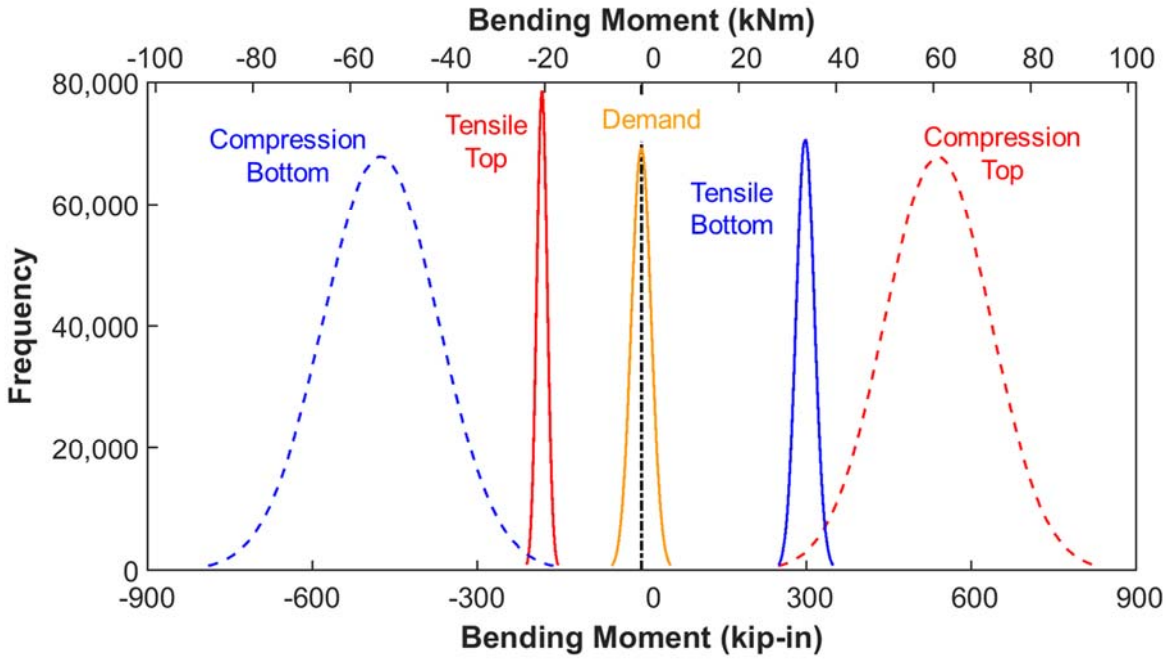

Figure 6.8: Results from MCS of crosstie rail seat bending moments for HRT.

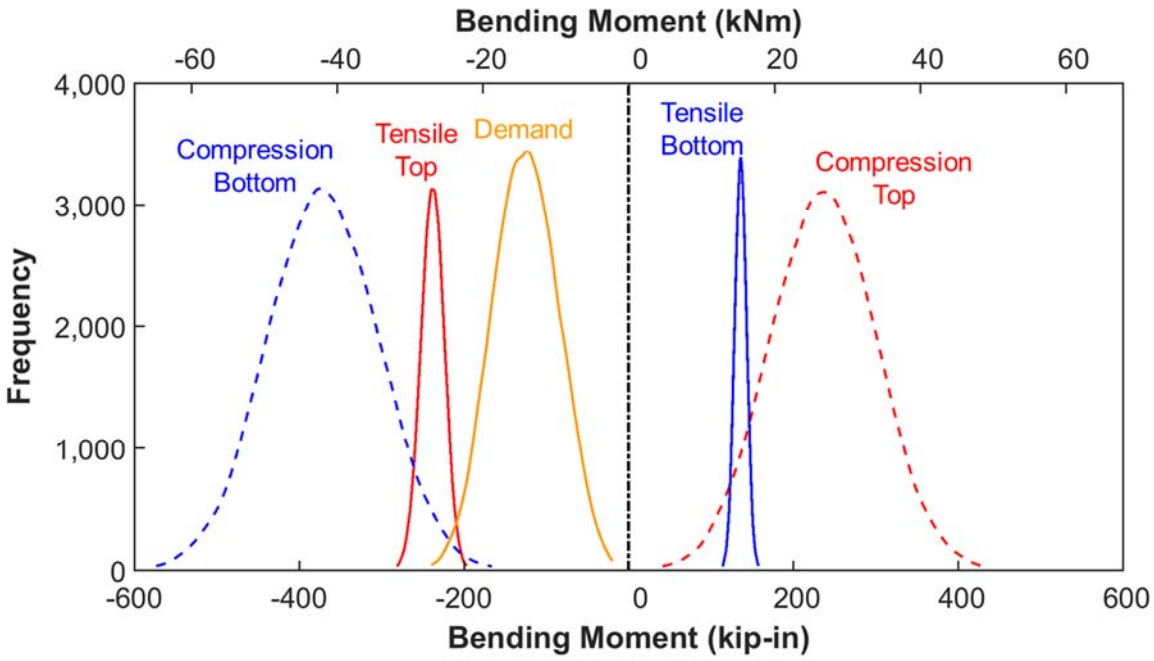

Figure 6.9: Results from MCS of crosstie center bending moments for HAL freight.

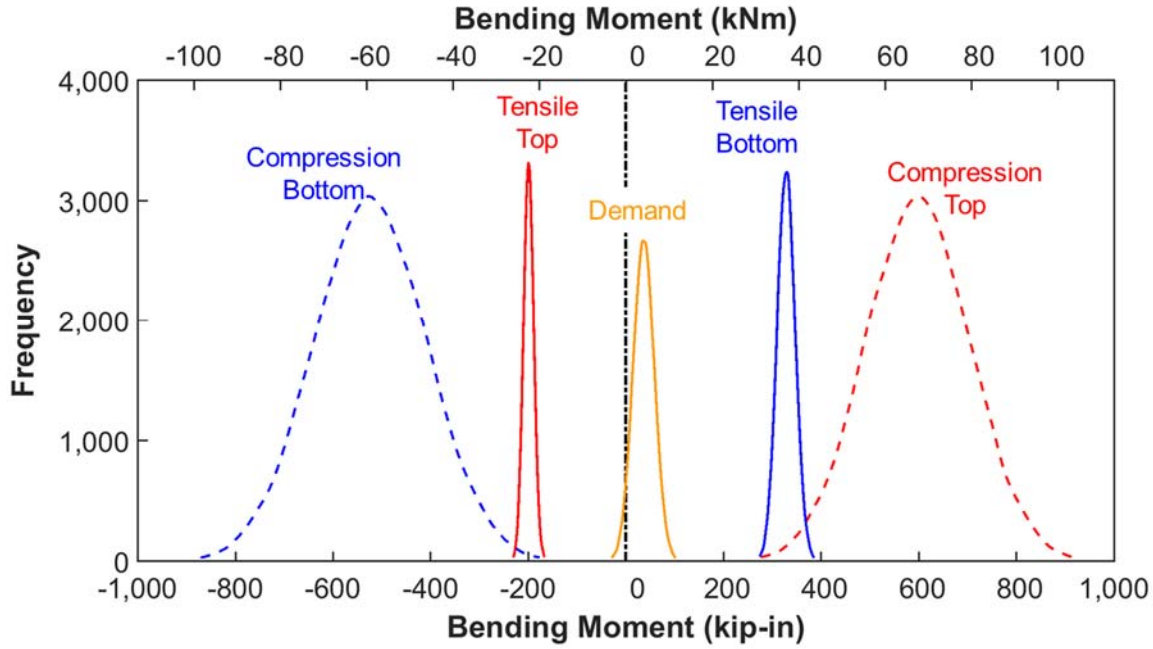

Figure 6.10: Results from MCS of crosstie rail seat bending moments for HAL freight.

In the field of SRA, the probability of failure is quantified using a "reliability index", defined as "β". This term is functionally related to the probability of failure (P_f), as shown in Equation 6.13 (Ditlevsen and Madsen, 2007; Nowak and Collins, 2013).

$$\beta = -\Phi^{-1}(P_f) \tag{6.13}$$

Where:
Φ^{-1} represents the inverse of the standard normal cumulative distribution function.
P_f represents the probability of failure.

Table 6.9 includes individual values for the reliability indices (β) that represent failures in either positive or negative bending at the center and rail seat sections.

Table 6.9: Reliability index and probability of failure for the studied limit state functions obtained using FORM

Extreme Fiber in Bending	HAL Freight		Heavy Rail Transit	
	β	P_f	β	P_f
Center Top	2.6614	0.0038908	5.0371	2.3633e-07
Center Bottom	2.6637	0.0038643	5.4090	3.1682e-08
Rail Seat Bottom	9.6322	2.9232e-22	6.4114	7.2071e-11
Rail Seat Top	6.4435	5.8375e-11	6.5298	3.2936e-11

The aforementioned analysis is based on the flexural strength at initial concrete cracking, and not the component's ultimate capacity or some location within the transition zone that is also specified by ACI 318-14 (2014). As discussed previously, this definition differs from the AREMA (2016) definition, which does not define a crosstie as failed until the crack has penetrated from the tensile surface to the first level of prestressing steel. In the future, the residual capacity could be defined in reference to ultimate capacity, which is approximately

double the cracking moment capacity as demonstrated experimentally by Cesar Bastos et al. (2018).

6.5 Part II - Design

6.5.1 Demand Model

For design, the same demand model that was used in the analysis of existing designs will be employed, given that the data are representative of conditions likely to be encountered in the field. The demand model could be further refined to consider a variety of possible support conditions. As mentioned earlier, this requires additional assumptions and is a topic that warrants further research. Data collected from the two rail transport modes will be used, with no extrapolation to other possible support conditions.

6.5.2 Capacity Model

The capacity models are generated using FORM, while incrementally changing crosstie geometry (height and width), number of prestressing wires, and prestress centroid within the bounds that are described in Table 6.10. The initial models were run at coarser increments for crosstie geometry, and I subsequently decided to re-run them at a finer increment (0.25 in). Final model increments were also selected to be compatible with reasonable prestressed concrete manufacturing tolerances.

Table 6.10: Bounds for crosstie design deterministic input parameters

Dimension / Value	Units	Range		Design Increment	Current Designs	
					HRT	HAL Freight
Bottom Width at Center (g_1)	in.	10	13	0.25	10.50	11.00
Top Width at Center (g_1)	in.	5	10	0.25	8.44	9.00
Height at Center	in.	5	10	0.25	6.75	6.75
Bottom Width at Rail Seat (g_1)	in.	10	13	0.25	10.50	11.00
Top Width at Rail Seat (g_1)	in.	7	11	0.25	8.44	9.00
Height at Rail Seat	in.	6	12	0.25	8.56	8.73
Number of Wires (g_4)	num	8	26	1	18	20
Height of Steel Centroid (y)	in.	2	4	0.25	3.67	3.75

Additional constraints placed on the model are infeasible cases in which 1) the crosstie top width exceeds the bottom width at either the rail seat or center, 2) the centroid of steel is less than the height of centroid of concrete at the center, and 3) the location of the centroid of steel is greater than the height of centroid of the concrete at the rail seat. For each set of discrete design variables selected, the random variables in Table 6.8 were simulated using FORM. The result of each simulation of the various design permutations were reliability indices (β) at the crosstie center and rail seat regions.

For selection of the optimized design, I assumed values for β that are representative of the current state of practice in the United States. Szerszen and Nowak (2003) concluded that the ultimate limit state (ULS) of prestressed beams designed using ACI 318 (2014) have an equivalent β ranging from 4.2 to 4.4. These values were calculated by varying material, geometry and load values, and resulted in a target reliability index (β_T) of 3.5 that will be used in this research to build upon previous work that treated load and resistance parameters from ACI as random variables to statistically determine reliability indices (Nowak and Szerszen, 2003).

This is related to earlier documentation and the field of SRA as described by Nowak and Collins (2013). This equivalent β defines what is an acceptable design following the concrete structures design code in the United States (Nowak and Collins, 2013; Canga Ruiz, 2018). The argument could be made for a lower value of β_T given the less-severe consequences of a single crosstie failure, compared to a bridge girder or other typical applications for prestressed concrete.

This discussion is akin to that of Szerszen and Nowak (2003) with respect to primary and secondary members, and the fact that secondary members can have a lower threshold for β_T. I am focusing on the reliability of a single element (a crosstie) as opposed to a system (the track, which has inherent redundancy due to load sharing among adjacent components).

Given that end users may desire different levels of risk for the center and rail seat, it is possible that the two values for β_T be considered independently. The reasoning behind different values for β_T at the center and rail seat relates to the consequences of failure at each location and the ease with which failures can be inspected at each location. After preliminary discussions with railroads and concrete crosstie manufacturers, acceptable values of β_T for the rail seat should be higher. This is because rail seat cracks are more difficult to detect, and the consequence of failure at this location can have an immediate effect on the crosstie's ability to fulfill its purpose of holding gauge and supporting the rail. Center cracking has been shown to be less critical by recent research by Cesar Bastos et al (2017), but is a location that is often found to be out of compliance with the FRA Track Safety Standards (CFR 213) (FRA, 2011) that require no visible prestressing strands or wires. For purposes of this analysis, which aims to create a balanced crosstie (e.g. equal risk assumed at rail seat and center), I will use values β_T = 3.5 at both rail seat and center.

6.5.3 Design Results

Using the model to design concrete crossties through a parametric study, values for β at the top and bottom of both center and rail seat sections were plotted as a function of changes in each deterministic input parameter (Figures 6.13 through 6.12). Figures 6.11 through 6.15 refer to HRT and Figures 6.16 through 6.20 refer to HAL freight. For all figures (6.11 through 6.15), the deterministic parameters that are not being addressed within the specific figure are held constant at the current design values shown in Table 6.10.

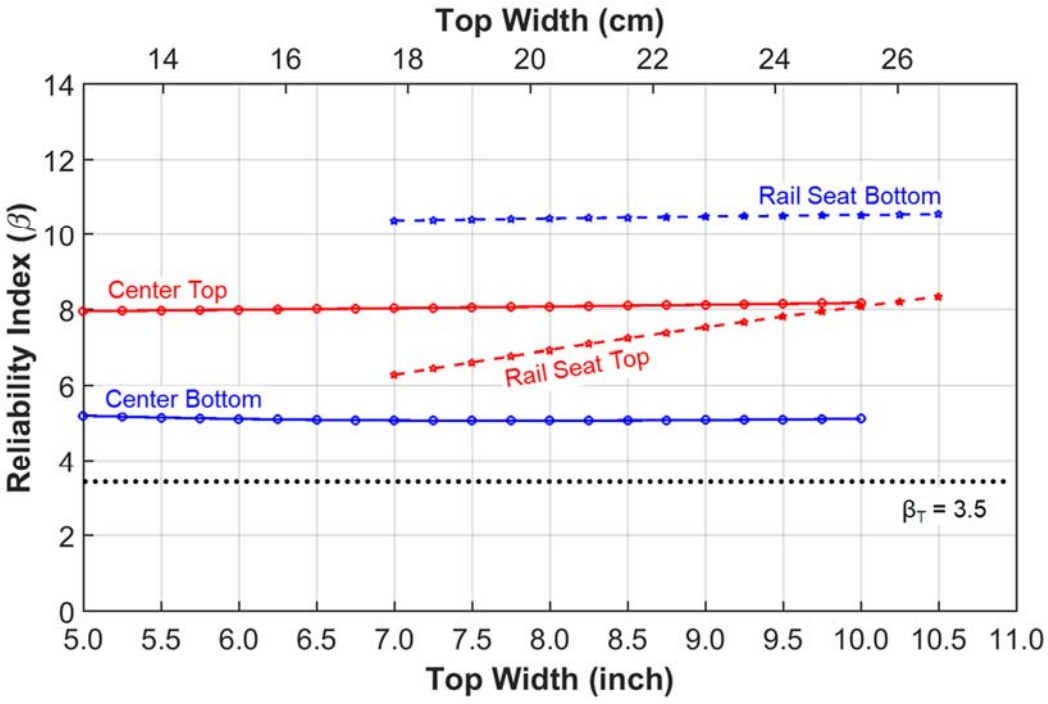

Figure 6.11: HRT center bending moment structural reliability indices (β) as a function of top width, while holding other parameters constant.

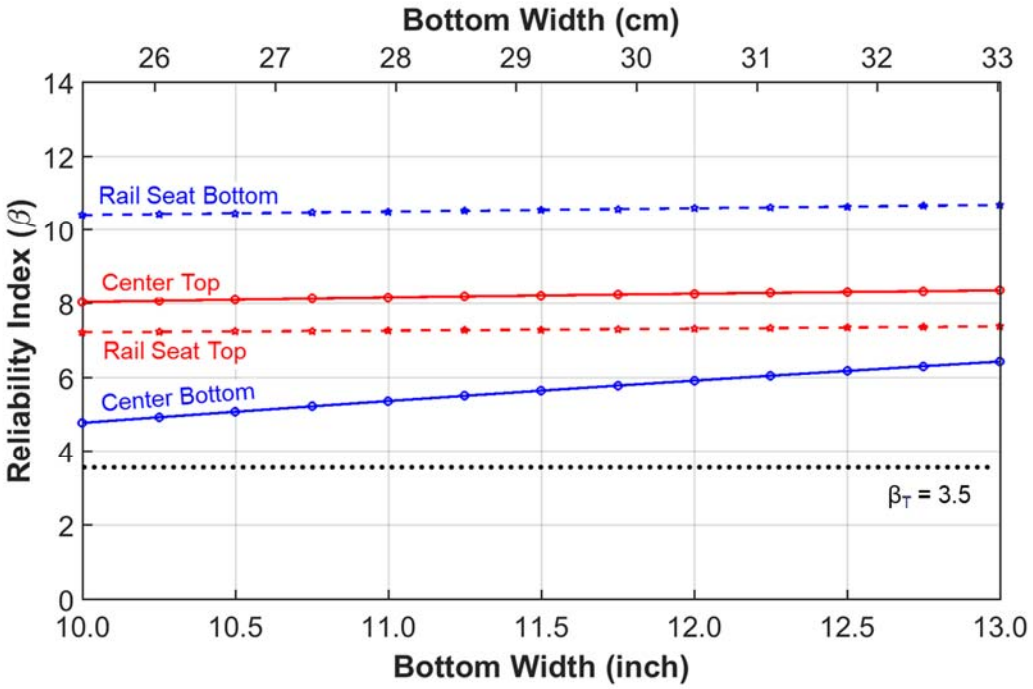

Figure 6.12: HRT center bending moment structural reliability indices (β) as a function of bottom width, while holding other parameters constant.

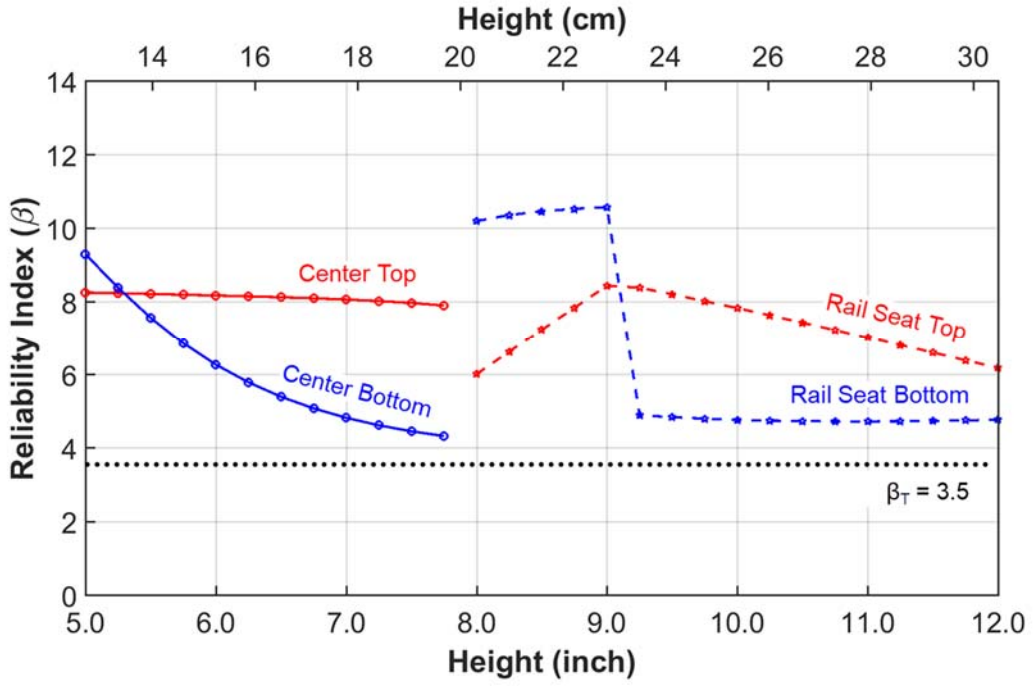

Figure 6.13: HRT center bending moment structural reliability indices (β) as a function of height, while holding other parameters constant.

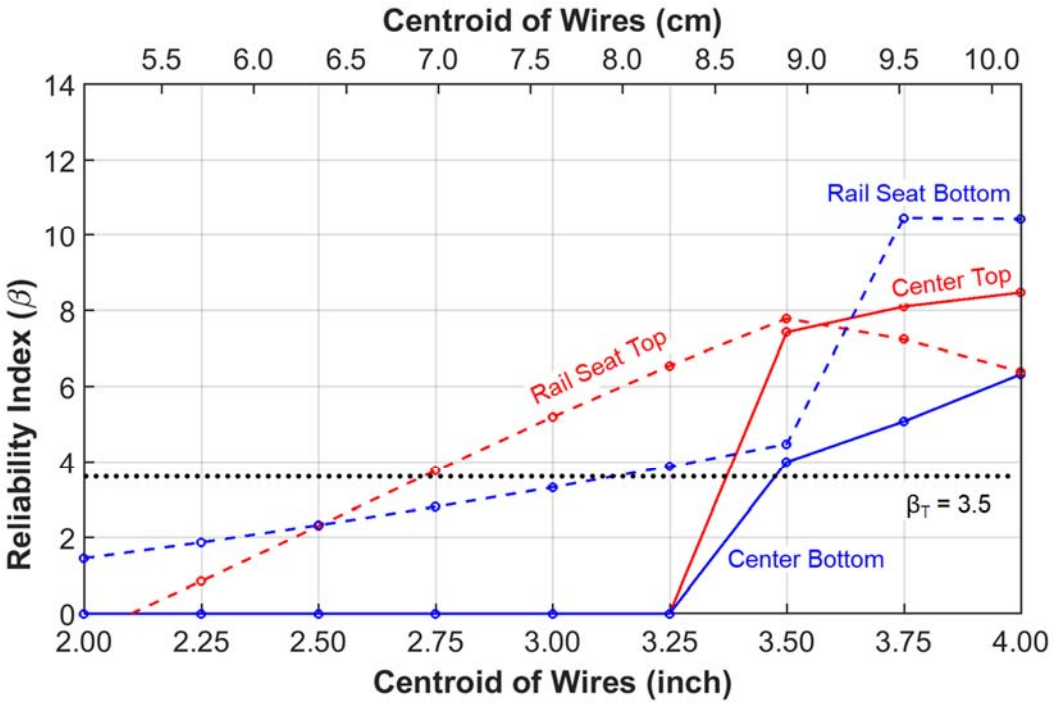

Figure 6.14: HRT center bending moment structural reliability indices (β) as a function of prestressing centroid, while holding other parameters constant.

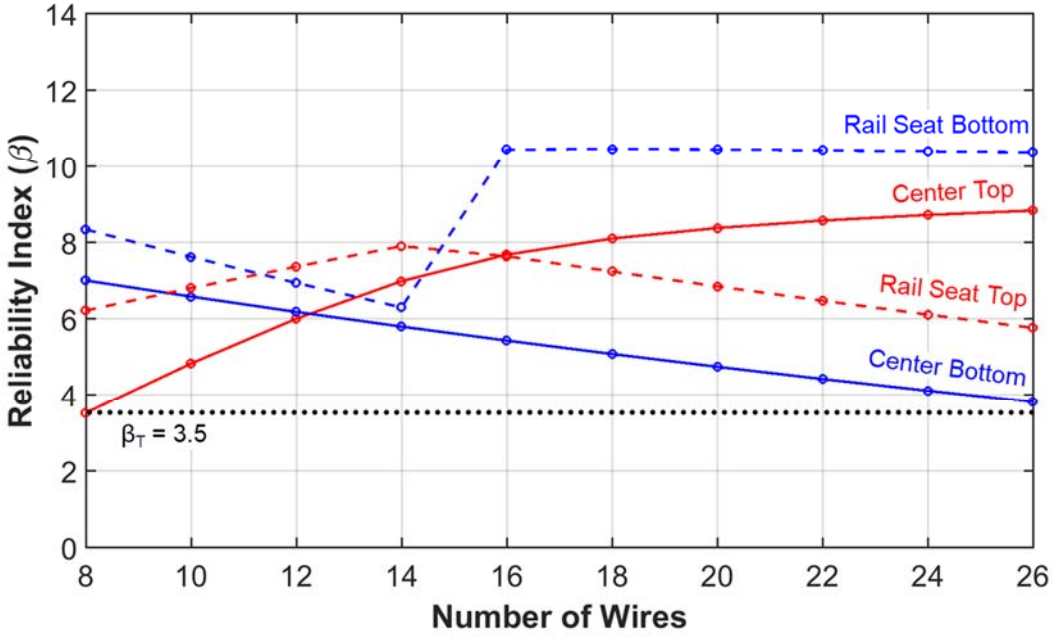

Figure 6.15: HRT center bending moment structural reliability indices (β) as a function of number of wires, while holding other parameters.

A review of HRT results provides insight into the sensitivity of design changes as a function of changes in deterministic input parameters. Negative slopes indicate a decrease in β as a function of larger size, more wires, etc.

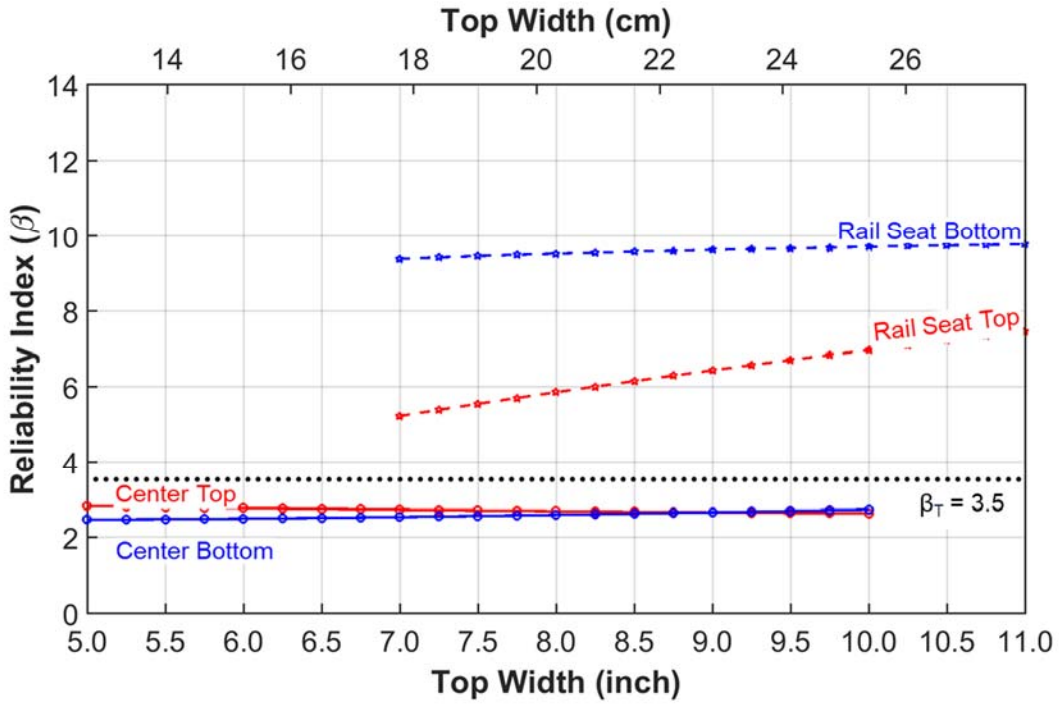

Figure 6.16: HAL freight center bending moment structural reliability indices (β) as a function of top width, while holding other parameters constant.

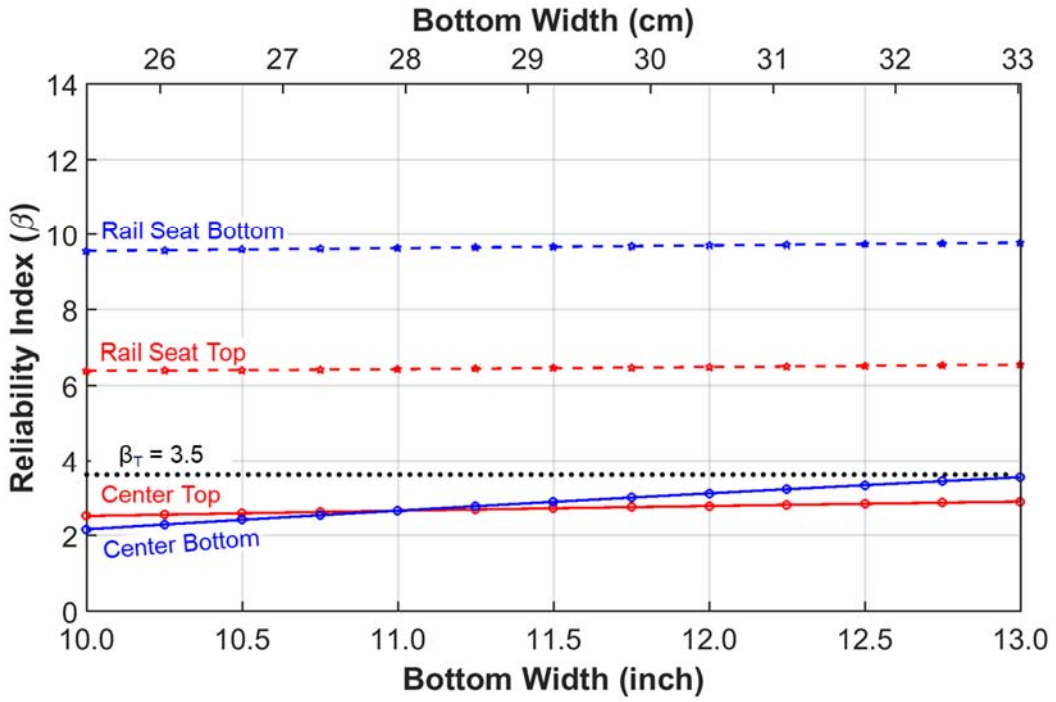

Figure 6.17: HAL freight center bending moment structural reliability indices (β) as a function of bottom width, while holding other parameters constant.

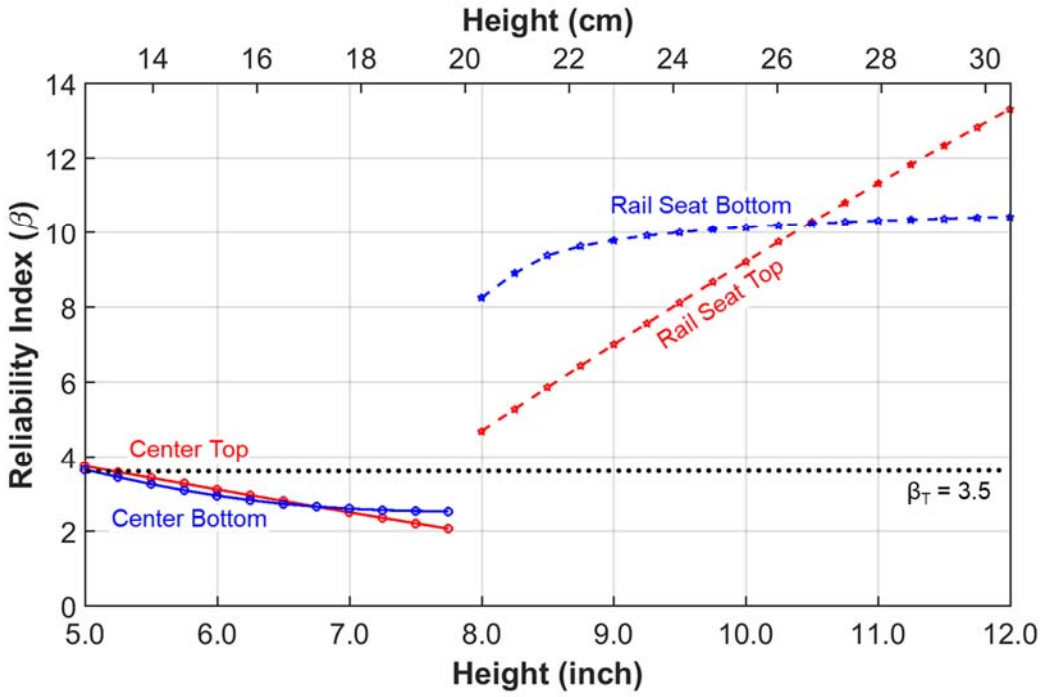

Figure 6.18: HAL freight center bending moment structural reliability indices (β) as a function of height, while holding other parameters constant.

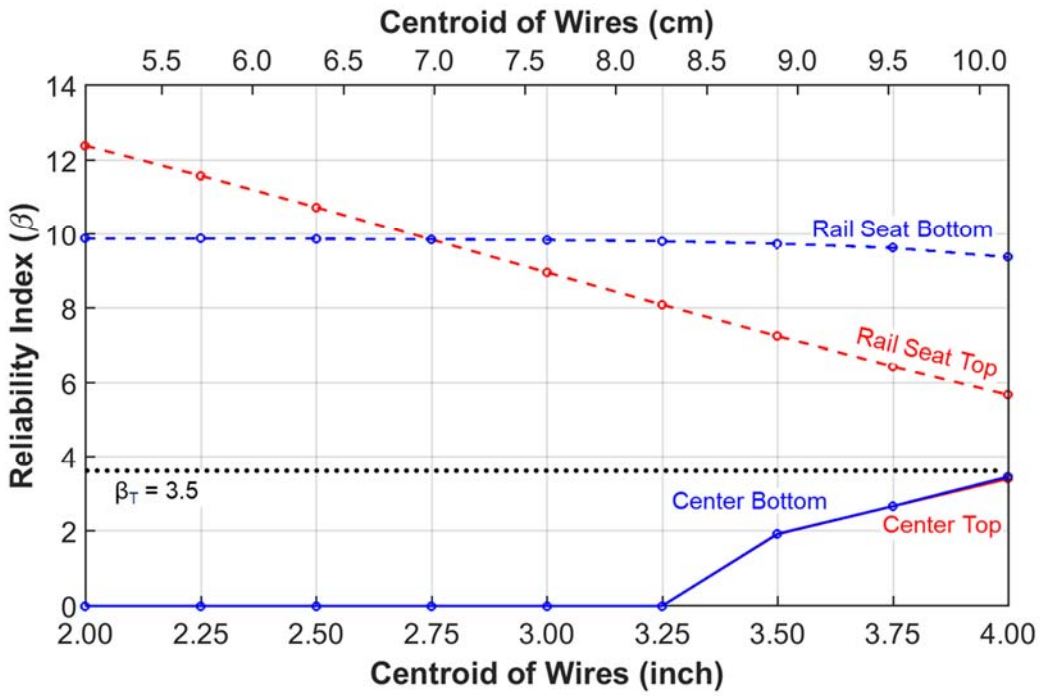

Figure 6.19: HAL freight center bending moment structural reliability indices (β) as a function of prestressing centroid, while holding other parameters constant.

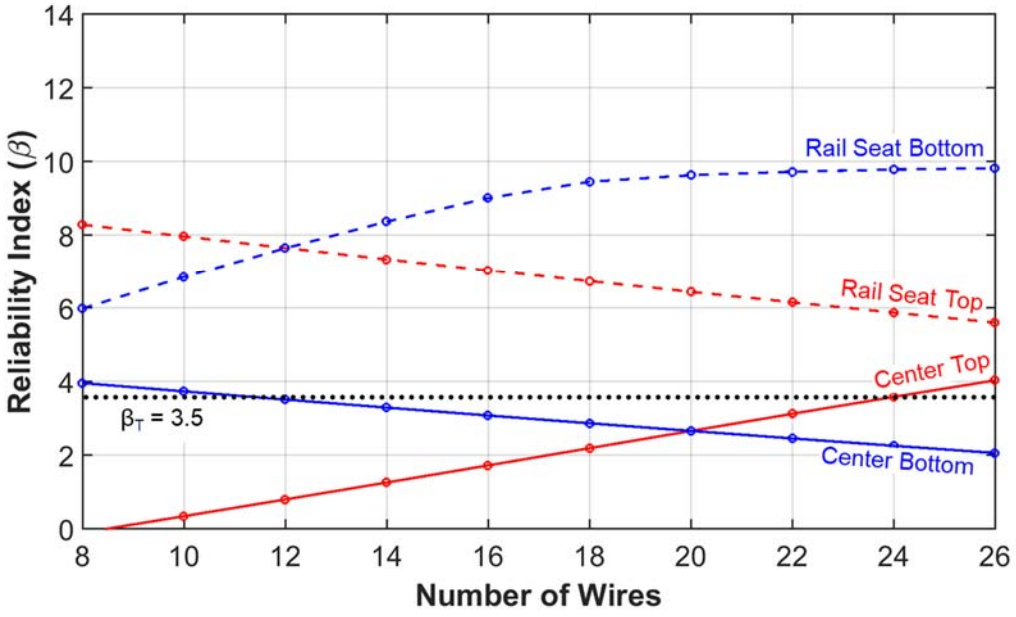

Figure 6.20: HAL freight center bending moment structural reliability indices (β) as a function of number of wires, while holding other parameters.

Similar to the HRT case, HAL freight results provide insight into the sensitivity of design changes as a function of changes in deterministic input parameters. Most of the positive slopes are intuitive, given that increases in deterministic input variables increase the reliability index.

For example, as the height of the crosstie changes (Figure 6.18) at both the center (left lines) and rail seat (right lines) I see distinct changes in reliability indices (β). For the crosstie center, as the height is increased, there is less conservatism in the designs due to a reversal of the eccentricity that works against the primary bending. Conversely, at the rail seats, any increase in depth of the section increases design conservatism given that the additional concrete material always improves the crosstie's resistance to positive bending given the section centroid is always above the prestressing steel centroid.

Changes in wire centroid (Figure 6.19) are of particular interest, given their relation to the eccentricity of the crosstie, a primary benefit of prestressing. As the centroid increases (moves upward in the cross section) values for β decrease for the rail seat and increase for the center. The center β values are especially sensitive to centroid location, as its role in resisting negative bending at the center is the most recognizable benefit of using prestressed concrete for crosstie applications. Negative slopes are also present for rail seat negative and center positive bending as a function of increased wires (Figure 6.20). This is due to the eccentricity of prestress that is designed to compensate for the primary bending modes; center positive and rail seat negative. By definition, the eccentricity will only add additional tensile capacity for either positive or negative bending, thus the less prevalent bending modes are the ones that are penalized.

6.5.4 Design Application

Focusing on designs that provide values of β for both center and rail seat that are closest to $\beta_T = 3.5$ leads to an initial, broad conclusion. For both HRT and HAL freight, values for β at

the center were consistently lower than at the rail seat. This is indicative of the need for a more balanced design, but also identifies a challenge when attempting to get all values of β_T near 3.5.

For HRT, 200,401 feasible designs were generated that have all values for β_T at the top and bottom of both center and rail seat $3.5 \leq \beta_T$. To narrow the design space, 137 designs were selected that had at least one instance of $3.5 \leq \beta_T < 3.8$. For HAL freight, 405,265 designs were generated that had values for both center and rail seat $3.5 \leq \beta_T$ and 117 designs were generated that had one or more instances of $3.5 \leq \beta_T < 3.65$. The top 137 and 117 designs for HRT and HAL freight, respectively, were selected for final visual inspection to determine the most feasible prototype crosstie designs.

Using the subset of designs described earlier, two proposed prototypes for each mode were selected for comparison to existing designs. These prototype designs are among the most reasonable choices from a constructability and manufacturing standpoint. A graphical representation of the cross-sectional geometries and changes in number of wires and prestress centroids are shown in Figure 6.21 for HRT and Figure 6.22 for HAL Freight.

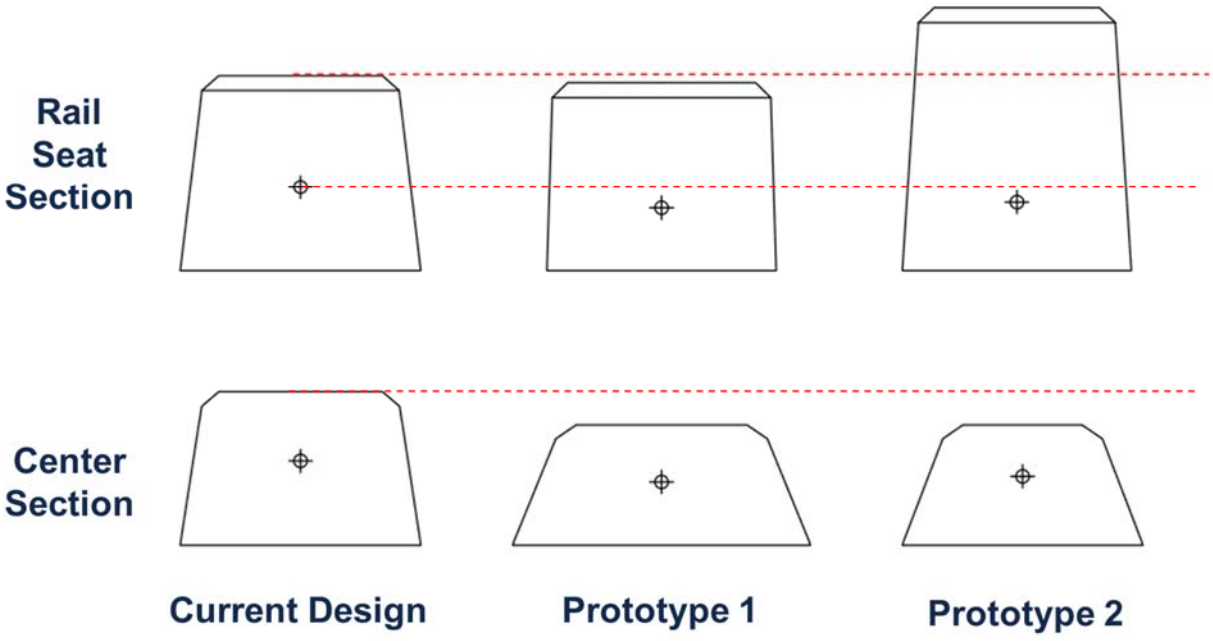

Figure 6.21: Graphical comparison of existing and optimized (prototype) crosstie cross sectional designs for HRT applications.

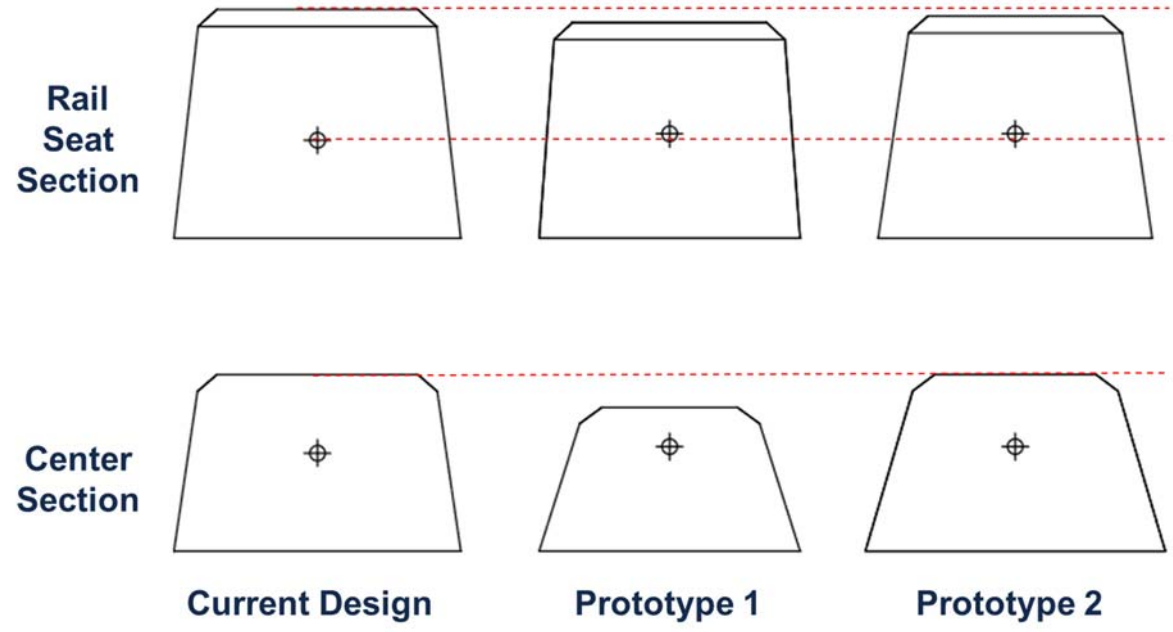

Figure 6.22: Graphical comparison of existing and optimized (prototype) crosstie cross sectional designs for HAL freight applications.

For HRT, when compared to the current crossties, proposed designs with $\beta_T \approx 3.5$ at the center typically have a shallower center and narrower rail seat section, fewer strands, and an eccentricity of 2.75 in to 4.00 in. For HAL freight, the crossties with $\beta_T \approx 3.5$ at the center typically have a narrower center and shallower depth for geometry, an equal or slightly fewer strands, and an eccentricity of 3.75 to 4.00 in.

Table 6.11: Bounds for prototype crosstie design deterministic input parameters

Dimension / Value	Units	Heavy Rail Transit		HAL Freight	
		Prot. 1	Prot. 2	Prot. 1	Prot. 2
Bottom Width at Center (g_1)	in.	13.00	10.50	10.00	11.50
Top Width at Center (g_1)	in.	8.75	6.50	6.50	7.50
Height at Center	in.	5.50	5.25	5.50	6.75
Bottom Width at Rail Seat (g_1)	in.	10.0	11.50	10.00	10.50
Top Width at Rail Seat (g_1)	in.	9.50	10.00	8.75	8.00
Height at Rail Seat	in.	8.25	12.00	8.25	8.50
Number of Wires (g_4)	num	14	12	18	20
Height of Steel Centroid (y)	in.	2.75	3.00	4.00	4.00

The flexural capacities of each of the two proposed prototype designs are shown in Tables 6.12 and 6.13, respectively. In terms of application of this procedure within a design specification, the suggested values for the random variables are also shown in Tables 6.12 and 6.13 (same for both designs and modes). They are consistent with conventional values for other specifications using prestressing wires and tendons and high strength concrete.

Table 6.12: Comparison of the magnitude of flexural capacity of existing and optimized (proposed) crosstie designs for HRT applications

Characteristic			Existing	Prototype 1	Prototype 2
Design Values	Compressive Strength (ksi)		7	7	7
	Length (ft)		8.5	8.5	8.5
	Tie Spacing (in)		24	24	24
	Number of Tendons		18	14	12
	Jacking Force (kips)		7	7	7
First Crack Flexural Capacity	Center Negative	Design (kip-in)	194	108	108
		B	5.03	3.57	3.57
	Center Positive	Design (kip-in)	132	48	48
		B	5.41	3.79	3.79
	Rail Seat Positive	Design (kip-in)	283	418	418
		B	6.41	5.78	5.78
	Rail Seat Negative	Design (kip-in)	178	78	78
		β	6.53	3.51	3.51

Table 6.13: Comparison of the magnitude of flexural capacity of existing and optimized (proposed) crosstie designs for HAL freight applications

Characteristic			Existing	Prototype 1	Prototype 2
Design Values	Compressive Strength (ksi)		7	7	7
	Length (ft)		8.5	8.5	8.5
	Tie Spacing (in)		24	24	24
	Number of Tendons		20	18	8
	Jacking Force (kips)		7	7	7
First Crack Flexural Capacity	Center Negative	Design (kip-in)	240	230	239
		B	2.66	3.50	3.57
	Center Positive	Design (kip-in)	186	0	83
		B	2.66	3.58	3.79
	Rail Seat Positive	Design (kip-in)	381	204	234
		B	9.63	4.01	7.52
	Rail Seat Negative	Design (kip-in)	219	189	202
		β	6.44	3.78	4.72

HRT prototypes demonstrate a reduction in center negative bending capacity of approximately 50% and an increase in rail seat positive capacity by as much as 100%. HAL freight prototypes have similar center negative capacities but rail seat positive reductions of approximately 40%. Selecting the most reasonable prototype for both HRT and HAL freight, values for bending moment reductions are shown in Tables 6.14 and 6.15.

Table 6.14: Comparison of the change in flexural capacity of existing and optimized (proposed) crosstie designs for HRT applications

Characteristic			Existing	Prototype	% Change
Design Values	Compressive Strength (ksi)		7	7	0
	Length (ft)		8.5	8.5	0
	Tie Spacing (in)		24	24	0
	Number of Tendons		18	14	-22
	Jacking Force (kips)		7	7	0
First Crack Flexural Capacity	Center Negative	Design (kip-in)	194	111	-43
		β	5.03	3.65	-27
	Center Positive	Design (kip-in)	132	79	-40
		β	5.41	3.79	-30
	Rail Seat Positive	Design (kip-in)	283	271	-4
		β	6.41	4.01	-37
	Rail Seat Negative	Design (kip-in)	178	71	-60
		β	6.53	3.78	-32

Table 6.15: Comparison of the change in flexural capacity of existing and optimized (proposed) crosstie designs for HAL freight applications

Characteristic			Existing	Prototype	% Change
Design Values	Compressive Strength (ksi)		7	7	0
	Length (ft)		8.5	8.5	0
	Tie Spacing (in)		24	24	0
	Number of Tendons		20	18	-10
	Jacking Force (kips)		7	7	0
First Crack Flexural Capacity	Center Negative	Design (kip-in)	230	239	4
		β	2.66	3.57	34
	Center Positive	Design (kip-in)	186	83	-55
		β	2.66	3.79	42
	Rail Seat Positive	Design (kip-in)	381	234	-39
		β	9.63	7.52	-22
	Rail Seat Negative	Design (kip-in)	219	202	-8
		β	6.44	4.72	-27

6.6 Conclusions

A probabilistic approach for the analysis and design of concrete crossties was undertaken. The approach incorporated the use of SRA principles that were implemented using both FORM and MCS. In the case of HRT, there was excess flexural capacity at both the center and rail seat sections in the current crosstie design that could be reduced by as much as 50%. For the HAL freight crosstie, the center section was under-designed. As such, the HAL design could benefit from having a similar or slightly higher bending moment at the crosstie center but much lower rail seat section to better balance the design.

The process I proposed and demonstrated in this chapter can be applied to concrete crosstie designs from other locations, and should be undertaken by considering demands that may not be representative of the exact location in which field data are collected. This requires extrapolation of support conditions, a challenging undertaking that involves multiple assumptions (Quirós-Orozco, 2018).

CHAPTER 7: CONCLUSION AND FUTURE WORK

In this dissertation, I describe the development and application of a method to quantify flexural demands on prestressed, monoblock concrete crossties for use in generating designs that are optimized for field loading conditions. Field testing and evaluation of a broad range of types of United States rail infrastructure ranging from light rail transit to heavy axle load (HAL) freight has proven useful in identifying variables that influence crosstie flexural demand. Collection of extensive data for more than one year at each field site provided a robust dataset that allowed me to develop a multivariate model for center and rail seat moment prediction. I then used the data to develop and implement a probabilistic design methodology using structural reliability analysis (SRA), leading to a number of conclusions that I summarize below.

7.1 Conclusions

7.1.1 Non-Destructive Bending Moment Instrumentation Methodology

A non-intrusive and non-destructive instrumentation method using concrete surface strain gauges was successfully developed and deployed to measure bending strains and resulting moments experienced by concrete crossties under a variety of types of rail infrastructure in the United States. This method was robust and yielded reliable and repeatable results over long time durations (up to three years) with very few in-service failures. Additionally, data collected using this method were generally clean and required minimal filtering in order to obtain peak bending responses.

7.1.2 Input Loading Environment at Wheel-Rail Interface

I investigated the aggregate effect of speed and other vehicle and track irregularities to generate accurate load factors that represent the total rail transit wheel load environment including dynamic and impact loads. The following conclusions were drawn from this research:

- Total load factor distributions for the three rail transit systems studied were statistically different, demonstrating that unique load factors are needed to adequately represent the existing wheel loads and improve the design of critical components that make up the track structure. Distributions indicate that the current AREMA impact factor of three could be reduced by as much as 50%.
- I analyzed existing dynamic load factors and found that the Talbot approach to estimating dynamic loading due to speed and wheel diameter was a poor predictor for rail transit modes. This method over-estimates light rail transit wheel loading environment by a factor of three. Conversely, heavy rail transit wheel loading factors are underestimated by approximately 50%. The Talbot method was, however, a good predictor for commuter rail transit wheel load factors.
- Focused wheel-rail interface instrumentation can be deployed in the field to answer loading questions within a given rail transit mode. The modest effort required to install instrumentation and process data from such an installation can provide substantial returns on investment (ROI) by helping develop more economically mechanistically designed track components.

7.1.3 Non-Destructive Field Quantification of Bending Moments

The concrete surface strain gauge instrumentation I developed was successful in measuring the bending strains and resulting moments experienced by concrete crossties under a

variety of types of rail traffic. The data were used to answer questions related to crosstie-to-crosstie variability, and the occurrence and magnitude of temperature-induced curl. The following conclusions were drawn from this research:

- Bending moments vary widely from crosstie-to-crosstie. This was demonstrated on a HAL freight railroad application, showing bending moments at the crosstie center that ranged from 0 kNm (0 kip-in) to 22.8 kNm (202 kip-in). This is consistent with prior research (Wolf et al., 2015; Wolf, 2015; Gao et al., 2016).
- Temperature-induced curl (e.g. warping of the crosstie due to different temperatures on the top and bottom) has a quantifiable impact on concrete crosstie flexural demand. Curl in concrete crossties was found to change over the course of the day as the temperature gradient changed. These changes affected the bending moments induced in the concrete crossties (Wolf, 2015a; Wolf et al., 2016b), a behavior similar to that which has been noted in rigid pavement applications (Beckemeyer et al., 2002).

7.1.4 Factors that Influence Rail Transit Bending Moments

Field deployments on MetroLink (light rail) and NYCTA (heavy rail) allowed me to address questions specific to rail transit concrete crosstie performance including quantification of bending moment magnitudes, calculation of reserve structural capacity, and measurement of crosstie-to-crosstie variability. The following conclusions were drawn from this research:

- Maximum center negative bending moments ranged from 25 kip-in (2.8 kNm) on MetroLink (light rail) to 120 kip-in (13.5 kNm) on NYCTA (heavy rail).
- Significant residual flexural capacity was also found. 99th percentile bending moments resulted in residual load factors of 6 and 2 for light and HRT systems, respectively.

- Bending moments experienced by concrete crossties on rail transit systems varied from crosstie-to-crosstie, ranging from as little as 10% for center negative (C-) bending on MetroLink to as much as 100% on NYCTA. The latter is similar to what was previously demonstrated in the HAL freight environment. Crosstie-to-crosstie variability between the two transit modes was also quite different, with the greatest variability associated with heavy rail transit center negative bending moments.

7.1.5 Probabilistic Crosstie Design

I developed and demonstrated a probabilistic design process based on structural reliability analysis concepts. Using first order reliability methods I obtained values for reliability indices (β) for new designs and compared them with existing designs. New, optimized designs had the following characteristics:

- New heavy rail transit designs had a reduced center negative moment capacity of 50%.
- New HAL freight designs had a reduction in rail seat bending capacity of 40%.
- In most cases, as compared to current designs, the proposed designs for both rail modes had fewer prestressing wires and a higher centroid of prestressing steel.
- In all cases, the flexural capacities at the crosstie center and rail seat are better balanced from a structural reliability standpoint when compared to current designs.

7.1.6 Impact on Mechanistic-Empirical Design of Railway Track Components

My dissertation focused on advancement of the mechanistic component of mechanistic-empirical design. This research is important because the response of components must be well understood before inferences can be made as to how they should be designed. Specific advancements were made to better understand the effects of various rail transport loading

conditions on bending moment magnitudes, reserve structural capacity, thermal gradient effects, and crosstie-to-crosstie variability.

A design process incorporating many of the elements proposed in this dissertation was used to develop a new crosstie for Amtrak's Northeast Corridor. This was the first instance in which a United States concrete crosstie design was based on mechanistic elements in a process that has traditionally relied on an iterative approach and assumptions based on empirical data. This design example was an initial step toward closing the gap between the current best practices and an ideal solution that incorporates an appropriate amount of both mechanistic and empirical design content (Figure 7.1).

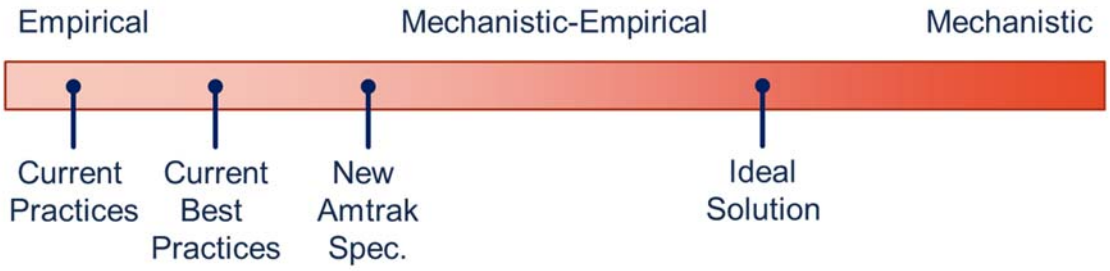

Figure 7.1: Flow chart representation of this dissertation's contribution to the application of mechanistic design to rail engineering in the context of concrete crossties.

The probabilistic design method using structural reliability analysis fundamentals demonstrated in this dissertation is a critical step in the development of mechanistic-empirical practices for the design of concrete crossties. The next steps for advancing the development of mechanistic design for railway track components are shown in Figure 7.2. Establishing failure criteria will be the most challenging. This is especially true for concrete crossties given new findings that have called into question the importance of cracking (César Bastos, 2016; César Bastos, et al. 2017).

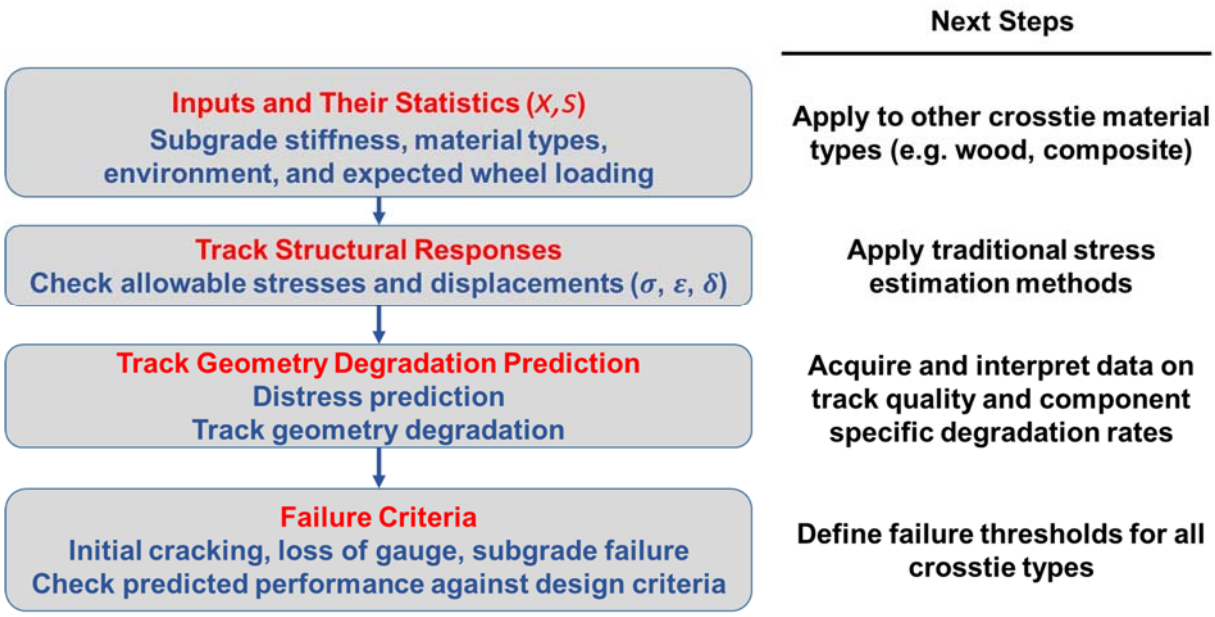

Figure 7.2: Next steps for advancement of proposed framework for mechanistic-empirical design of railroad track infrastructure components.

Beyond crossties, the proposed framework will enable future application of mechanistic-empirical design practices to other railway track components. Track components and materials adjacent to the crosstie (e.g. ballast and fastening systems) are the most reasonable candidate for near-term adoption. The rate of deterioration of the ballast layer has been extensively investigated. The deterioration of ballast and overall track substructure health as a function of tonnage has been quantified through experimentation and modeling (Selig and Waters 1994; Moaveni et al. 2016; Hou et al. 2018). The fastening system has received comparatively little research, but emerging mechanistic work on premium fastening systems for timber crossties lends itself to the mechanistic design process. Additionally, prior work on lateral load transfer and magnitude within the fastening system is relevant and can be applied to the design process (Edwards et al., 2017b; Holder et al. 2017). The application of the mechanistic component of mechanistic design to a variety of track superstructure components was also preliminary

documented by Edwards et al. (2017b).

7.2 Future Research

The results I present in this dissertation facilitate the optimization of future concrete crosstie bending moment requirements based on flexural demands recorded during revenue service field tests. Given the accuracy and repeatability of data from surface strain gauging of concrete crossties, broader deployment is warranted to investigate scenarios that were not previously considered. Specific track conditions and manufacturing processes that warrant additional study are described in the following sub-sections.

7.2.1 Variations in Track Quality

Given that much of the work I describe in this dissertation pertains to collection of data on track that is well-maintained, future work focusing on the deployment of this method in more demanding or partially degraded field conditions would be of value such as track transition zones and areas with fouled ballast. These are areas that have received considerable attention for track substructure reasons, but are also of interest in the area of superstructure performance.

7.2.2 Concrete Crosstie Design

Alternative methods of prestressing concrete crossties have begun to emerge in the North American market, including end-plated systems that eliminate many of the challenges associated with the transfer of prestressing forces to the concrete. These, along with post-tensioned concrete crosstie designs that are beginning to appear, should be the subject of research aimed at understanding their long-term performance. Such a study should also ensure that the methods by which their initial structural capacity and load versus deflection behavior are accurate. Additionally, as alternative crosstie types emerge, it is important to understand whether the

analysis and design methods and procedures proposed in this dissertation are robust to changes in crosstie manufacturing method (e.g. pre-tensioned vs. post-tensioned designs) and design geometries (e.g. length, depth, etc.).

Finally, I suggest further study of concrete crosstie life cycle cost (LCC). There has been little focus on this topic within the realm of track superstructure components, and is of particular importance if capital and maintenance dollars are scarce. It also provides a logical method to include the quantification of other environmental impacts to ensure concrete crossties are being designed, manufactured, maintained, and disposed of in a sustainable manner.

7.2.3 Concrete Crosstie Performance

The transient behavior of concrete crossties should be considered. This is a subject whose importance has recently been illustrated by a study of the track support structure and its transient performance (Stark and Wilk, 2016; Wilk, 2017; Hou et al., 2018). Initial data on the flexural response of the crosstie to a passing wheel load indicates that the response can vary widely depending on load magnitude and duration, something noted decades ago on Amtrak's NEC in their study of rail pad effectiveness. Understanding the relative importance and trade-offs between flexural demand magnitude and moment duration could influence the design of other resilient track components such as under tie pads (UTPs) and ballast mats.

7.2.4 Other Crosstie Materials

Beyond concrete crossties, there is ongoing interest in performing similar instrumentation on composite crossties. If surface strain gauging similar to that described in this dissertation is indeed feasible on composite materials, this would provide an opportunity to understand the behavior of a crosstie material that is inherently different than concrete. This would allow for an analysis of how the flexural rigidity of the composite crosstie and its interaction with the ballast

impact overall track performance. Both short and long-term impacts of composite crosstie use should be investigated. Finally, the other obvious crosstie material to investigate through this procedure is steel, given the applicability of strain gauges to steel products. Such research would be particularly important outside North America where steel crossties are more commonly used.

REFERENCES

Albahttiti, M.T., A.A. Ghadban, K.A. Riding, and D. Lange. 2015. Air entrainment and the fabrication of concrete railroad ties. In: *Proceedings of the 2015 Joint Rail Conference*, American Society of Mechanical Engineers (ASME), San Jose, CA, USA.

Al-Qadi, I. 2018. Class Notes, CEE 310 (Transportation Engineering), Department of Civil and Environmental Engineering (CEE), University of Illinois at Urbana-Champaign, Urbana, IL, USA.

American Association of State Highway and Transportation Officials (AASHTO). 2008. *Mechanistic-Empirical Pavement Design Guide*. American Association of State Highway and Transportation Officials (AASHTO). Washington, DC, USA.

American Concrete Institute (ACI). 1997. *Committee 215: Considerations For Design Of Concrete Structures Subjected To Fatigue Loading*. American Concrete Institute (ACI). Farmington Hills, MI, USA.

American Concrete Institute (ACI). 2002. *Evaluation of Strength Test Results of Concrete*. American Concrete Institute (ACI). Farmington Hills, MI, USA.

American Concrete Institute (ACI). 2014. *ACI 318-14 Building Code Requirements for Structural Concrete and Commentary*. American Concrete Institute (ACI), Farmington Hills, MI, USA.

American Public Transportation Association (APTA). 2019. *Fact Book Glossary*. URL https://www.apta.com/resources/statistics/Pages/glossary.aspx. Accessed 2019-01-01.

American Railway Engineering and Maintenance-of-Way Association (AREMA). 2016. Manual for Railway Engineering, Chapter 30, Part 4: Concrete Ties. The American Railway Engineering and Maintenance-of-Way Association, Lanham, MD, USA.

American Railway Engineering and Maintenance-of-Way Association (AREMA). 2017. Manual for Railway Engineering, Chapter 30, Part 4: Concrete Ties. The American Railway Engineering and Maintenance-of-Way Association, Lanham, MD, USA.

Ang, A.H. and W.H. Tang. 2006. *Probability Concepts in Engineering: Emphasis on Applications to Civil and Environmental Engineering,* 2nd ed. John Wiley & Sons, New York, NY, USA.

Applied Research Associates (ARA). 2004. *Guide for Mechanistic-Empirical Design of New and Rehabilitated Pavement Structures.* Applied Research Associates (ARA), Inc., ERES Division. Champaign, IL, USA.

Askarinejad, H., M. Dhanasekar, and C. Cole. 2013. Assessing the effects of track input on the response of insulated rail joints using field experiments. *Proceedings of the Institution of Mechanical Engineers, Part F: Journal of Rail and Rapid Transit*, 227(2): 176–187.

Bartlett, F.M. and J.G. MacGregor. 1999. Variation of in-place concrete strength in structures. *American Concrete Institute Materials Journal*, 96(2):261-27.

Beckemeyer, C., L. Khazanovich, and H. Thomas Yu. 2002. Determining amount of built-in curling in jointed plain concrete pavement: case study of Pennsylvania 1-80. *Transportation Research Record: Journal of the Transportation Research Board*, 1809: 85–92.

Bodapati, N.N.B, R.J. Peterman, W. Zhao, T. Beck, C.-H.J. Wu, J. Holste, M. Arnold, R. Benteman, and R. Schweiger. 2013. Transfer-length measurements on concrete railroad ties fabricated with 15 different prestressing reinforcements. In: *Proceedings of the 2013 PCI Convention and National Bridge Conference*, Grapevine, TX, USA, pp. 21–24.

Bodapati, N.N.B., R.J. Peterman, B.T. Beck, and C.-H.J. Wu. 2014. Effect of concrete properties on transfer lengths in concrete rail-road ties. In: *Proceedings of the 2014 Joint Rail Conference*, American Society of Mechanical Engineers (ASME), Colorado Springs, CO, USA.

Cai, Z., G.P. Raymond, and R.J. Bathurst. 1994. Estimate of static track modulus using elastic foundation models. *Transportation Research Record: Journal of the Transportation Research Board*, 1470: 65-72.

Canadian National (CN). 2011. Wheel Impact Load Detectors: The early history on CN. In: *Proceedings of the 31st Annual North American Rail Mechanical Operations Seminar*, St. Louis, MO, USA.

Canga Ruiz, Á.E. 2018. *Analysis of the Design of Railroad Track Superstructure Components for Rail Transit Applications*. Master's Thesis, University of Illinois at Urbana-Champaign, Department of Civil and Environmental Engineering, Urbana, IL, USA.

Canga Ruiz, Á.E., Y. Qian, J.R. Edwards, and M.S. Dersch. 2019. Analysis of the temperature effect on concrete crosstie flexural behavior. *Construction and Building Materials*, 196: 362–374.

César Bastos, J. 2016. *Analysis of the Performance and Failure of Railroad Concrete Crossties with Various Track Support Conditions*. Master's Thesis, University of Illinois at Urbana-Champaign, Department of Civil and Environmental Engineering, Urbana, IL, USA.

César Bastos, J., M.S. Dersch, J.R. Edwards, and B.O. Andrawes. 2016. Determination of the influences of deteriorated track conditions on gauge widening in concrete sleeper track. In: *Proceedings of the 2016 World Congress on Railway Research*, Milan, Italy.

César Bastos, J., M.S. Dersch, J.R. Edwards, and B.O. Andrawes. 2017. Flexural behavior of concrete crossties under different support conditions. *American Society of Civil Engineers Journal of Transportation Engineering*, 143(12): 04017064.

César Bastos, J., A. Álvarez-Reyes, M.S. Dersch, J.R. Edwards, and C.P.L. Barkan. 2018. Laboratory Characterization of Structural Capacity of North American Heavy Haul Concrete Crossties. In Press: *Transportation Research Record: Journal of the Transportation Research Board*.

Chen, R., X. Zhao, Z. Wang, H. Jiang, and X. Bian. 2013. Experimental study on dynamic load magnification factor for ballastless track-subgrade of high-speed railway. *Journal of Rock Mechanics and Geotechnical Engineering*, 5(4): 306–311.

Chen, Z., B. Andrawes, and J.R. Edwards. 2016. Finite element modelling and field validation of prestressed concrete sleepers and fastening systems. *Structure and Infrastructure Engineering*, 12(5): 631–646.

Chen, Z., M. Shin, B. Andrawes, and J.R. Edwards. 2014a. Parametric study on damage and load demand of prestressed concrete crosstie and fastening systems. *Engineering Failure Analysis*, 46: 49–61.

Chen, Z., M. Shin, S. Wei, B. Andrawes, and D.A. Kuchma. 2014b. Finite element modeling and validation of the fastening systems and concrete sleepers used in North America. *Proceedings of the Institution of Mechanical Engineers, Part F: Journal of Rail and Rapid Transit*, 228(6): 590–602.

Cheng, C., X. Bian, H. Jiang, and J. Jiang. 2014. Model testing on dynamic behaviors of the slab track of high-speed railway. In: *Proceedings of the 9th International Conference on Structural Dynamics (EURODYN 2014)*, Porto, Portugal, pp. 813–818.

Choros, J., M.N. Coltman, and B. Marquis. 2007. Prevention of derailments due to concrete tie rail seat deterioration. In: *Proceedings of the 2007 Joint Rail Conference and Internal Combustion Engine Division Spring Technical Conference*, American Society of Mechanical Engineers (ASME), Pueblo, Colorado, USA, pp. 173–181.

Consolis. 2017. *SMART SLEEPERS® A Concrete Sleeper with Accurate and Resistant Embedded Sensors.* URL https://www.consolis.com. Accessed 2017-03-10.

Cortis, D., M. Bruner, G. Malavasi, S. Rossi, M. Catena, and M. Testa. 2017. Estimation of the wheel-rail lateral contact force through the analysis of the rail web bending strains. *Measurement - Journal of the International Measurement Confederation*, 99: 23–35.

Csenge, M.V., X. Lin, H. Wolf, M.S. Dersch, and J.R. Edwards. 2015. Mechanistic design of concrete monoblock crossties for rail transit loading conditions. In: *Proceedings of the 2015 APTA Rail Conference*, American Public Transportation Association (APTA), Salt Lake City, UT, USA.

Darling, D.A. 1957. The Kolmogorov-Smirnov, Cramer-von Mises Tests. *The Annals of Mathematical Statistics*, 28(4): 823–838.

Der Kiureghian, A. 2008. Analysis of structural reliability under parameter uncertainties. *Probabilistic Engineering Mechanics*, 23(4): 351–358.

Der Kiureghian, A., T. Haukaas, and K. Fujimura. 2006. Structural reliability software at the University of California, Berkeley. *Structural Safety*, 28(1): 44–67.

Ditlevsen, O. and H.O. Madsen. 2007. *Structural Reliability Methods*. John Wiley & Sons, Chichester, New York, USA.

Domingo, L., C.Z. Martín, C.P. Avilés, and J.I.R. Herráiz. 2014. Analysis of the influence of cracked sleepers under static loading on ballasted railway tracks. *The Scientific World Journal*, 2014: 363547.

Doyle, N.F. 1980. *Railway Track Design: A Review of Current Practice*. Canberra: Australian Government Publishing Service, Melbourne, Australia.

Edwards, J.R., A. Cook, M.S. Dersch, and Y. Qian. 2018a. Quantification of rail transit wheel loads and development of improved dynamic and impact loading factors for design. *Proceedings of the Institution of Mechanical Engineers, Part F: Journal of Rail and Rapid Transit*, 232(10): 2406–2417.

Edwards, J.R., M.S. Dersch, and R.G. Kernes. 2017a. *Improved Concrete Crosstie And Fastening Systems For US High Speed Passenger Rail And Joint Corridors - Project Summary Report (Volume 1)*. US Department of Transportation, Federal Railroad Administration DOT/FRA/ORD-17/23. Washington, DC, USA.

Edwards, J.R., M.S. Dersch, and R.G. Kernes. 2017b. *Improved Concrete Crosstie And Fastening Systems For US High Speed Passenger Rail And Joint Corridors - Technical Report (Volume 2)*. US Department of Transportation, Federal Railroad Administration DOT/FRA/ORD-17/23, Washington, DC, USA.

Edwards, J.R., Z. Gao, H.E. Wolf, M.S. Dersch, and Y. Qian. 2017c. Quantification of concrete railway sleeper bending moments using surface strain gauges. *Measurement - Journal of the International Measurement Confederation*, 111: 197–207.

Edwards, J.R., A.E.C. Ruiz, A.A. Cook, M.S. Dersch, and Y. Qian. 2018b. Quantifying bending moments in rail-transit concrete sleepers. *American Society of Civil Engineers Journal of Transportation Engineering*, 144(3): 04018003.

Elishakoff, I. 2017. *Probabilistic Methods in the Theory of Structures: Strength of Materials, Random Vibrations, and Random Buckling*. World Scientific, Hackensack, NJ, USA.

Elsaleiby, A.A.S. 2014. *Wheel Imbalance Effect on the Output of Wheel Impact Load Detector System (WILD)*. Master's Thesis, Department of Industrial and Systems Engineering, Colorado State University, Pueblo, CO, USA.

Engmann, S. and D. Cousineau. 2011. Comparing distributions: the two-sample Anderson-Darling Test as an alternative to the Kolmogorov-Smirnoff Test. *Journal of Applied Quantitative Mechanics,* 6(2):17.

Federal Railroad Administration (FRA). 2011. 49 CFR 213 - Track Safety Standards. In: *Title 49 of the Code of Federal Registrations*, US Department of Transportation, Federal Railroad Administration, Washington, DC, USA.

Federal Transit Administration (FTA). 2013. *Revenue Vehicle Inventory, National Transit Database (NTD)*. Federal Transit Administration. Washington, DC, USA.

Frangopol, D.M., R.B. Corotis, and R. Rackwitz. 1997. *Reliability and Optimization of Structural Systems*, 1st ed. Pergamon, Oxford, United Kingdom.

Gao, Z., H.E. Wolf, M.S. Dersch, Y. Qian, and J.R. Edwards. 2016. Field measurements and proposed analysis of concrete crosstie bending moments. In: *Proceedings of the American Railway Engineering and Maintenance-of-Way Association Annual Conference*, Orlando, FL, USA.

Gettu, R., Z.P. Bazant, and M.E. Karr. 1990. Fracture properties and brittleness of high-strength concrete. *American Concrete Institute Materials Journal*, 87(6): 608–618.

Grassé, J.S. 2013. *Field Test Program of the Concrete Crosstie and Fastening System*. Master's Thesis, University of Illinois at Urbana-Champaign, Department of Civil and Environmental Engineering, Urbana, IL, USA.

Grassé, J.S., S. Wei, J.R. Edwards, D. Kuchma, and D.A. Lange. 2014. Field study of load path in rail and concrete crosstie system. *Electronic Journal of Structural Engineering*, 14(2014): 29–38.

Hannah, R.L. and S.E. Reed. 1992. *Strain Gage Users' Handbook*. Society of Experimental Mechanics, Bethel, CT, USA.

Harris, D.K., R.H. Lutch, T.M. Ahlborn, and P. Duong. 2011. Optimization of a prestressed concrete railroad crosstie for heavy-haul applications. *American Society of Civil Engineers Journal of Transportation Engineering*, 137(11): 815–822.

Harrison, H.D., L.R. Cheng, and W. GeMeiner. 2006. Tracking the performance of heavy axle load vehicles in revenue service. In: *Proceedings of the 2006 ASME International Mechanical Engineering Congress and Exposition*, American Society of Mechanical Engineers (ASME) Rail Transportation Division (RTD), Chicago, IL, USA.

Harrison, H.D., F.E Dean, E.T, Selig, and H.F. Stewart. 1984. *Correlation of Concrete Tie Track Performance in Revenue Service and at the Facility for Accelerated Service Testing. Volume A - A Detailed Summary*. Battelle Columbus Laboratories, Columbus, OH, USA.

Hay, W.W. 1953. *Railroad Engineering*, 1st ed. John Wiley & Sons, New York, NY, USA.

Hay, W.W. 1982. *Railroad Engineering*, 2nd ed. John Wiley & Sons, New York, NY, USA.

HBM. 2017. *Strain Gauges – Absolute precision from HBM*. URL https://www.hbm.com/fileadmin/mediapool/hbmdoc/technical/s3996.pdf. Accessed 2017-03-10.

Holder, D.E., M.V. Csenge, Y. Qian, M.S. Dersch, and J.R. Edwards. 2017. Laboratory investigation of the Skl-style fastening system's lateral load performance under heavy haul freight railroad loads. *Engineering Structures*, 139 (2017) 71-80.

Hou, W., B. Feng, W. Li, and E. Tutumluer. 2018. Evaluation of ballast behavior under different tie support conditions using discrete element modeling. In Press: *Transportation Research Record: Journal of the Transportation Research Board*.

Jamshidi, A., S. Faghih-Roohi, S. Hajizadeh, A. Núñez, R. Babuska, R. Dollevoet, Z. Li, and B. De Schutter. 2017. A big data analysis approach for rail failure risk assessment, *Risk Analysis*, 37(8): 1495–1507.

Jimenez, R. and J. LoPresti. 2004. Performance of alternative tie material under heavy-axle-load traffic. *Railway Track and Structures*, January, pp. 16–18.

Jokūbaitis, A., J. Valivonis, and G. Marčiukaitis. 2016. Influence of static and dynamic loads on the behavior of prestressed concrete railway sleepers. *Solid State Phenomena*, 249: 278–283.

Kaewunruen, S. and A.M. Remennikov. 2009a. Dynamic crack propagations in prestressed concrete sleepers in railway track systems subjected to severe impact loads. *Journal of Structural Engineering*, 136(6): 749–754.

Kaewunruen, S. and A.M. Remennikov. 2009b. Progressive failure of prestressed concrete sleepers under multiple high-intensity impact loads. *Engineering Structures*, 31(10): 2460–2473.

Kalay, S. and J. Samuels. 2002. Reducing the stress state of the railroad. *Railway Track and Structures,* March, pp. 13–16.

Kernes, R. 2014. *The Mechanics of Abrasion on Concrete Crosstie Rail Seats*. Master's Thesis, University of Illinois at Urbana-Champaign, Department of Civil and Environmental Engineering, Urbana, IL, USA.

Kerokoski, O., T. Rantala, and A. Nurmikolu. 2016. Deterioration mechanisms and life cycle of concrete monoblock railway sleepers in Finnish conditions. In: *Proceedings of the 11th World Congress on Railway Research*, Milan, Italy.

Kerr, A.D. 2000. On the determination of the rail support modulus k. *International Journal of Solids and Structures*, 37(32): 4335–4351.

Kerr, A.D. 2003. *Fundamentals of Railway Track Engineering*. Simmons Boardman, Omaha, NE, USA.

Khan, A.S. and X. Wang. 2001. *Strain Measurements And Stress Analysis*. Prentice Hall, Upper Saddle River, NJ, USA.

Knothe, K. and S. Stichel. 2013. *Rail Vehicle Dynamics*. Springer, New York, NY, USA.

Kutner, M.H. 2005. *Applied Linear Statistical Models*, 5th ed. McGraw-Hill Irwin, New York, NY, USA.

Lee, S. 2013. Probabilistic approach on railway infrastructure stability and settlement analysis. *IJR International Journal of Railway*, 6(2): 45–52.

Leong, J. and M.H. Murray. 2008. Probabilistic analysis of train–track vertical impact forces. In: *Proceedings of the Institution of Civil Engineers Transport 2008*, Thomas Telford Ltd., pp. 15–21.

Lin, T.Y. and N.H. Burns. 1981. *Design of Prestressed Concrete Structures*, 3rd ed. John Wiley & Sons, Hoboken, NJ, USA.

Lin, X., J.R. Edwards, M.S. Dersch, T.A. Roadcap, and C. Ruppert. 2017. Load quantification of the wheel–rail interface of rail vehicles for the infrastructure of light rail, heavy rail, and commuter rail transit. *Proceedings of the Institution of Mechanical Engineers, Part F: Journal of Rail and Rapid* Transit: 232(2) 596–605.

Lovett, A. 2017. *Railroad Decision Support Tools for Track Maintenance*. Doctoral Thesis, Master's Thesis, University of Illinois at Urbana-Champaign, Department of Civil and Environmental Engineering, Urbana, IL, USA.

MATLAB. 2012. *MATLAB and Statistics Toolbox Release*. The MathWorks, Inc., Natick, MA, USA.

Mayville, R.A., L. Jiang, and M. Sherman. 2014. *Performance Evaluation of Concrete Railroad Ties on the Northeast Corridor*. US Department of Transportation, Federal Railroad Administration DOT/FRA/RPD-14/03. Washington, DC, USA.

McHenry, M. and J. LoPresti. 2016. Field evaluation of sleeper and fastener designs for freight operations. In: *Proceedings of the 11th World Congress on Railway Research*, Milan, Italy.

McHenry, M.T. 2013. *Pressure Measurement At The Ballast-Tie Interface Of Railroad Track Using Matrix Based Tactile Surface Sensors*. Master's Thesis, University of Kentucky, Department of Civil Engineering, Lexington, KY, USA.

McNeely, D.J. and S.D. Lash. 1963. Tensile strength of concrete. *Journal of the American Concrete Institute*, 60(38): 751–759.

Mertol, H.C., S. Rizkalla, P. Zia, and A. Mirmiran. 2008. Characteristics of compressive stress distribution in high-strength concrete. *American Concrete Institute Structural Journal*, 105(5): 626-633.

Mindess, S., J.F. Young, and D. Darwin. 2003. *Concrete*, 2nd ed. Prentice Hall, Upper Saddle River, NJ, USA.

Moaveni, M., I. Qamhia, E. Tutumluer, C. Basye, D. Li, and S.C. Douglas. 2016. Morphological characterization of railroad ballast degradation trends in the field and laboratory, *Transportation Research Record: Journal of the Transportation Research Board*, 2545: 89-99.

Murray, M. 2015. Heavy haul sleeper design - a rational cost-saving method. In: *Proceedings of the 2015 International Heavy Haul Association Conference*, Perth, Australia.

Naaman, A.E. 2004. *Prestressed Concrete Analysis and Design: Fundamentals, 2nd ed.* Techno Press 3000, Ann Arbor, MI, USA.

National Instruments. 2017. *CompactDAQ Systems*. URL http://www.ni.com/dataacquisition/compactdaq. Accessed 2017-03-11.

Ngamkhanong, C., D. Li, and S. Kaewunruen. 2017. Impact capacity reduction in railway prestressed concrete sleepers with surface abrasions. *IOP Conference Series: Materials Science and Engineering*, 245: 032048.

Nowak, A.S. and K.R. Collins. 2013. *Reliability Of Structures*, 2nd ed. Taylor and Francis Group, CRC Press, Boca Raton, FL, USA.

Nowak, A.S. and M.M. Szerszen. 2003. Calibration of design code for buildings (ACI 318): Part 1 - statistical models for resistance. *American Concrete Institute Structural Journal*. 100(3):377-382.

Ott, R.L. and M. Longnecker. 2008. *An Introduction to Statistical Methods and Data Analysis*, 6th ed. Brooks/Cole, Belmont, CA, USA.

Pavement Interactive. 2012. *What Is Mechanistic-Empirical Design? – The MEPDG and You.* URL http://www.pavementinteractive.org/2012/10/02/what-is-mechanistic-empirical-design-the-mepdg-and-you/. Accessed 2018-04-18.

Prause, R.H., H.D. Harrison, J.C. Kennedy, and R.C. Arnlund. 1977. *An Analytical and Experimental Evaluation of Concrete Crosstie and Fastener Loads*. US Department of Transportation, Federal Railroad Administration DOT/FRA/RPD-77/71. Washington, DC, USA.

Prause, R.H. and A. Kish. 1978. Statistical description of service loads for concrete crosstie track. *Transportation Research Record: Journal of the Transportation Research Board*, 694: 30–39.

Press, W.H., S.A. Teukolsky, W.T. Vetterling, and B.P. Flannery. 2002. *Numerical Recipes in C++: The Art of Scientific Computing*, 2nd ed. Cambridge University Press, Cambridge, UK.

Quirós-Orozco, R.J. 2018. *Prestressed Concrete Railway Crosstie Support Variability and its Effect on Flexural Demand*. Master's Thesis, University of Illinois at Urbana-Champaign, Department of Civil and Environmental Engineering, Urbana, IL, USA.

Quirós-Orozco, R.J., J.R. Edwards, Y. Qian, and M.S. Dersch. 2018. Quantification of loading environment and flexural demand of prestressed concrete crossties under shared corridor operating conditions. *Transportation Research Record: Journal of the Transportation Research Board*. 2672: 136–145.

Radford, G.S. 1922. *The Control of Quality in Manufacturing*. The Ronald Press Company, New York, NY, USA.

Railway Systems and Management Association (RSMA). 1970. *International Forum - The Dynamics and Economics of Railway Track Systems*. Railway Systems and Management Association, Chicago, IL, USA.

Rakoczy, A.M. and A.S. Nowak. 2013. Resistance model of lightweight concrete members. *American Concrete Institute Materials Journal*, 110: 99–107.

Rakoczy, A.M. and A.S. Nowak. 2014. Resistance factors for lightweight concrete members. *American Concrete Institute Structural Journal*, 115: 103–111.

Remennikov, A.M., M.H. Murray, and S. Kaewunruen. 2012. Reliability-based conversion of a structural design code for railway prestressed concrete sleepers. *Proceedings of the Institution of Mechanical Engineers, Part F: Journal of Rail and Rapid Transit*, 226(2): 155–173.

Roesler, J. and E. Barenberg. 1999. Fatigue and static testing of concrete slabs. *Transportation Research Record: Journal of the Transportation Research Board*, 1684: 71–80.

Sadeghi, J. 2012. New advances in analysis and design of railway track system, In: X. Perpinya (Ed.) *Reliability and Safety in Railway*. InTech, London, United Kingdom.

Sadeghi, J. and P. Barati. 2010. Comparisons of the mechanical properties of timber, steel and concrete sleepers. *Structure and Infrastructure Engineering*, 8(12): 1151–1159.

Selig, E.T. and J.M. Waters 1994. *Track Geotechnology and Substructure Management Engineering*, 1st ed. Thomas Telford, London, United Kingdom.

Senese, K. 2016. Annual Crosstie Update. *Railway Track and Structures*, October, pp 22–33.

Shurpali, A.A., J.R. Edwards, R.G. Kernes, D.A. Lange, and C.P.L. Barkan. 2014. Investigation of material improvements to mitigate the effects of the abrasion mechanism of concrete crosstie rail seat deterioration. *American Society of Civil Engineers Journal of Transportation Engineering*, 140(2): 04013009.

Shurpali, A.A., J.R. Edwards, R.G. Kernes, D.A. Lange, and C.P.L. Barkan. 2017. Improving the abrasion resistance of concrete to mitigate concrete crosstie rail seat deterioration (RSD).

American Society of Testing and Materials International Materials Performance and Characterization, 6(1): 521–534.

Soares, C.G. 1997. *Probabilistic Methods for Structural Design*. Springer, Dordrecht, Netherlands.

Song, W., X. Shu, B. Huang, Y. Sun, H. Gong, and D. Clarke. 2017a. Pressure distribution under steel and timber crossties in railway tracks. *American Society of Civil Engineers Journal of Transportation Engineering*, 143(9): 04017046.

Song, Y., R. Zou, D.I. Castaneda, K.A. Riding, and D.A. Lange. 2017b. Advances in measuring air-void parameters in hardened concrete using a flatbed scanner. *Journal of Testing and Evaluation*, 45(5): 1713–1725.

Standards Australia. 2003. *Railway Track Material, Part 14: Prestressed Concrete Sleepers*. Standards Australia Committee CE-002. Sydney, NSW, Australia.

Stark, T.D. and S.T. Wilk. 2016. Root cause of differential movement at bridge transition zones. *Proceedings of the Institution of Mechanical Engineers, Part F: Journal of Rail and Rapid Transit*, 230(4): 1257–1269.

Steenbergen, R.D.J.M., P.H.A.J.M. Van Gelder, S. Miraglia, and A.C.W.M. Vrouwenvelder. 2013. *Safety, Reliability and Risk Analysis: Beyond the Horizon*, 1st ed. CRC Press, Boca Raton, FL, USA.

Stratman, B., Y. Liu, and S. Mahadevan. 2007. Structural health monitoring of railroad wheels using wheel impact load detectors. *Journal of Failure Analysis and Prevention*, 7(3): 218–225.

Szerszen, M.M. and A.S. Nowak. 2003. Calibration of design code for buildings (ACI 318): Part 2 - reliability analysis and resistance factors. *American Concrete Institute Structural Journal*, 100(3): 383–391.

Taherinezhad, J., M. Sofi, P.A. Mendis, and T. Ngo. 2013. A review of behaviour of prestressed concrete sleepers. *Electronic Journal of Structural Engineering*, 13(1): 1–16.

Talbot, A.N. 1980. *Stresses in Railroad Track: Bulletins of the Special Committee on Stresses in Railroad Track 1918-1940,* American Railway Engineering Association (AREA). Washington, DC, USA.

Thompson, M.R. 1996. Mechanistic-empirical flexible pavement design: an overview. *Transportation Research Record: Journal of the Transportation Research Board*, 1539: 1–5.

Timoshenko, S.P. 1953. *History of Strength of Materials*. McGraw-Hill, New York, NY, USA.

TML. 2017. *Developing Strain Gauges and Instruments* – Polyester Strain Gauges. URL http://www.tml.jp/e/product/strain_gauge/catalog_pdf/P_PFseries.pdf. Accessed 2017-03-10.

Van Dam, E. 2014. *Abrasion Resistance of Concrete and the Use of High Performance Concrete for Concrete Railway Crossties*. Master's Thesis, University of Illinois at Urbana-Champaign, Department of Civil and Environmental Engineering, Urbana, IL, USA.

Van Dyk, B., M. Dersch, J. Edwards, C. Ruppert Jr., and C. Barkan. 2014. Load characterization techniques and overview of loading environment in North America. *Transportation Research Record: Journal of the Transportation Research Board*, 2448: 80–86.

Van Dyk, B.J. 2014. *Characterization of the Loading Environment for Shared-Use Railway Superstructure in North America*. Master's Thesis, University of Illinois at Urbana-Champaign, Department of Civil and Environmental Engineering, Urbana, IL, USA.

Van Dyk, B.J., J.R. Edwards, M.S. Dersch, C.J. Ruppert Jr., and C.P. Barkan. 2017. Evaluation of dynamic and impact wheel load factors and their application in design processes. *Proceedings of the Institution of Mechanical Engineers, Part F: Journal of Rail and Rapid Transit*, 231(1): 33–43.

Van Dyk, B.J., J.R. Edwards, C.J. Ruppert Jr., and C.P. Barkan. 2013. Considerations for mechanistic design of concrete sleepers and elastic fastening systems in North America. In: *Proceedings of the 2013 International Heavy Haul Association Conference*, New Delhi, India.

Van Dyk, B.J., A.J. Scheppe, J.R. Edwards, M.S. Dersch, and C.P. Barkan. 2016. Methods for quantifying rail seat loads and a review of previous experimentation. *Proceedings of the Institution of Mechanical Engineers, Part F: Journal of Rail and Rapid Transit*, 230(3): 935–945.

Venuti, W. 1970. *Field Investigation of the Gerwick RT-7 Prestress Concrete Tie*. Department of Civil and Environmental Engineering, San Jose State University. San Jose, CA, USA.

Venuti, W. 1990. *Report On The Structural Response Of The BART Concrete Ties*. Department of Civil and Environmental Engineering, San Jose State University. San Jose, CA, USA.

Vishay Micro-Measurements. 2015a. *Strain Gage Installations for Concrete Structures*. URL http://www.vishaypg.com/docs/11091/tt611.pdf. Accessed 2017-03-11.

Vishay Micro-Measurements. 2015b. *Strain gage selection: criteria, procedures, recommendations* URL https://www.vishay.com/docs/11055/tn505.pdf. Accessed 2013-11-17.

Von Quintus, H. L. and J.S. Moulthrop. 2007. *Mechanistic-Empirical Pavement Design Guide Flexible Pavement Performance Prediction Models For Montana--Volume I Executive Research Summary*. US Department of Transportation, Federal Highway Administration FHWA/MT-07-008/8158-1 Washington, DC, USA.

Wakui, H. and H. Okuda. 1997. A study on limit state design method for prestressed concrete sleepers. *Doboku Gakkai Ronbunshu*, (557): 35–54.

Weibull, W. 1951. A statistical distribution function of wide applicability. *American Society of Mechanical Engineers Journal of Applied Mechanics*, 18(3): 293–297.

Wiley, R. and A. Elsaleiby. 2007. *A review of wheel impact measurement variation*. Technology Digest TD-11-007, Transportation Technology Center, Inc. Pueblo, CO, USA.

Wilk, S.T. 2017. *Mitigation of Differential Movements at Railroad Bridge Transition Zones*. Doctoral Thesis, University of Illinois at Urbana-Champaign, Department of Civil and Environmental Engineering, Urbana, IL, USA.

Windisch, A. 1970. Safety to brittle failure in prestressed concrete structures with bond. *Periodica Polytechnica Civil Engineering*, 14(4): 341.

Window, A.L. 1992. *Strain Gauge Technology*. Springer, Dordrecht, Netherlands.

Wolf, H.E. 2015a. *Flexural Behavior of Prestressed Concrete Monoblock Crossties*. Master's Thesis, University of Illinois at Urbana-Champaign, Department of Civil and Environmental Engineering, Urbana, IL, USA.

Wolf, H.E. 2015b. *Application of Surface Strain Gauges*. University of Illinois at Urbana-Champaign, Department of Civil and Environmental Engineering, Urbana, IL, USA.

Wolf, H.E., J.R. Edwards, M.S. Dersch, and C.P. Barkan. 2015. Flexural analysis of prestressed concrete monoblock sleepers for heavy-haul applications: methodologies and sensitivity to support conditions. In: *Proceedings of the 11th International Heavy Haul Association Conference*, Perth, Australia.

Wolf, H.E., J.R. Edwards, M.S. Dersch, Y. Qian, and D.A. Lange. 2016a. Field measurement of bending moments in prestressed concrete monoblock sleepers. *Proceedings of the World Congress on Railway Research*, Milan, Italy.

Wolf, H.E., S. Mattson, J.R. Edwards, M.S. Dersch, and C.P. Barkan. 2014. Flexural analysis of prestressed concrete monoblock crossties: comparison of current methodologies and sensitivity to support conditions. In: *Proceedings of the 94th Annual Meeting of the Transportation Research Board of the National Academies*, Washington, DC, USA.

Wolf, H.E., Y. Qian, J.R. Edwards, M.S. Dersch, and D.A. Lange. 2016b. Temperature-induced curl behavior of prestressed concrete and its effect on railroad crossties. *Construction and Building Materials*, 115: 319–326.

Yang, S.K., T.S. Liu, and Y.C. Cheng. 2008. Automatic measurement of payload for heavy vehicles using strain gages. *Measurement - Journal of the International Measurement Confederation*, 41(5): 491–502.

Yu, H. and D.Y. Jeong. 2014. Bond between smooth prestressing wires and concrete: finite element model and transfer length analysis for pretensioned concrete crossties. In: *Proceedings of the American Society of Civil Engineers Structures Congress*, Boston, MA, USA.

Yu, H., L. Khazanovich, M. Darter, and A. Ardani. 1998. Analysis of concrete pavement responses to temperature and wheel loads measured from instrumented slabs. *Transportation Research Record: Journal of the Transportation Research Board*, (1639): 94–101.

Zakeri, J. and F.H. Rezvani. 2012. Failures of railway concrete sleepers during service life. *International Journal of Construction Engineering and Management*, 1(1): 1–5.

Zarembski, A. 2010. *Assessment of Concrete Tie Life on US Freight Railroads.* Prepared by ZETA-TECH A Harsco Rail Business Unit. North Cherry Hill, NJ, USA.

Zeman, J.C. 2010. *Hydraulic Mechanisms of Concrete-Tie Rail Seat Deterioration*. Master's Thesis, University of Illinois at Urbana-Champaign, Department of Civil and Environmental Engineering, Urbana, IL, USA.

Zhao, W., B.T. Beck, R.J. Peterman, R. Murphy, C.J. Wu, and G. Lee. 2013a. A direct comparison of the traditional method and a new approach in determining 220 transfer lengths in prestressed concrete railroad ties. In: *Proceedings of the 2013 Joint Rail Conference*, American Society of Mechanical Engineers, Knoxville, TN, USA.

Zhao, W., B.T. Beck, R.J. Peterman, C.J. Wu, N.N.B. Bodapati, and G. Lee. 2014. Reliable transfer length assessment for real-time monitoring of railroad crosstie production. In: *Proceedings Of The 2014 Joint Rail Conference*, American Society of Mechanical Engineers, Colorado Springs, CO, USA.

Zhao, W., B.T. Beck, R.J. Peterman, C.J. Wu, G. Lee, and N.N.B. Bodapati. 2013b. Determining transfer length in pre-tensioned concrete railroad ties: is a new evaluation method needed? In: *Proceedings of the 2013 Rail Transportation Division Fall Technical Conference*, American Society of Mechanical Engineers, Altoona, PA, USA.

Zhao, W., K. Larson, R.J. Peterman, B.T. Beck, and C.J. Wu. 2012. Development of a laser-speckle imaging device to determine the transfer length in pretensioned concrete members. *Precast Concrete Institute Journal*, 57(1): 135.

Zhao, Y. and T. Ono. 1999. A general procedure for first/second-order reliability method (FORM/SORM). *Structural Safety*, 21(2): 95–112.

Zong, N., H. Askarinejad, T.B. Heva, and M. Dhanasekar. 2013. Service condition of railroad corridors around the insulated rail joints. *American Society of Engineers Journal of Transportation Engineering*, 139(6): 643–650.